Proteome Turnover in Mouse Aging: In Vivo Studies by Stable Isotope Mass Spectrometry

Natan Basisty

A dissertation

submitted in partial fulfillment of the

requirements for the degree of

Doctor of Philosophy

University of Washington

2015

Reading Committee:

Peter S. Rabinovitch, Chair

George Martin

Richard G. Gardner

Program Authorized to Offer Degree:

Pathology

University of Washington

Abstract

Proteome Turnover in Mouse Aging: In Vivo Studies by Stable Isotope Mass Spectrometry

Natan Basisty

Chair of the Supervisory Committee:
Professor Peter Rabinovitch, M.D., Ph.D.
Department of Pathology

Abstract

Introduction: Maintenance of proper protein homeostasis (proteostasis) is essential to cellular and organismal health. A wealth of research has shown that age-related diseases and conditions are associated with the inability of the cell to maintain healthy proteins or get rid of defective proteins, including: neurodegenerative disease, cardiac dysfunction, cataracts, and sarcopenia. Calorie restriction (CR) and rapamycin (RP), two interventions known to alter protein degradation and synthesis rates, effectively extend lifespan and improve health in many model organisms. Overexpression of mitochondria-targeted catalase (mCAT), an antioxidant enzyme, similarly extends lifespan and healthspan in mammals, protects against protein damage and unfolding, and preserves proteostasis machinery. While a general observation of improved

proteome quality and activation of proteostasis machinery can be observed in all three aging-interventions, the downstream proteins targeted by the affected processes remain unknown. Identifying these targets, their functional relevance to health and aging, and the mechanisms by which they change is the focus of this thesis.

Methods: Utilizing a combination of stable isotope labeling and nano-scale liquid chromatography tandem mass spectrometry (nLC-MS/MS), we performed large-scale estimation of changes in protein abundances and turnover rates simultaneously for each treatment, followed by clustering, pathway enrichment, correlations, and statistical analysis.

Calorie restriction and rapamycin in the aging heart and liver: In several tissues, we examined changes in protein abundances and in vivo turnover rates of young and old mice treated with either CR or RP for 10 weeks. Our data shows that global protein turnover tends to increase with age in the heart and liver, while both RP and CR reverse this aging effect. In old mice treated with CR, protein abundances closely recapitulated young levels in both heart and liver among the top significantly altered pathways. Treatment with RP recapitulated young levels in heart, but had the opposite effect in liver. The top pathways altered by treatment consisted mostly of metabolic pathways, including mitochondrial function, oxidative phosphorylation, and fatty acid beta-oxidation and decreases in glycolytic pathways.

Poly-ubiquitin mediated proteostasis: To determine the relative contribution of ubiquitin-mediated homeostasis to changes in turnover, we also performed an antibody-based enrichment of the poly-ubiquitin modified fraction (ubiquitinome) of liver tissue, followed by a novel

analysis of "poly-ubiquitinome" kinetics. Our data demonstrates that a large number of poly-ub-proteins show a preferential increase in abundance compared to their unmodified counterparts, and in several cases significantly correlate with previously observed increases in half-lives (HLs). These correlations extended to pathway-level changes during aging and treatment. Furthermore, we demonstrate how label kinetics can be used to distinguish accumulating poly-ub-proteins from readily degraded ones. Overall, our results demonstrate that proteomic analysis of sub-populations of proteins may be a promising approach to identifying the targets and dynamics of major cellular processes.

Mitochondrial respiratory chain turnover: The turnover rates of subunits of the mitochondrial respiratory chain were observed from over 40 unique experimental conditions representing a wide range of proteome compositions and turnover rates. We show that across highly divergent conditions, the relative differences in half-lives of respiratory proteins are highly conserved. This conserved heterogeneity can be partly explained by several factors.

Mitochondria-targeted catalase (mCAT) and reverse antagonistic pleiotropy: A comprehensive examination of changes in abundance and turnover during normal and mCAT aging. The effects of mCAT on global turnover rates as well as a number of changes in top pathways are comparable to the effects of CR and RP. Interestingly, the YmCAT proteome is largely different in abundances and turnover rates from the YWT proteome and more closely resembles the OWT proteome – exhibiting a pattern of "reverse antagonistic pleiotropy".

CONTENTS

LIST OF FIGURES*

* Supplementary figures can be found online: http://blogs.uw.edu/nbasisty/home/136-2/

LIST OF TABLES*

* Supplementary tables can be found online: http://blogs.uw.edu/nbasisty/home/136-2/

INTRODUCTION

1.1 THE ROLE OF AGING IN DISEASE

Aging can be loosely defined as the progressive decline in organismal function over time. Quantitatively, one can think of it as an increase in our mortality, or likelihood of death, over time due to a collection of biological changes [5]. Despite the extensive research on aging and age-associated diseases that exists today, the underlying cause(s) of aging are not known. In fact, the view that a single process could underlie the multitude of biological changes with advancing age has been a point of contention among researchers for many years. On one hand, some have argued that aging could be driven by a small number of fundamental cellular mechanisms, which are presumably universal to all cell types [6], or alternatively, the endocrine action of a single tissue could be the dominant force behind aging in many tissues [7]. On the other extreme, "aging" may be a singular term describing a large number of separate processes that are specific to pathologies, tissues, or cell types [8]. The current popular opinion leans toward the notion that there are a relatively small number of cellular processes underlying the progression toward many diseases of aging, although most will agree some biological changes are separable from these. Some of the evidence consistent with the current mainstream view will be discussed in the

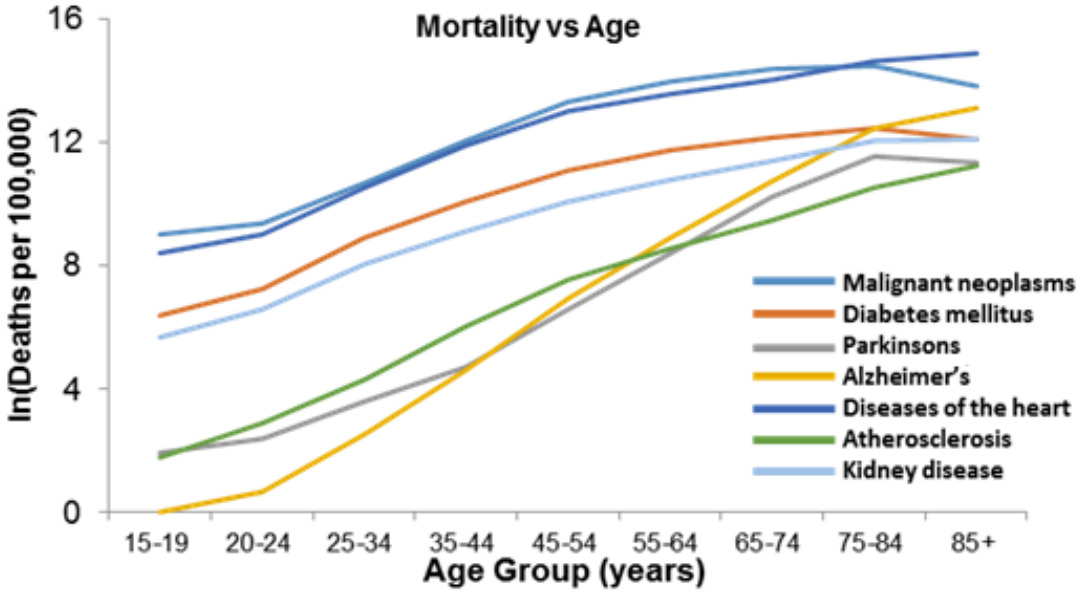

Figure 1-1 Mortality data from the Center for Disease Control (CDC) showing death rates in the U.S. from 1999-2010 from a several diseases. Death rates are in units of 1 per 100,000 people (on a natural log scale) as a function of age. This information is freely accessible using the WONDER database tools located on the CDC webpage (CDC WONDER) [9].

sections below.

Regardless of underlying causes, there is a vast amount of data describing observable changes that are characteristic of aging. Notably, statistical data on the U.S. population illustrates that the risk of many diseases, including all of the top killers, consistently increase with advancing age [9] (Figure 1-1). With the exception of neurodegenerative diseases, the progressions of these diseases in the provided example (slope of each line) are relatively parallel across tissue types, and all of them clearly have a strong age component, perhaps consistent with the idea of some common underlying mechanisms.

Age is also the single greatest risk factor for a number of diseases including Alzheimer's and heart disease [10]. This has been largely overlooked, as aging research receives only a fraction of the funding awarded to any of the individual diseases of aging [2]. In terms of improving health, research on the diseases among the top causes of death in developed countries, such as heart disease and cancer, are giving diminishing returns in extending lifespan and the period of healthy life ("healthspan") [2]. As these returns are continuing to decline and scientific research increasingly demonstrates the potential of aging interventions, it is becoming evident that aging research may be a much more effective and fruitful investment (Figure 1-2).

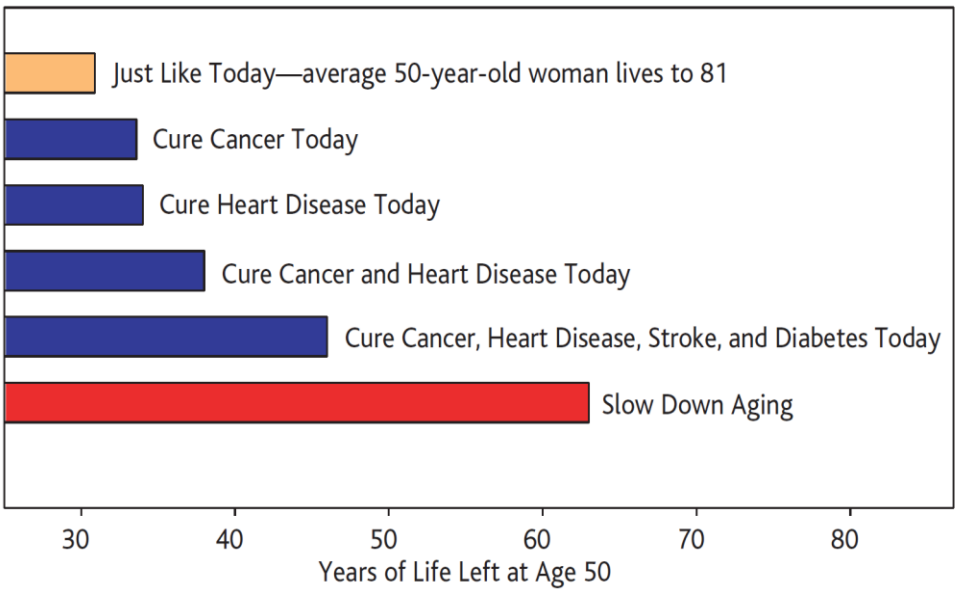

Figure 1-2 The remaining life expectancy of a 50 year old Caucasian woman in the U.S. in 1985, based on mortality risk at the time (top bar), and the projected years remaining if the mortality risk for specific diseases were reduced to zero (blue bars). The bottom bar projects years of life remaining if mortality risks were reduced to the same extent that calorie restriction reduces mortality risk in mice. 2.

1.2 PROTEIN QUALITY CONTROL IN AGING

Proteins directly participate in virtually all processes of the cell, so it is no surprise that the various declines in function associated with aging are evident on the protein level; however, increasing evidence suggests that protein quality control mechanisms have a more relevant role in aging and may be therapeutic targets for aging and a range of diseases.

Protein homeostasis is the equilibrium between protein synthesis, maintenance, and degradation. Maintenance of proper protein homeostasis (proteostasis) is essential to cellular and organismal health – illustrated by many studies indicating that age-related diseases and conditions are associated with the inability of the cell to maintain healthy proteins or get rid of defective proteins [11]. Some of these conditions include neurodegenerative disease [12], cardiac dysfunction [13,14], cataracts [15], and sarcopenia [16]. Similar dysfunctions in proteostasis have been observed in "normally" aging cells which are free of disease, indicating a potentially important role for protein regulation in both health and aging.

Aging interventions have also suggested an important role of protein homeostasis in health and aging. While dysfunction of protein quality control mechanisms is a hallmark of aging, improvement of these mechanisms is a hallmark of longevity and improved health. For example, the characteristic accumulation of damaged proteins and decline in quality control machinery have been alleviated in longevity models utilizing overexpression of mitochondrial-targeted catalase [17-20], calorie restriction [21], reduced IGF1 signaling [16,22,23], and rapamycin treatment [24,25].

Aside from the correlative association between aging, health, and protein quality control, direct intervention of quality control mechanisms may potentially increase lifespan and improve health. An example of this is the inhibition of mechanistic Target of rapamycin (mTOR), a regulator of protein homeostasis, which has been extensively shown to increase lifespan and healthspan in a variety of animal models and various intervention protocols [26]. The major role of mTOR in protein homeostasis, among other functions (discussed in more detail below), is to mediate protein translation and degradation in response to nutrient availability [26]. Both rapamycin and calorie restriction effectively inhibit mTOR and

are widely believed to confer benefits by this mechanism, although this has not been clearly established. Various protein quality control interventions have been shown to improve health and aging in both invertebrate and mammalian models[11,12,22,27].

Collectively, studies in this area may suggest that dysfunctional proteostasis has some causative role in aging or, alternatively, restoration of protein homeostasis machinery is protective against some other driving force in aging and age-related disease. In either scenario, the major mechanistic question of how these processes extend lifespan and healthspan remains unanswered and will pose a major challenge to researchers. An incomplete understanding of the various interactions, specificity, and targets of quality control pathways currently limits the ability of researchers to close this gap. Fortunately, several quality control pathways, such as autophagy and ubiquitin-mediated degradation, are receiving increased attention from several areas of biomedical research as their roles are recognized in a number of diseases[11,27]. In addition, emergence of sophisticated tools in proteomics and improved computer processing power have proven to be powerful tools in cellular biology, allowing researchers to acquire and analyze an unprecedented depth and volume of data.

1.3 AUTOPHAGY

Autophagy is one of two primary cellular systems that degrade the vast majority of proteins in the cell (its counterpart, the ubiquitin proteasome, is discussed in the next section). Any cellular degradation involving lysosomes, a single membrane vesicle containing various enzymes for the digestion of macromolecules, is generally categorized under the umbrella term “autophagy” [27]. There are three major ways by which proteins can be delivered to a lysosome for degradation, which define three primary categories of autophagy: macroautophagy, microautophagy, and chaperone-mediated autophagy (Figure 1-3). For brevity these will not be covered in detail, however, readers are referred to a number of detailed reviews on each topic [11,27,28].

Lysosomal degradation serves four primary physiological roles: cell and protein quality control, conserving cellular resources, cell remodeling, and cell defense [28]. In the context of quality control, autophagy is responsible for the clearance of damaged proteins, insoluble protein inclusions, and abnormal organelles, all of which are hallmarks of aged and dysfunctional tissues. Knocking down components of autophagy leaves cells unable to remove damaged organelles and proteins [28-31], demonstrating that autophagy plays a key role in protein homeostasis.

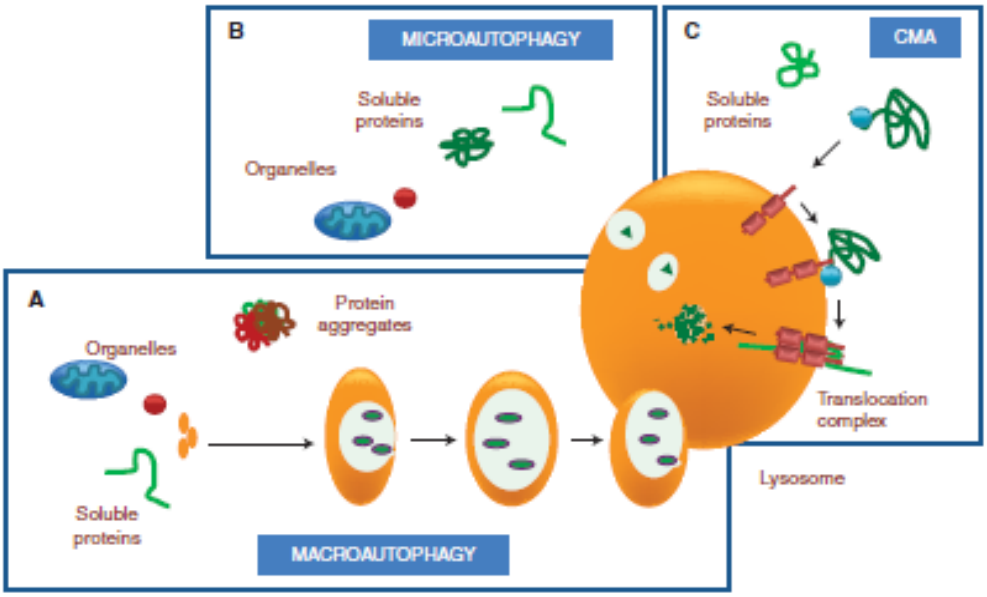

Figure 1-3 Autophagic pathways illustrated by Cuervo et al. (Wong & Cuervo 2010). Three primary types of autophagy (A) macroautophagy, a whole region of the cytosol is sequestered into a membrane-bound vesicle, which then fuses with lysosomes. (B) Microautophagy, the lysosome directly takes in small regions of cytosol (C) chaperone-mediated autophagy, soluble proteins are recognized and delivered to the lysosome by a targeting sequence, and translocated through the membrane via lamp2a, a receptor on the lysosomal membrane.

Numerous lines of evidence suggest that autophagy is likely to have an important role in aging, however, there has been no smoking gun study. Many studies, mostly those in C. *elegans*, have demonstrated that autophagy components are required for lifespan extension by CR, mTOR inhibition, IGF-1 inhibition, and a few other longevity pathways [32] – though these have not as yet been confirmed in other model systems. Unfortunately, there is no genetic or pharmacological intervention known to specifically increase autophagy without targeting other processes (and it may not be possible to do so), hence the lack of a definitive study. Though genetic overexpression of ATG5, a vital autophagy protein involved in autophagosome formation, has been reported to extend lifespan in mice [33]. ATG5 has also been shown to have pro-apoptotic functions, which cannot be excluded as the longevity-promoting component ATG5.

The mTOR pathway, when inhibited, is well known to increase both lifespan and autophagy. In fact, rapamycin is one of the few drugs available that can be used to activate autophagy. Longevity studies with rapamycin, and other forms of mTOR inhibition, have reported increased autophagy in treated animals [21,24-26], and offer further evidence that autophagy may play a central role in aging. Again, because autophagy is tightly linked to most cellular processes in some way, including growth, immunity, metabolism, energy and protein homeostasis, the key to understanding the role of autophagy will likely require a deep understanding of its interactions with other processes.

1.4 UBIQUITIN-MEDIATED TURNOVER

The ubiquitin-proteasome system (UPS) is the primary non-lysosomal protein degradation pathway. In contrast to autophagy, its action is limited specifically to individual proteins, and cannot degrade other macromolecules, organelles, or groups of proteins. Where autophagy often degrades its targets in bulk, the UPS very specifically targets thousands of proteins and utilizes a sophisticated array of mechanisms to do so with special and temporal precision. The UPS is also active in all regions of the cell, and targets proteins localized within organelles. For most proteins, degradation through this pathway is characterized by 2 major steps: recognition and "tagging" of a protein for elimination with a poly-ubiquitin modification, and translocation to the proteasome for degradation [28] (summarized in Figure 1-4). This process is very complex and has been extensively studied and described in detail in various reviews[11,27,28,34].

Similar to autophagy, the UPS is essential for maintaining overall cellular homeostasis. Inhibiting or deleting its components often leads to toxicity with severely altered cellular phenotypes and cellular death[34,35]. Almost immediately after inhibition, an accumulation of protein inclusions can be observed in cells. Interestingly these resemble the inclusions described in a number of neurodegenerative diseases[34-37]. Genetic depletion of proteasome subunits in the brains of mice has been shown to induce a neurodegenerative phenotype, suggesting a role in neurodegenerative diseases characterized by protein inclusions [36].

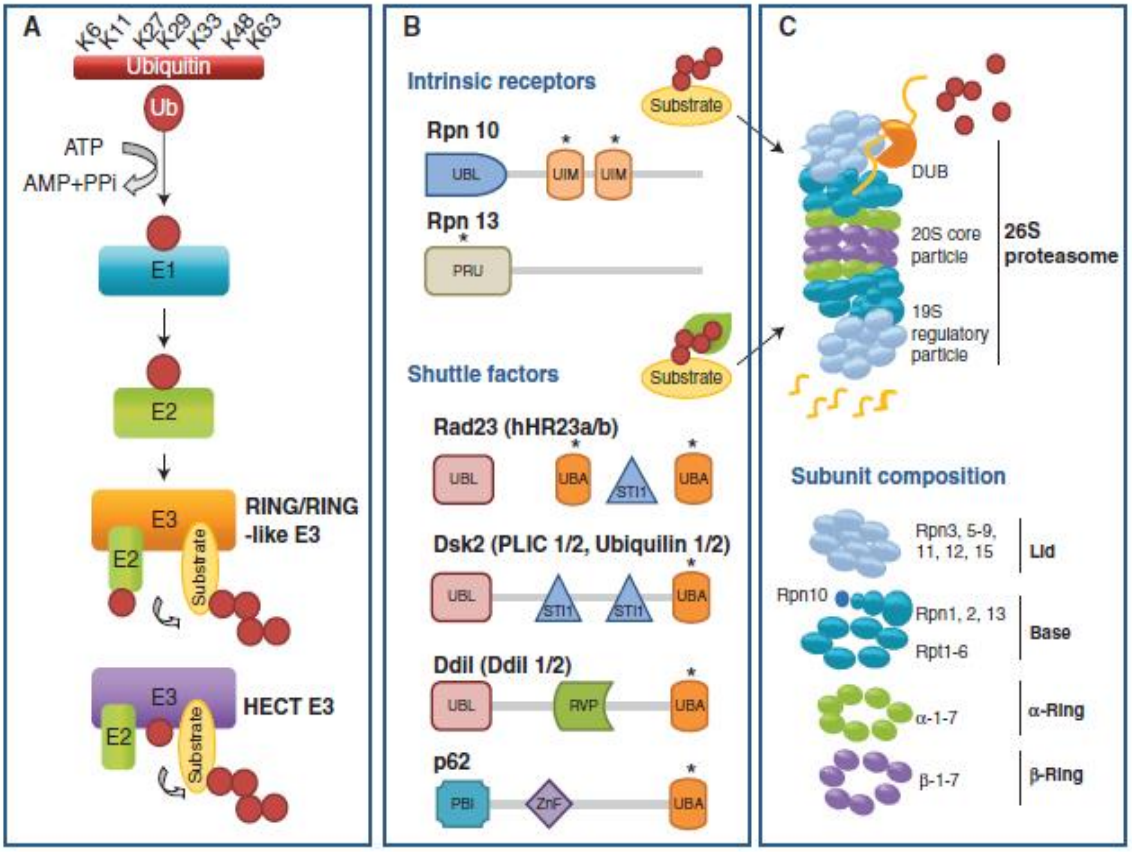

Figure 1-4 Components of the UPS broken down and illustrated by Cuervo et al. (Wong & Cuervo 2010) First, a protein in need of degradation (because of unfolding, oxidation, etc.) is recognized by an E3 ligase enzyme, and A) the protein is tagged with a ubiquitin chain over repeated cycles of ubiquitin activation (E1), conjugation (E2), and ligation (E3). B) A poly-ubiquitinated protein may directly bind to receptors on the proteasome or may be shuttled by factors. C) Once bound to the proteasome, de-ubiquitinating enzymes (DUBs) remove the ubiquitin modification and the protein is translocated into the proteolytic core of the proteasome, where it is digested into short peptides.

Most of the evidence linking the UPS-intervention to longevity comes from C. *elegans* studies [34]. Generally, these can be explained by the specific action of UPS on longevity pathways, rather than a global change in the proteolytic system. The ubiquitin ligase RLE-1, for example, selectively targets and poly-ubiquitinates daf-16, a key component in the insulin/IGF pathway in worms, leading to its degradation by the proteasome [38]. As a result, inhibition of RLE-1 extends lifespan in C. *elegans*. In flies it has been shown that overexpression of parkin-1, a ubiquitin ligase involved in familial Parkinson's disease, extends lifespan [39].

On a broad scale, it is not known if general protein maintenance by the UPS is involved in aging. Correlatively, proteasomal activity becomes less functional with age and is restored in long-lived animals under CR [11,27]. It is also important to note that autophagy and the UPS must work in harmony to direct protein homeostasis, and an intervention in either process is inevitably going to lead to changes in both. Unsurprisingly, there is extensive crosstalk between these processes - for example, it has been shown

that poly-ubiquitination can promote the clearance of depolarized mitochondria through mitophagy [40]. There also exists interaction between these systems in host-cell autonomous immunity, where the autophagic destruction of invading pathogens relies on the extensive ubiquitination of pathogen components in order to recognize pathogens as "non-self" [41].

The roles of poly- and mono- ubiquitination extend far beyond the widely known proteasomal degradation. This thesis, however, will focus directly on the aspects related to protein homeostasis – which itself also encompasses several fields of study. A few mechanisms of ubiquitin-mediated-homeostasis will be later revisited and are not discussed in detail here, but are worth noting. For example, poly-ubiquitin mediated proteostasis serves diverse roles including formation of insoluble protein inclusions characteristic of aged tissue [39], signaling protein turnover through autophagy [42], and the decoration of pathogen containing vacuoles to facilitate host-cell defense [43].

1.5 CALORIE RESTRICTION, MTOR, AND RAPAMYCIN

Calorie restriction (CR) was first associated with longevity in the 1930s [44], and to this day is the most robust non-genetic aging intervention in a variety of model organisms, including yeast, flies, worms, rats, mice, and dogs [45-47]. In addition to long-life, CR provides a number of health benefits, and has been reported to improve nearly every major pathway of interest in the field of aging, and through various mechanisms, including the insulin/IGF pathway, mTOR, hormone signaling, oxidative stress, DNA damage, protein homeostasis, and hormesis[48]. It has also demonstrated the potential to extend life, or prolong age-related diseases, in non-human primates [49,50]. Despite this vast amount of characterization and research, much of the data that exists is correlative and mechanism(s) by which CR confers longevity remains unclear.

Mechanistic target of rapamycin (mTOR) has been popularly pursued as an aging intervention since it was discovered that CR is a potent inhibitor of this pathway. Like with CR, inhibition of mTOR is a known aging intervention that is conserved – increasing lifespan in yeast, worms, flies, and mice. Rapamycin, an FDA approved drug (which the mTOR pathway was named after), effectively inhibits mTOR activity and

improves health and aging in both invertebrates and mammals. Though there have been other popular anti-aging drug candidates proposed as “CR mimetics”, such as resveratrol, rapamycin was the only one to increase longevity in several independent mouse studies [24,25].

mTOR is a nutrient responsive pathway which, when active, inhibits protein degradation through autophagy and promotes cell growth and protein synthesis. When mTOR is inhibited by CR or RP, autophagy is promoted and protein synthesis is reduced. Although these alterations in protein homeostasis have been generally associated with both CR and RP treatments, the specific actions of each intervention are not well known. A deeper study of the proteins that are being targeted by homeostatic machinery will more directly address the specific differences in these treatments. Additionally, an increase in degradation coupled with a decrease in protein synthesis is clearly not a viable long-term strategy to maintain homeostasis, so the kinetics of treatment with CR and RP are also important to investigate.

1.6 OVEREXPRESSION OF MITOCHONDRIA-TARGETED CATALASE

One of the most popular and well-known, yet highly controversial theories of aging is the Free Radical Theory of Aging (FRTA) and the various versions of it that exist today. FRTA, first proposed by Denham Harman in the 1950s [51] and later renamed the “Mitochondrial” FRTA [52], views aging as an accumulation of macromolecular damage over time. It hypothesizes that highly reactive molecules, collectively referred to as reactive oxygen species (ROS), which are unavoidably created as a side effect of essential cellular metabolism, damage various macromolecular components in the cell including proteins, lipids and DNA, and thereby drive a progressive decline in health and function seen with advancing age.

ROS are associated with the progression of a broad spectrum of pathologies including aging [51], neurodegeneration, metabolic syndrome [53-55], heart disease [56-58], cancer , and others [59]. Mechanistically, this has largely been attributed to oxidative modification of cellular macromolecules, including lipids [60], DNA [61] and proteins [62]. Given the propensity for ROS to cause damage and modification on proteins, it is perhaps not surprising that it can have large impacts on protein homeostasis. Compounds with the ability

to inhibit the oxidative modification of molecules by ROS, antioxidants, are widely believed to promote health and longevity. Unfortunately, this widely held view is largely unsupported by scientific evidence. In human clinical trials, antioxidants have largely failed to have a therapeutic use [63-65] and have occasionally reported negative outcomes[66-68].

The results have been mixed in animal models as well, with invertebrate studies reporting that *increasing* rather than decreasing ROS promotes longevity [69]. Likewise, antioxidant models in mice have failed to show benefits from either overexpression of endogenous cellular antioxidants or treatment with pharmacological ones [70]. However, a transgenic mouse model in which the antioxidant enzyme catalase, normally found in the peroxisomes, is overexpressed and targeted to mitochondria is a notable exception. Created in the Martin and Rabinovitch labs, the mitochondria-targeted catalase (mCAT) mice live about 15-20% longer [18]. Numerous studies [61,71-76] have now supported the exceptional health and resilience of these mice including heart failure models and cardiac aging studies in our lab, and numerous measures of health reported by other labs.

In chapter 6, I examine the relationship between mCAT and the proteome more closely. Additionally, I discuss how global alterations in proteome abundances and turnover rates, in the context of a few recent mCAT papers, provide clues as to how to reconcile contradictory antioxidant studies.

1.7 STABLE ISOTOPE LABELING AND PROTEIN TURNOVER

Studies of in vivo protein kinetics with stable isotopes have been conducted at least as far back as the early 1960's [77,78], and the value of doing so was recognized much earlier [79]. Early experiments utilized pulse-chase or continuous radiolabeling of tissues to perform bulk measurements of protein turnover. A typical experiment could involve administering metabolically active biological precursors (amino acids, glucose, ammonia, etc) that contained a radioactive tracer (isotopes of carbon, hydrogen, and sulphur) in an animal or cell culture model. After an initial labeling period, radioactive decay is generally monitored by collecting specimens and measuring radioactivity over several time points. Tissue collection and cell fractionation often aided these techniques. In early studies of mitochondrial turnover, preparation of

mitochondrial inner membrane, outer membrane, and matrix fractions allowed for the comparison of bulk protein turnover among compartments of this organelle [77]. Gel-based separations aided in collecting data on more specific protein isolates. The use of radioactive tracers to perform turnover studies did face some serious challenges, however. Some obvious examples are the adverse health effects of injecting radioactive isotopes into live animals, which emit radiation and can induce effects that may affect the disease model or the biological system of interest. Perhaps the most significant limitations of these methods was the 1) lack of protein-specific data and 2) the fact that degree of enrichment of radioactive isotopes in the amino acid precursor pool of higher organisms is difficult to determine, which is required if one is to know the proportion that would be expected to appear in newly synthesized proteins.

Owing to modern proteomic technologies, software tools, and improved computing power, researchers now have the ability to estimate turnover rates at the individual protein level of thousands of proteins simultaneously [80]. Mass spectrometers rely on mass measurements to identify proteins, rather than measuring radioactivity, allowing for the use of stable-isotopes rather than radioactive ones and reducing the risk of inducing unwanted effects in animals. With the exception of deuterium or tritium, which can be highly toxic or fatal, stable isotopes have shown no evidence of significant disruption of biological systems, and near-complete labeling of higher organisms with ^{13}C and ^{18}O has been achieved without adverse effects [81]. There have been few investigations of biological effects of stable isotopes, however, and it should be noted that even if changes to the physical properties of heavy-isotope containing molecules are subtle or undetectable, there might be larger and more apparent effects on a biological system.

Metabolic labeling can be done with a number of molecules with various advantages and disadvantages [82,83]. Generally, outside of nuclear magnetic resonance studies, amino acids are superior for metabolic labeling because their incorporation into proteins is predictable, although researchers have had success estimating protein turnover with other precursors such as deuterated water [84]. Several considerations are taken when choosing the correct amino acid label: the number of biosynthetic pathways that a model organism can utilize to create it, whether the isotopic atom can be redistributed to other precursors that

incorporate into peptides, the prevalence of the amino acid in the proteome, and whether available instrumentation can reliably detect the mass differential between the heavy and light molecules. Essential amino acids are the most commonly used because they cannot be synthesized by the organism of study and are more likely to incorporate into the amino acid precursor pool used to synthesize new proteins. For all studies described in this thesis, we performed metabolic labeling with deuterated leucine. Leucine is an essential amino acid as well as the most prevalent amino acid in the proteome, increasing the likelihood that it will appear in tryptic peptides and proteins.

One of the major challenges in turnover studies is the difficulty in assessing the enrichment of label in the amino acid precursor pool throughout the labeling period [85-87]. The studies outlined in this thesis overcome these challenges using Topograph, an open-source software program developed in the MacCoss Lab at the University of Washington [88]. The Topograph algorithm is capable of calculating the enrichment of heavy-label (leucine in our case) in the amino acid precursor pool based on the isotopomer abundances of peptides containing 2 or more labels. Topograph corrects to these precursor enrichments to make an accurate estimation of turnover regardless of whether the precursor pool is fully labeled. Further details on the design and analysis of our turnover studies are given in the methods section of each chapter below. For more information about metabolic labeling or Topograph, readers are referred to several informative papers as well as the Topograph publication [86-89].

1.8 CARDIAC AGING

Physiologically, age-related heart failure in humans is closely recapitulated by mouse models, including the development of left-ventricular hypertrophy, diastolic dysfunction, and fibrosis [17,90]. In mice, we have shown these functional declines are accompanied with proteomic remodeling of both energetic and structural pathways [91]. Levels of mitochondrial respiratory proteins, key proteins in the production of most of the cardiac ATP, decline in the old heart, leading to concurrent loss of energy homeostasis. Additional declines in metabolic proteins involved in fatty acid beta oxidation, amino acid metabolism, ketogenesis, and the TCA cycle likely contribute to an overall energy deficiency [91]. Conversely, glycolytic metabolic pathways as well as extracellular structural proteins are often significantly *increasing* in protein

abundance with age [91]. Glycolytic proteins rise significantly during age, which together with the loss of fatty acid oxidation and amino acid metabolism suggests a metabolic fuel switch has occurred. These findings are consistent with a number of proteomic studies focused on cardiac aging and disease. These changes may owe to an underlying decline in major protein quality control systems with age, leading to increases in low quality and damaged proteins which less able to perform their roles efficiently.

The aging cardiac proteome recapitulates most hallmarks of the aged cellular proteome including the appearance of protein aggregates and lipofuscin, increased protein oxidation and damage, increased ubiquitination, and declines in autophagy and the ubiquitin proteasome system [26,27]. All of these changes will have an impact on global levels of proteostasis to some degree, consistent with a notion of proteome remodeling during aging. It is unlikely, however, that all protein changes are equally or significantly contributing to the aging phenotype – presenting a challenge for researchers to identify the most phenotypically relevant downstream targets and their changes during aging.

The majority of studies in mice have reported a decline in the efficiency of protein degradation machinery with advanced age, contributing to a popular notion that aging is associated with a decrease in overall protein turnover. In contrast, our group has consistently observed that proteome turnover is either unchanged or modestly increased in the various mouse tissues examined to date, including mouse heart [91] as well as skeletal muscle [92] and unpublished data in brain. Unlike earlier studies, these finding were based on direct measurements of individual protein turnover rates *in vivo* [88], rather than using cellular markers of degradation as a proxy. Additionally, other recent studies utilizing a similar metabolic labeling-based MS approach to assess in vivo protein turnover have observed turnover rates consistent with our observations in aging mice [85,93]. The relative contribution of various homeostatic processes to the many changes in protein turnover and abundance remains unknown. It is clear that several closely connected quality control mechanisms are required in order to maintain healthy cardiac function.

1.8.1 **Autophagy in cardiac aging**

Macroautophagy has shown a mix of positive and negative results in various heart disease models; however, numerous lines of evidence have shown that macroautophagy does indeed have an important role in organismal and cardiac ageing. For example, a recent report found that genetic over-expression of ATG5, a vital autophagy protein involved in autophagosome formation, improved mitochondrial morphology, respiratory rates, and extended lifespan in mice [33]. ATG5 has been shown to have a pro-apoptotic function, and this activity in reducing cancer deaths in C57BL/6 mice may be a longevity-promoting component. Cardiac-specific knockdown of ATG5 in mice has conversely been shown to accelerate aspects of ageing in the heart, suggesting that autophagy plays an important role in maintaining normal heart function and mediating cardiac ageing. Like normally ageing mice, cardiac specific ATG5 mutants develop left-ventricular hypertrophy, but they also develop accelerated heart failure with decreased fractional shortening, abnormal mitochondrial morphology, decreased respiratory capacity, and premature death[94-96]. While the mechanism by which autophagy maintains cardiac function is not fully understood, fragmentation of mitochondria and accumulation of ubiquitinated proteins and p62 in mice lacking ATG5 suggests that this is an essential protective mechanism [34,95]. In agreement with this, a study performed on cardiomyocyte cell lines found that induction of autophagy was protective against oxidative stress-induced protein aggregation, reduced levels of protein ubiquitination, improved mitochondrial function, and reduced cell death [95].

Inhibition of the mTOR pathway (see above) is well known to increase autophagy and extend lifespan. In fact, the mTOR inhibitor rapamycin is one of the few drugs available which can be used to increase autophagy. Longevity studies with rapamycin and other forms of mTOR inhibition have reported increased autophagy in animals across many studies [26,27,32], and offer further evidence that autophagy may play a central role in ageing. Even so, due to the difficulty of specifically over-expressing autophagy components without targeting non-specific processes, direct evidence that activating autophagy can extend lifespan is not yet available.

1.8.2 **Ubiquitin-mediated turnover in cardiac aging**

In the heart, the role of the UPS is less well known. Some evidence exists of proteasomal degradation of various cardiac proteins including myofibrillar proteins, connexins, actin, and myosin [97], although many of these mechanisms have not been well established. Pharmacological and genetic intervention of the UPS with proteasome inhibitors, however, has made it evident that the proteasome can have powerful effects on the heart. In models of ischemia reperfusion injury, for instance, proteasome inhibitors decrease infarct size - sometimes by over 50% [97]. Little has been reported in the literature about the role of the ubiquitin proteasome in the context of cardiac aging specifically.

1.8.3 **Mitochondrial Fusion/Fission**

Mitochondrial dysfunction, particularly bioenergetic deficiencies, is an important hallmark of cardiac ageing. Age-related decline in mitochondrial activity and impaired mitochondrial dynamics offer a potent explanation for deteriorating cardiac performance with age. Dysregulation of mitochondria quality control processes are widely reported in ageing and although few studies have focused on the role of dysfunctional mitochondrial dynamics in cardiac senescence, there is extensive evidence to indicate that healthy cardiac performance is highly reliant on precise balance of mitochondrial fission and fusion.

Mitochondria are highly motile organelles that constantly change morphology, fuse, divide, and move depending on energy demands and integrity of individual mitochondria. Following fission, segments of mitochondrial that are dysfunctional, sensed as reduced membrane potential, are targeted for mitophagy [98]. This homeostatic process helps to ensure optimal mitochondrial quality and supply of ATP to meet energy demand [99]. The key regulators of mitochondrial dynamics, Mfn1, Mfn2, Opa1, hFis1, Drp1, and Fss, show high expression in normal cardiac tissue, consistent with their pivotal role in mitochondrial dynamics and bioenergetics [100,101]. Genetic defects of proteins regulating fusion/fission are correlated with severe alterations in mitochondria morphology, decreased mtDNA integrity, increased oxidative stress, susceptibility to apoptosis, and metabolic dysregulation [102]. Mitofusion 1 and mitofusion 2 null mice are embryonic lethal, while knock-downs have fragmented mitochondria, characteristic of declining mitochondrial fusion; mfn1 deficiency is observed in giant cells similar to those present in age-related

cardiac hypertrophy [103]. Genetic aberrations of mfn1 and 2 are consistent with increased respiratory dysfunction and higher frequencies of mtDNA mutations [104]. Dysregulation of fission may cause permeabilization of the mitochondrial membrane and release of caspase-3, a key modulator of myopathic apoptosis observed in senescent heart [105-107] that can trigger several other cytosolic death pathways [108,109] likely similar to those observed in heart failure [93] and possibly other cardiac pathologies.

Mitochondrial fusion is regulated by Mfn1, Mfn2, and Opa1. Opa1 mice missing one allele develop cardiomyopathy late in life, and the acetylation of Opa1 has been linked to the development of heart disease when mice are pharmacologically, dietary, or surgically stressed [110]. The general loss of Opa1 in MEFs has been shown to give fragmented mitochondrial populations. Cardiac specific Mfn1/Mfn2 KOs have been shown to develop early onset heart disease [111]. Mfn1/2 are found on the outer mitochondrial membrane, where they can make hetero- or homo-dimeric interactions with neighboring mitochondria. Mfn1/2, unlike Opa1, are increased in some forms of heart failure [112]. Mfn1/Mfn2 plays a large role in autophagy that is often difficult to separate from their roles in fusion, which is an area of intense research. Mfn2 plays a key role in mitochondria–sarcoplasmic reticulum tethering for calcium signaling. In fact, loss of outer membrane mitofusins (MARF) led to fragmented mitochondria with higher ROS, which was repaired by increasing XBP1 expression, a protein involved in ER stress [113].

Mitochondrial fission is managed by Drp1, Fis1, and Mff. Drp1 is localized to the cytosol until it is attracted to the mitochondrial surface for a fission event [114]. Drp1 has recently been suggested to help protect cardiac cells from ischemia repurfusion injury by allowing them to be less reliant on oxidative phosphorylation and delaying or suppressing apoptosis [114,115]. The depletion of Drp1 in cardiomyocytes or in mouse hearts leads to mitochondrial dysfunction and heart disease, respectively. A study by Ikeda et al. demonstrated that unchecked mitochondrial fusion, by Drp1 knock out was just as detrimental as is unchecked fission [111].

Despite the recent illumination of the roles and mechanisms of fission and fusion, challenges remain in studying these processes in ageing cardiac tissue. Much of what is known about mitochondria dynamics

and its relationship to energetic deficiencies in the ageing heart comes from studies of cultured cardiomyocytes and surgically stressed hearts, not from ageing hearts.

1.8.4 **Mitophagy**

Mitochondrial-specific autophagy, or "mitophagy", is a process by which (usually) defective mitochondria are turned over through the lysosomal pathway. Knocking down components of macroautophagy strongly diminishes mitochondrial function [28,90,116], demonstrating that it plays a key role in mitochondrial maintenance and homeostasis. Two well characterized regulators of mitophagy are PINK1 and Parkin [117,118]. PINK1, aka phosphatase and tensin (PTEN) homologue-induced kinase 1, is a mitochondria-targeted serine/threonine kinase which serves to protect the cell from mitochondrial dysfunction and apoptosis [119]. Mutations in this protein are the most common cause of recessive familial Parkinsonism in humans [120]. In addition, PINK1 KO mice have severe deficiencies in mitochondrial homeostasis accompanied by morphological changes in the mitochondrial network, increased ROS, and susceptibility to heat shock [119]. Together this evidence suggests PINK1 has an important role in Parkinson's disease as well as mitochondrial quality in normal cells, and possibly plays an important role in ageing.

Under healthy conditions, PINK1 is imported into mitochondria via the TOM complex and is actively degraded by mitochondrial processing peptidase (MPP) and presenilin-associated rhomboid-like protease [121 94,119,122]. Upon loss of mitochondrial membrane potential, PINK1 accumulates on the mitochondrial outer membrane and recruits Parkin, an E3 ubiquitin ligase, leading to the poly-ubiquitination of many mitochondrial outer membrane proteins such as Hexokinase I, VCAC1, MFN1/2, and Miro [123]. These ubquitinated proteins are recognized by autophagy proteins P62, LC3 II, and BNIP3 to promote fusion with the lysosome and clearance of the dysfunctional organelle via mitophagy [123,124]. Many of the details surrounding this pathway and the interactions starting at PINK1 and leading up to mitophagy have been studied in detail and reviewed elsewhere [117,119,123,124].

A few studies have shown that PINK1/Parkin mediated mitophagy is important for heart function, particularly in the context of adaptation and recovery from stress. Parkin KO rats, in contrast to wild type,

lack cardioprotection following ischemic preconditioning [125]. Parkin deficient mice exhibit impaired recovery of cardiac function after sepsis [126] and have reduced survival and larger infarct size following myocardial infarction [127]. All of these studies noted that Parkin deficient animals show disorganized mitochondrial networks, small or fragmented mitochondria, and an increase in cardiomyocyte cell death. The infarct study additionally showed that overexpression of Parkin in isolated cardiomyocytes protects against hypoxia mediated cell death[128]. Interestingly, protein ubiquitination and LC3II, markers of mitophagy, were not higher in control mice than in Parkin deficient animals after sepsis or in the remote zone after myocardial infarction. However, there was evidence of compensatory increases in macroautophagy, and possibly an induction of alternative BNIP3-mediated mitophagy, where Parkin-dependent mitophagy is absent. A more detailed review details the role of mitophagy, including the less known role of BNIP3, in the heart [129].

Even though there were obvious morphological differences in the mitochondria of Parkin deficient animals, one common observation of these studies was that under normal conditions there was no apparent difference in cardiac function compared to wild type mice until advanced age or animals were first subjected to stress. PINK1 KO mice also show increased vulnerability to ischemic injury [130], but unlike Parkin deficiency, loss of PINK1 has been reported to show signs of cardiac dysfunction in mice as young as 2 months [131]. By six months of age, PINK1 KO and heterozygous mutants show increased heart weight, cardiomyocyte hypertrophy, decreased fractional shortening, and increases in hypertrophic gene expression [131]. Again in contrast to Parkin deficient mice under normal conditions, this study also reported reductions in mitochondrial biogenesis and bioenergetics starting at 2 months of age. Collectively, studies in PINK1/Parkin have shown that these mediators are important for cardiac function, particularly in response to stressors, and compensatory increases in other degradation pathways may alleviate the dysfunction resulting in reduced mitophagy. However, further studies in the context of ageing will be needed to determine the precise roles of PINK1/Parkin and mitophagy related to age-related cardiac dysfunction.

ALTERED PROTEOME TURNOVER AND REMODELING BY SHORT-TERM CALORIC RESTRICTION OR RAPAMYCIN REJUVENATE THE AGING HEART

2.1 SUMMARY

Chronic caloric restriction (CR) and rapamycin inhibit the mechanistic target of rapamycin (mTOR) signaling, thereby regulating metabolism and suppressing protein synthesis. CR or rapamycin extend murine lifespan and ameliorate many aging-associated disorders; however, the beneficial effects of shorter treatment on cardiac aging are not as well understood. Using a recently developed deuterated-leucine labeling method, we investigated the effect of short-term (10 weeks) CR or rapamycin on the proteomics turnover and remodeling of the aging mouse heart. Functionally, we observed that short-term CR and rapamycin both reversed the pre-existing age-dependent cardiac hypertrophy and diastolic dysfunction. There was no significant change in the cardiac global proteome (823 proteins) turnover with age, with a median half-life 9.1 days in the 5-month old hearts and 8.8 days in the 27-month old hearts. However, proteome half-lives of old hearts significantly increased after short-term CR (30%) or rapamycin (12%). This was accompanied by attenuation of age-dependent protein oxidative damage and ubiquitination. Quantitative proteomics and pathway analysis revealed an age-dependent decreased abundance of proteins involved in mitochondrial function, electron transport chain, citric acid cycle and fatty acid metabolism as well as increased abundance of proteins involved in glycolysis and oxidative stress response. This age-dependent cardiac proteome remodeling was significantly reversed by short-term CR or rapamycin, demonstrating a concordance with the beneficial effect on cardiac physiology. The metabolic shift induced by rapamycin was confirmed by metabolomic analysis.

2.2 INTRODUCTION

Caloric restriction (CR) extends lifespan in a wide variety of organisms ranging from yeast to mice and may attenuate several age-related diseases including diabetes, cancer and neurodegenerative disease [46,132]. Long term caloric restriction has been shown to ameliorate age-associated cardiac hypertrophy and diastolic dysfunction [133-135] as well as cardiomyopathy in rodents and in monkeys [48,136]. Although short term caloric restriction improved ischemic tolerance in the aged heart [135], the beneficial effect of short-term caloric restriction on cardiac hypertrophy and diastolic dysfunction is not well understood.

Several nutrient sensing pathways have been implicated in the beneficial effect of caloric restriction on aging process [137], however, interest in the mechanistic target of rapamycin (TOR) has increased following the demonstration that long-term rapamycin (RP) treatment, initiated at 9 or 18 mo of age, extends lifespan in murine models [25,138]. mTOR regulates metabolism and cellular growth by sensing nutrient status and the growth factor signaling. The mechanisms by which TOR exerts its effects on aging involve the modulation of protein synthesis [139], ribosomal biogenesis and autophagy through mTOR Complex 1 (mTORC1) and downstream targets ribosomal S6 kinase (S6K) and the translational repressor 4E-BP1 [140,141]. Mice with deletion of S6K1 have increased life span and resistance to age-related pathologies [142], and activation of 4E-BP has been shown to mediate the lifespan extension effect of dietary restriction in Drosophila [143]. Furthermore, 4E-BP has been shown to act downstream of TOR to modulate cardiac functional aging in Drosophila [144].

Although the inhibition of mTOR is well known to ameliorate pressure-overload induced cardiac hypertrophy [145], the effect of RP on murine cardiac aging is less established. Both CR and RP have been shown to suppress protein synthesis and increase autophagy. We have recently developed a novel method to measure proteome dynamics using 2H3 Leucine heavy isotope labeling [88]. In this study we applied this novel method to investigate the effect of short-term CR or RP on cardiac aging, proteome dynamics and protein abundance.

2.3 RESULTS*

2.3.1 Experimental diet and deuterated leucine labeling.

The experimental design is summarized in Figure 2-1. C57BL6 mice were acclimatized to synthetic diet for 3 weeks. During the first week there was a 7% decline of mouse body weight, after which it stabilized. At week three, 4 and 26 mo old mice were fed *ad libitum* synthetic chow control diet (CL), caloric restricted (CR) or *ad libitum* plus rapamycin (RP) for 10 weeks. RP was used at the concentration and formulation previously shown by the NIA Interventions Testing Program to extend mouse lifespan [25]. Old mice fed caloric restricted synthetic chow diet lost 25% of body weight over the first three weeks, after which weight stabilized (Fig. S1). The body weight of old CL and old RP remained unaltered throughout the 10 week period; young mice CL gained 7.8% of body weight, normal growth for age. Mice are then

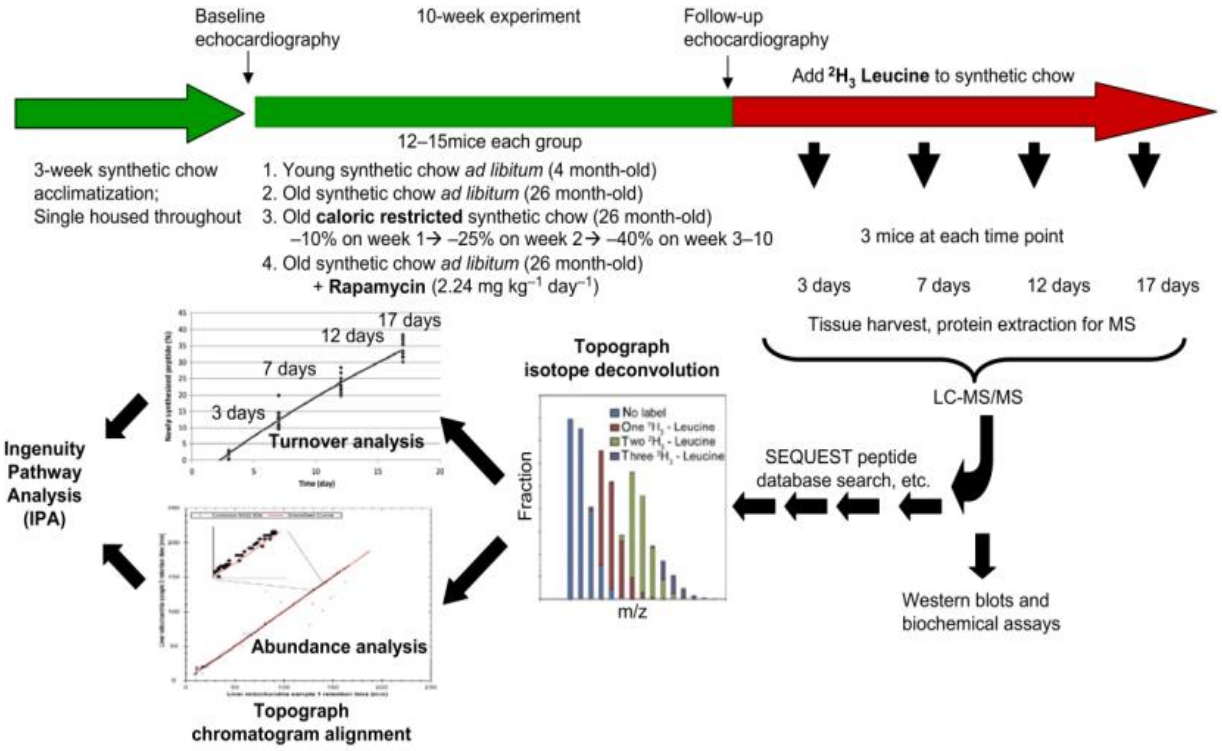

Figure 2-1 Summary of experimental design. After 3 weeks on synthetic chow diet for acclimatization, young (4 month old) and old (26 month old) female mice had baseline echocardiography and were placed on a synthetic diet ad libitum (control group), 40% caloric restriction (progressively over 3 weeks), or ad libitum plus microencapsulated rapamycin 2.24 mg kg-1day-1. After 10 weeks, echocardiography was repeated and the mice were switched to the same synthetic diet but with 2H3-leucine fully substituted for normal leucine. Tissue from 3 mice per treatment were harvested 3, 7, 12, and 17 days thereafter. Protein extraction was followed by LC-MS/MS. Topograph was applied to calculate the fraction of newly synthesized peptides, as well as the relative abundance of all isotopomers. The percentage newly synthesized peptides for each protein were plotted for the triplicate mice at each time point to derive the rate constant and half-lives based on first order kinetics. For abundance analysis, Topograph aligned the chromatograms to normalize the recovery times of the corresponding ions in each sample and obtain the areas under the curve for every peptide identified in any one sample. (see method S1 for further detail).

placed on a deuterated leucine diet while maintaining CR, RP or CL conditions. At 4 time points thereafter, mice were euthanized and cardiac proteins analyzed by LC-MCS/MS. Topograph software was used to deconvolute the mass spectra to determine the isotope distributions of deuterated label in each peptide and used this to calculate the precursor-pool adjusted turnover rate of proteins (Fig. S2, Stab1, supplementary method)[88].

2.3.2 **Reversal of aging cardiac dysfunction by short-term rapamycin or CR.**

At baseline, the aged heart phenotype in mice recapitulates the age-related changes of the human heart [73], including left ventricular hypertrophy and impairment of myocardial performance and diastolic

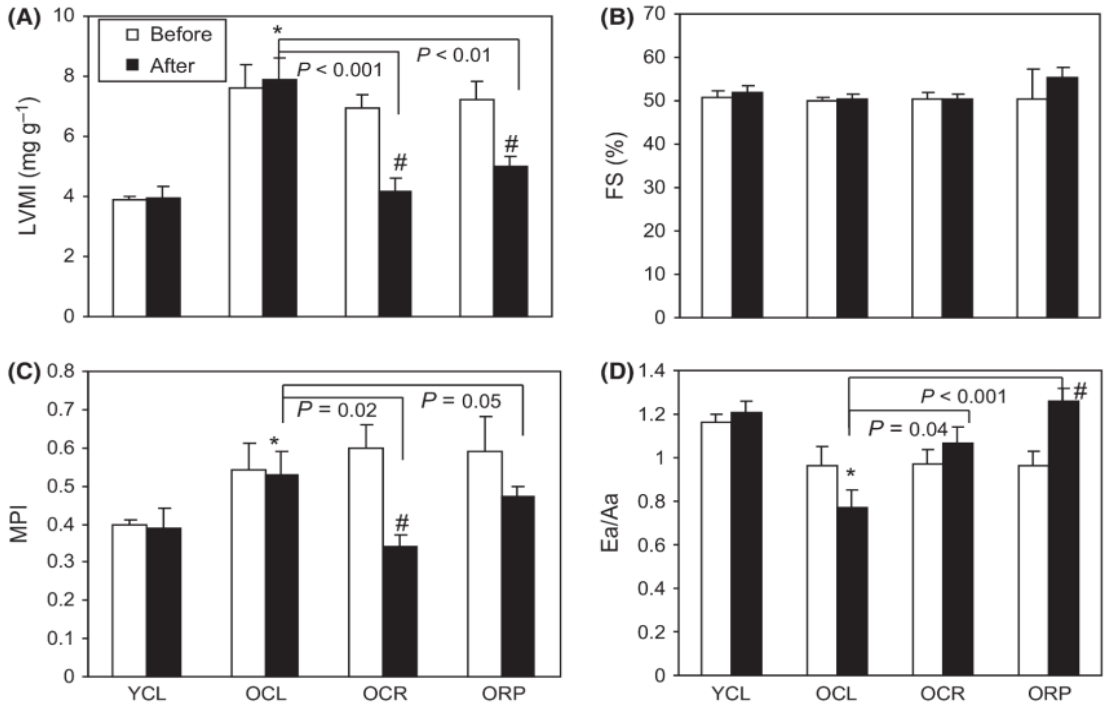

Figure 2-2 Echocardiography. (A) Left ventricular mass index (LVMI) is significantly higher in old hearts at baseline (25 months old), when compared to young hearts (3 months old), indicating age-dependent left ventricular hypertrophy. After 10 weeks of CR or RP in old mice, LVMI is significantly lower than old control mice ($P < 0.001$ and $P = 0.004$, respectively). It is also significantly reversed when compared with the baseline echocardiography of each mouse ($P < 0.01$ for both CR and RP), indicating reversal of age-dependent ventricular hypertrophy. (B) Fractional shortening does not significantly change with age or treatment group. (C). Myocardial performance index 4 significantly worsened (increased) in old mice at baseline. CR or RP significantly improved the MPI in old hearts when compared with control mice. ($P = 0.02$ and 0.05, respectively). (D) Diastolic function measured by tissue Doppler imaging Ea/Aa significantly declined in old hearts. While old CL mice have progressive decline of Ea/Aa after 10 weeks, treatment with CR or RP significantly increased Ea/Aa. CL: ad libitum control diet, and CR: caloric restriction. *$P < 0.05$ vs. YCL; #$P < 0.05$ versus pretreatment. n = 5–8.

dysfunction, as measured by echocardiography (Figure 2-2). Old mice fed *ad libitum* with a control diet (OCL) had an approximately 2-fold increase in left ventricular mass index (LVMI, Figure 2-2A) compared to young controls (YCL), indicating left ventricular hypertrophy. There was no significant change in systolic function measured by fractional shortening (Figure 2-2B). The myocardial performance index [4], a sensitive marker of systolic and diastolic function, significantly increased with age (Figure 2-2C), indicating a greater fraction of inefficient time spent without ejection in systole. Diastolic function measured by tissue Doppler Ea/Aa significantly decreased in OCL mice (Figure 2-2D), falling below the value of 1.0 which is the definition of diastolic dysfunction. While 10 weeks of control diet did not affect any of the above parameters, OCR mice demonstrated a large decline of LVMI, falling to a level comparable to YCL young mice and significantly lower than that of OCL mice ($p<0.001$, Figure 2-2A). This was closely recapitulated by 10 week RP ($p=0.004$). The worsening of myocardial performance [4] in old mice was also significantly reversed by both CR and RP ($p=0.016$ and 0.05, respectively, Figure 2-2C), to levels comparable to YCL. Likewise, the age-related decline in diastolic function was significantly improved by both CR and RP ($p=0.04$ and $p<0.001$, respectively, Figure 2-2D) as compared to OCL. These findings suggest that short-term CR or RP effectively induce regression of age-related left ventricular hypertrophy, amelioration of myocardial performance and reversal of diastolic dysfunction.

2.3.3 **Measurement of global cardiac proteome dynamics in aged heart and its modification by short-term rapamycin or CR**

CR and RP are associated with the reduction of mTOR signaling and reduced protein synthesis [146]. Alterations in mTOR signaling observed in this study included a significant increase in S6 ribosomal protein phosphorylation in the aged heart, which was significantly attenuated by both CR and RP (Fig. S3). There was no significant change of 4EBP1 phosphorylation with aging, CR or RP (Fig S3).

The proteomics analysis of turnover rates found a wide distribution in protein half-lives (Figure 2-3A, Stab 1). The median half-lives of 823 proteins in the YCL heart were 9.1 days, similar to 8.8 days in the OCL heart. Short-term CR significantly increased proteome half-lives by approximately 30% (11.4 days), when compared with OCL ($p<0.001$). Short-term RP also significantly increased old heart proteome half-lives by 12% to a median of 9.8 days ($p=0.04$ compared to OCL),

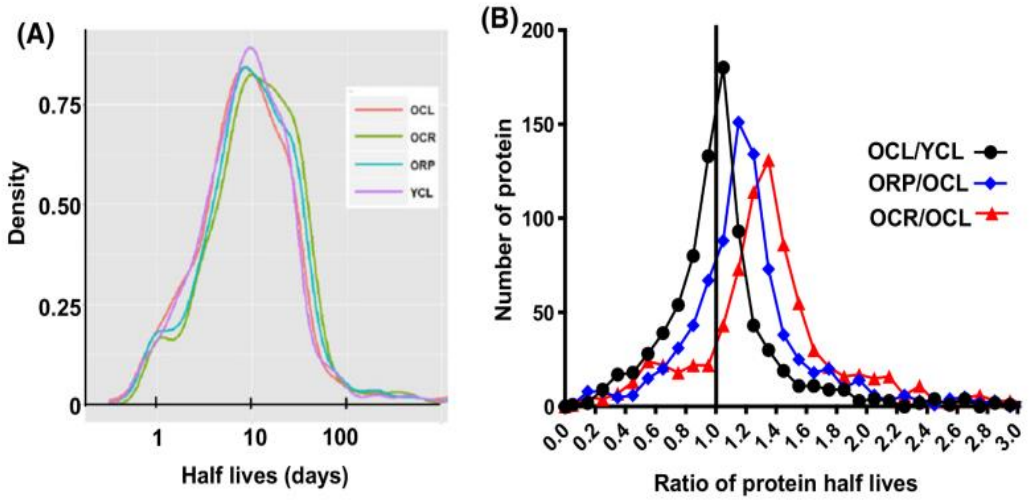

Figure 2-3 Global proteomic half-lives. (A) Histograms of half-lives (days). YCL versus OCL: n.s., OCL versus OCR $P < 0.001$; OCL versus ORP, $P = 0.038$; OCR versus OR, $P = 0.08$. (B) Histograms of half-life ratios for two-group comparisons. $P = 0.09$ for YCL/OCL >1, $P < 0.001$ for both OCR/OCL and ORP/OCL >1.

A more sensitive analysis of treatment differences is performed by comparing the ratio of half-lives of each individual protein in two treatment groups. The pairwise comparison in Figure 2-3B shows that the median half-lives of OCL are 10% longer than YCL ($p=0.09$). Both short-term CR and RP significantly increased the half-lives of old heart proteins: OCR are 45% longer than OCL and ORP are 27% longer than OCL (both $p<0.001$, Figure 2-3B).

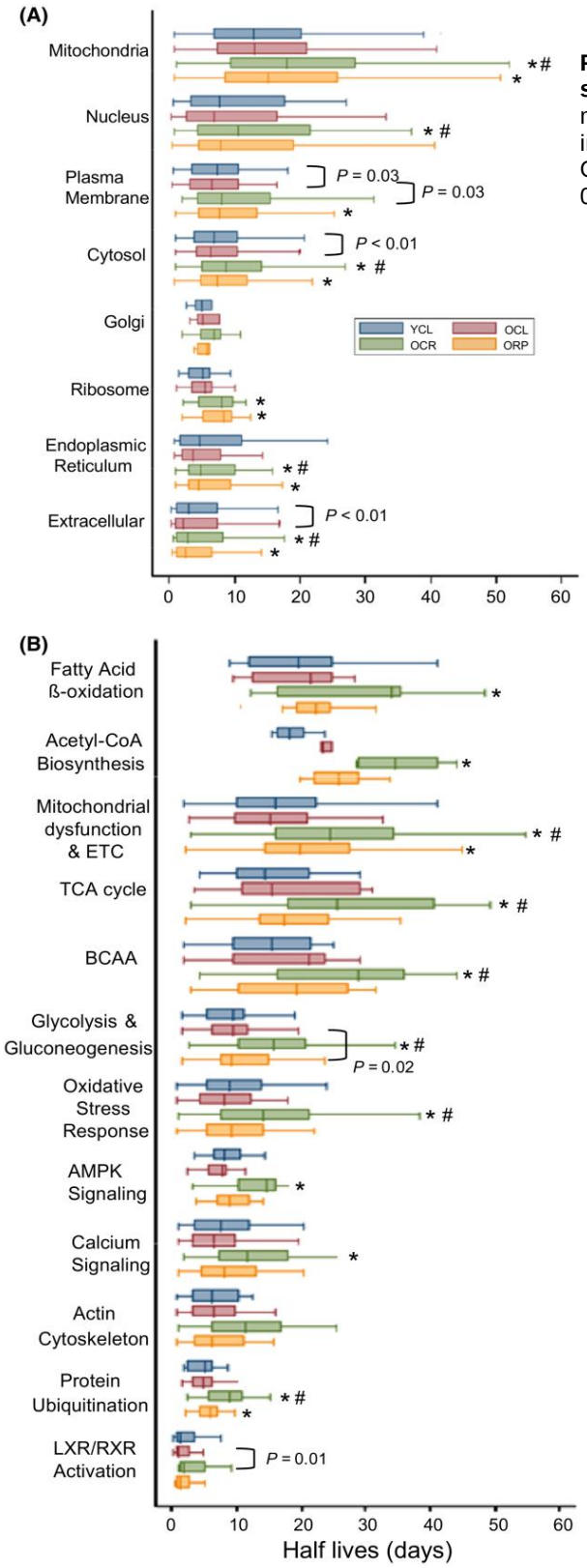

Figure 2-4 Protein half-lives (days) stratified by (A) cellular compartment, (B) most significant canonical pathways in ingenuity pathway analysis. *P < 0.01 for OCR versus OCL or ORP versus OCL, #P < 0.01 for OCR versus ORP.

To describe the variation of protein half-lives in different cellular compartments, we grouped the components proteins of 8 chief compartments. As shown in Figure 2-4A, extracellular proteins have the shortest half-lives in YCL, with the median of 3.4 days, and mitochondrial proteins have the longest half-lives, with the median of 13.2 days, with other compartments falling in between. The half-lives of plasma membrane and cytosolic proteins in OCL are ~8% and ~17% shorter, respectively, than those of YCL ($p=0.03$ and $p<0.01$, Figure 2-4A). CR significantly increased protein half-lives in old mice in all compartments except for Golgi; the magnitude of increase are: 42.8% for mitochondria, 38% for cytosol, 39.5%for extracellular, 46%for ER, 47.3% for ribosome, 74.8% for nucleus and 75.4% for plasma membrane ($p<0.01$ for all except for nucleus, $p=0.03$, Figure 2-4A). ORP mice had significantly increased protein half-lives in mitochondria (27.8%), plasma membrane (32.1%), cytosol (23.2%) and ribosome (54.0%) compartments ($p<0.01$ for all, Figure 2-4A).

2.3.4 **Pathway analysis of proteome dynamics and remodeling in aged heart and the effect of CR and rapamycin**

To identify protein pathways that are differentially regulated by CR and RP, we used Ingenuity pathway analysis [147]. A complete list of the significantly altered protein abundances with aging and their canonical pathways are given in Stab. 2 There were 589 proteins whose turnover was significantly changed in one or more group comparison ($q<0.05$). The 12 pathways that were most significantly altered in protein turnover are shown in Figure 2-4B. Proteins involved in signaling have the shortest half-lives, including proteins in LXR/RXR activation, protein ubiquitination, actin cytoskeleton, calcium and AMPK signaling as well as oxidative stress response pathways. Proteins involved in metabolism have longer half-lives, including those involved in glycolysis/gluconeogenesis, branched-chain amino acid (BCAA) degradation, TCA cycle, mitochondrial dysfunction and electron transport chain (ETC), acetyl CoA and fatty acid beta-oxidation. CR significantly increased the half-lives of proteins in all these IPA pathways by 48-94% ($p\leq0.01$ for all), except for actin cytoskeleton. Rapamycin in old mice significantly increased half-lives only for mitochondrial dysfunction (24.9%, $p<0.01$), glycolysis/gluconeogenesis (12.8%, $p=0.02$) and protein ubiquitin pathways (20.3%, $p<0.01$), each to a much lesser extent than the effect of CR.

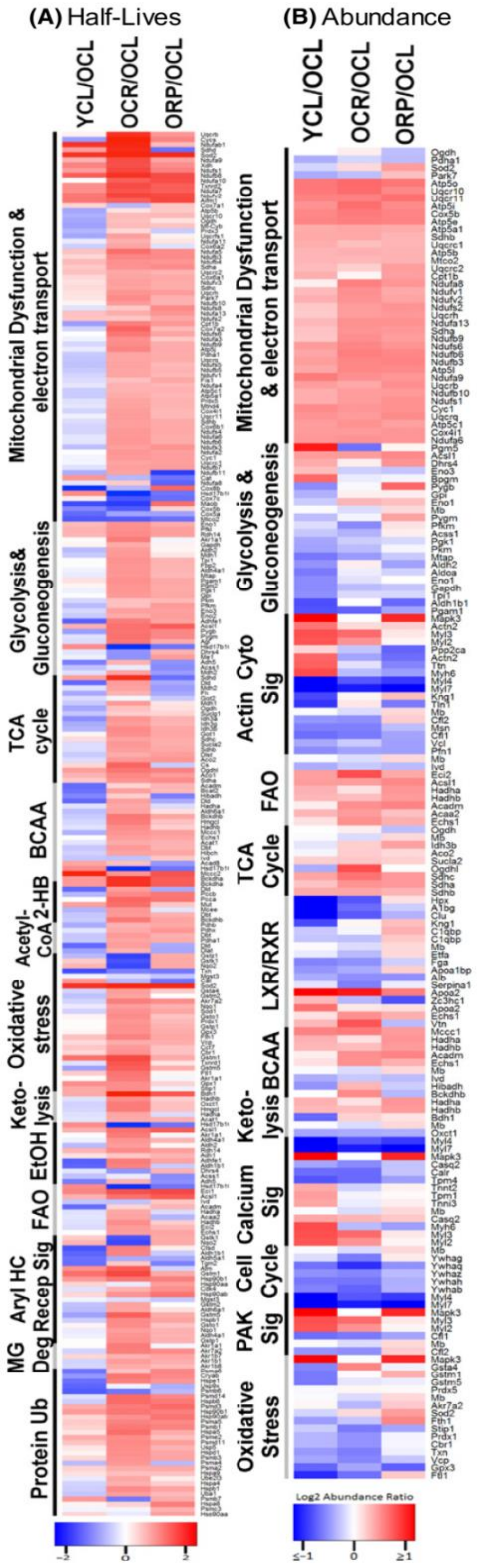

Figure 2-5 Heatmaps of (A) half-life differences, (B) abundance differences for YCL/OCL,OCR/OCL, and ORP/OCL comparisons, ordered by the rank of significance of differences in ingenuity pathway analysis. In part A, red indicates longer and blue indicates shorter half-lives. In part B, red indicates higher and blue indicates lower abundance. The component protein IDs are listed in Tables S4 for abundance difference and Table S5 for turnover differences.

FAO: fatty acid oxidation, BCAA: branched-chain amino acid metabolism; 2-HB: 2 oxobutanoate; MG:methylglyoxal; and Ub: Ubiquitination.

To examine and compare differences between groups for protein turnover (Stab 1) and protein abundance (Stab 3), we created heat map of proteins in IPA canonical pathways, ordered by the significance of the IPA pathway (Figure 2-5). Figure 2-5A displays the heat maps of the protein half-life ratios. Compared with OCL, YCL has shorter half-lives for 58% of proteins involved in mitochondrial dysfunction and ETC, and longer half-lives for the remainder. Consistent with Figure 2-3, short-term CR in old age hearts confers significantly longer half-lives, and this is true for the great majority of the proteins. Interestingly, the heat map shows that RP closely recapitulates CR in increasing mitochondrial dysfunction and ETC protein half-lives, despite its weaker effect than CR overall (Figure 2-3).

Figure 2-5B shows the heat map of protein abundance ratios between groups. There were 327 proteins whose abundance was significantly changed in one or more group comparison ($q<0.05$). Proteins involved in mitochondrial dysfunction and ETC are significantly more abundant in YCL as compared to OCL, indicating a significant decrease in these proteins with age; this difference is concordant for the great majority of proteins of mitochondrial dysfunction and ETC. CR and RP in old mice significantly reverse the aging difference, restoring protein abundances in this pathway to levels very comparable to YCL. The increased mitochondrial protein abundance by CR and RP was not associated with increased in mitochondrial copy number (Fig.S4A), mRNA levels of mitochondrial biogenesis regulator, PGC1α, or its downstream transcriptional factor, TFAM (Fig. S4B and C). Similar effects on proteome, though not as consistent across all proteins, were seen in proteins involved in fatty acid beta oxidation and TCA cycle pathways. Conversely, YCL has significantly lower abundance of the majority of proteins involved in glycolysis/gluconeogenesis, oxidative stress response and cell cycle than OCL. CR is effective in reducing abundance of most of these proteins in these three pathways in old mice towards the youthful levels, in contrast, RP had mixed effects within all but the cell cycle pathway, which was effectively restored to the young phenotype. The decrease in protein abundance in glycolysis together with the increased abundance in fatty acid oxidation by RP in old mice suggested that RP shifts substrate utilization in old heart from glucose to fatty acid, similar to previous observation from skeletal muscle cells [148].

To confirm this observation, we performed a targeted metabolic profiling of aged heart tissue in OCL and ORP mice. Figure 2-6A-B and Stab 6 show that when compared with OCL, ORP has significantly higher TCA cycle metabolites: α-ketoglutarate, fumarate, malate and citrate, with ratios of 1.32-1.41 ($p=0.001$ to 0.02); and higher succinate and oxaloacetate with borderline significance ($p=0.08$-0.09). For glycolytic intermediates, ORP has significantly lower glucose-6 phosphate (ratio: 0.45, $p=0.05$) and fructose-6 phosphate (ratio: 0.45, $p=0.05$), and non-significant decrease in the remaining glycolytic intermediates, when compared with OCL (Figure 2-6A-B, Stab 6).

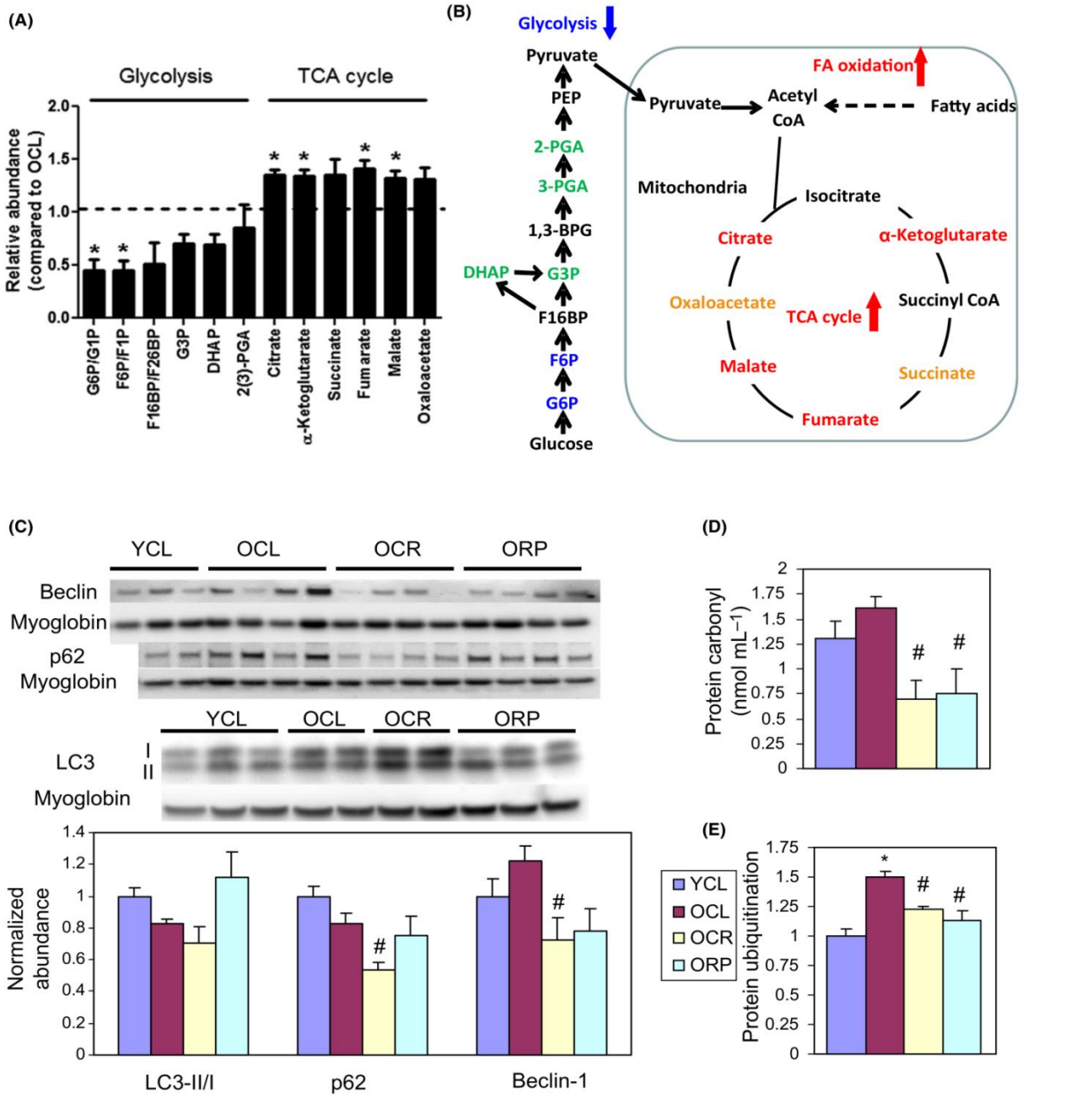

Figure 2-6 Metabolic profiling and biochemical assay. (A) Relative abundance of the substrates in the glycolytic pathway and TCA cycle in ORP compared to OCL by targeted metabolic profiling. When compared with OCL heart, ORP hearts have significantly lower glucose-6-phosphate and fructose-6-phosphate (both are glycolytic metabolites), and significantly higher a-ketoglutarate, fumarate, malate, and citrate (all are TCA cycle metabolites). *P < 0.05 compared with OCL. See Table S6 for numerical data. (B) A schematic diagram summarizing the changes in metabolism by rapamycin in old heart. (C) Western blots of autophagic markers show no significant change of LC3II/I, p62, or beclin-1 in cardiac aging. However, OCR has significantly lower p62 than that in OCL. #P < 0.05 compared with OCL. (D) Both CR and RP significantly reduce the age-dependent increase in protein carbonyls (nmol mL-1). #P < 0.05 compared with OCL. (E). Both CR and RP significantly reduce the age dependent increase in protein ubiquitination.*P < 0.05 compared with YCL and #P < 0.05 compared with OCL. n = 3–8. G6P: glucose 6-phosphate; G1P: glucose 1-phosphate; F6P: fructose 6-phosphate; F1P: fructose 1-phosphate; F16BP: fructose 1,6 bisphosphate; F26BP: fructose 2,6-biphosphate; G3P: glyceraldehyde 3-phosphate; DHAP:dihydroxyacetone phosphate; 2(3)-PGA: 2- or 3- phosphoglycerate; and PEP: phosphoenolpyruvate. Isomers of same molecular weight, that is, G6P versus G1P, F6P versus F1P, and F16BP versus F26BP,were not distinguishable by the LC-MS/MS-based metabolic profiling method.

2.3.5 **Alterations in protein autophagy, ubiquitination and damage by rapamycin and caloric restriction**

We observed no significant change in LC3 II/I, p62 and beclin-1, markers of autophagy, in cardiac aging (Figure 2-6C). However, OCR substantially reduced p62 ($p<0.05$). Consistent with our previous observation [73], there is an increase in oxidative damage in old hearts, as shown by a higher level of protein carbonylation. This increase is significantly reversed by CR and RP (Figure 2-6D). The ubiquitin-proteosomal pathway is one of the major mechanisms for degradation of damaged proteins. Figure 2-6E shows that protein ubiquitination significantly increased in OCL hearts, and this was significantly reversed by CR and RP. The reduction of protein damage and ubiquitination is consistent with the slower rate of protein turnover seen in CR and RP treated old hearts.

2.4 DISCUSSION

This study demonstrates that short-term, 10 week treatment with CR or RP, initiated at old age, reverses many of the pre-existing functional deficits of cardiac aging, rather than just slowing down the aging process. This rejuvenation of the heart includes reversal of age-dependent cardiac hypertrophy, diastolic dysfunction and impairment of myocardial performance (Figure 2-2). In parallel with the effect on cardiac physiology, short-term RP closely recapitulate CR to restore key components of the mitochondrial proteome to youthful levels, including those involved in mitochondrial function and electron transport chains, fatty acid oxidation and TCA cycles (Figure 2-5A, Stab 3). In some other pathways, such as glycolysis/gluconeogenesis, oxidative stress response and cell cycle, CR was effective in reducing abundance of most of these proteins in old mice towards the youthful levels, in contrast, RP had mixed effects and reversed to a smaller extent.

This study is also the first to elucidate the global dynamics of the aging cardiac proteome, calculating the turnover rate of 823 proteins (containing at least one leucine) in a single experiment (Figure 2-3, 4, 5B, Stab 1). It was done by analyzing LC-MS data with the Topograph software program. Topograph deconvolutes the isotopologue distributions to determine the amount of heavy label in the amino acid precursor pool (Figure S2 and S5, and from this correctly calculates the percentage of peptides that are newly synthesized (18). This novel method of turnover analysis does, however, have several limitations. First, it requires feeding mice with a synthetic diet, not regular mouse chow. Second, the analysis of the protein turnover is limited to proteins containing at least one leucine. Some important proteins without leucine, such as collagen (which increased in age-dependent cardiac fibrosis) were therefore not included in the turnover analysis (these were, however, included in the abundance analysis). Third, the errors in half-life measurement of proteins with very short (less than 3 days) or very long (greater than 50 days) half-lives are higher using our current labeling protocol (Figure S6).

The proteome in the aged heart is notable for the significant decline in proteins involved in mitochondrial function, ETC and fatty acid metabolism. Conversely, aged hearts have significantly increased protein abundance in glycolysis/gluconeogenesis, acute phase response and LXR/RXR and other signaling

pathways. This remodeling is similar to our previous observations in pressure-overload induced heart failure, including the decline in proteins in mitochondrial function, ETC, and fatty acid oxidation, as well as an increase in proteins of glycolysis/gluconeogenesis pathways [75]. This switch in preferential substrate utilization from more efficient fatty acid oxidation in the mitochondrial-rich normal heart to less efficient glycolysis/glucose oxidation in failing hearts has been extensively described in human and animal models of heart failure [149]. Although aged hearts do not demonstrate the full-blown phenotypes of end-stage heart failure, the concomitant changes in both functional performance (Figure 2-2) and metabolic proteomes (Figure 2-5B) are obvious. The age-related decline in proteins in mitochondrial function, ETC and fatty acid metabolism is reversed by 10 week CR or RP treatment. As the increased mitochondrial protein abundance following CR and RP occurred without increasing mitochondrial biogenesis and mtDNA copy number, this suggests that the proteomic remodeling may be due to increased abundance of these mitochondrial proteins that resulted from better preserved protein quality and slower turnover. These findings emphasize the crucial roles of mitochondria in aging and are consistent with previous studies showing that preservation of mitochondria by overexpression of catalase targeted to mitochondria [73] or by inhibition of insulin signaling [53,150] attenuates age-dependent cardiomyopathy [151].

RP has been shown to reduce glycolysis and facilitate a switch in fat metabolism by increasing fatty acid oxidation in skeletal muscle [148]. By using a targeted metabolomics approach, we confirm that RP significantly reduces glycolytic metabolites and significantly increases TCA cycle metabolites (Figure 2-6A-B and Stab 6) in old mouse hearts. The increased TCA cycle metabolites despite the lower glycolytic intermediates suggests increased proportion of TCA cycle substrate are coming from fatty acid oxidation. The concerted effect of RP on these metabolic pathways are consistent with the changes in protein levels: increase in proteins involved in TCA cycle and fatty acid oxidation and decrease in proteins involved in glycolysis (Figure 2-5B). In contrast to this beneficial effect, RP treatment has been reported to induce detrimental metabolic phenotypes, including insulin resistance, hyperlipidemia and glucose intolerance, all of which are associated with shortened lifespan. Some of these effects may be due to inhibition of mTORC2 [152]. This RP paradox may be reconciled, at least in part, by the differential effects of acute vs short-term RP treatment; as recently reported, 2 or 6 weeks of RP result in detrimental metabolic

alterations, while 20 week RP treatment conferred beneficial metabolic profiles, including improved insulin sensitivity and increased oxygen consumption [153]. The current study using a 10-week protocol of CR or RP is consistent with these 20-week short-term effects, as it ameliorated the age-dependent decline in metabolic proteins and reversed the adverse metabolic remodeling in the aged heart. The involvement of mTOCR2 in these metabolic changes will require further investigation.

Two recent studies have reported contradictory results of RP on the aging mouse heart. Neff et al reported that chronic RP treatment for 1 year initiated at late life (20-22 months) reduced aging heart's increased dimensional measures, but did not show any effect on systolic function, mean flow velocity or pressure gradient across aortic and pulmonic valves in male mice [154]. Flynn et al reported that short-term RP treatment for 12 weeks initiated at late life (24 months) attenuates age-related cardiac hypertrophy and marginally improves systolic function in female mice, with a reduction in age-related inflammation [155]. The discrepancy observed in these studies could be explained by both difference in duration of treatment and gender differences. It is notable that neither of these studies have reported the effect of RP on diastolic dysfunction, which is one of the most prominent findings in aged hearts of mice and humans [73,156]. In this study, CR and RP improve diastolic function in old mice; this reversal of diastolic dysfunction is potentially related to better preserved mitochondria [73]. It is well known that diastolic heart failure (heart failure with preserved ejection fraction) is the predominant type in elderly human patients without structural or coronary heart disease and there is no effective treatment to date. Hence, our observation that short-term CR or RP ameliorates age-dependent diastolic dysfunction is clinically relevant and supports the potential of therapeutics development for the treatment of age-associated diastolic heart failure.

Our study further shows that both CR and RP decreased protein oxidative damage in the aged heart (Figure 2-6D). This is consistent with the observed decrease in protein ubiquitination (Figure 2-6E), the rate-limiting step for the proteosomal degradation of oxidized proteins [157]. Also consistent with this, CR and RP decreased the proteomics turnover rate globally (extended half-lives), and this is especially true for mitochondrial proteins. Whether CR increases or decreases proteomics turnover has previously been

a topic of debate, and the effect of RP on protein turnover has not been well established. CR and RP induce autophagy, which would suggest increased protein turnover. However, Miller and colleagues recently reported that CR and RP do not alter overall protein synthesis in heart [158,159]. Price et al, on the other hand, showed that CR reduces protein turnover of 80% of proteins in liver [160]. Our study showed that CR greatly reduced protein turnover in the heart, which is consistent with the study in liver [160]. We showed that RP also reduced turnover in the heart. The absence of CR or RP effect on protein synthesis rate in the studies by Miller and colleagues is likely due to the limitation of the method of "bulk measurement". Bulk analysis of overall protein labeling level is skewed by the synthesis rate of a few highly abundant structural proteins, whereas in our study and the study by Price et al, measurements of average protein turnover changes in large numbers of individual proteins are not weighted toward the most abundant structural proteins.

Both CR and RP have been shown to induce autophagy [146], which is consistent with our unpublished observation that RP for 1-2 weeks induced autophagy (data not shown). Interestingly, the current study demonstrates that at the end of the 10 week CR or RP treatment does not increase the levels of autophagic markers, LC3-II/I and beclin-1 (Figure 2-6C). The absence of persistent induction of autophagy by CR or RP after 10-weeks undoubtedly relates to the temporal response of protein homeostasis. Upregulation of autophagy is generally observed acutely and allows damaged or aggregated proteins to be recycled, reaching a new equilibrium with proteins of better quality by 10 weeks. Likewise, a recent study shows that constitutive activation of TORC1 decreased translational fidelity and increased amino acid misincorporation errors and that RP reversed these effects as it slowed the rate of ribosomal elongation in mouse embryonic fibroblasts [161]. A further mechanism of preservation of protein quality by CR depends of mitochondrial SIRT3-mediated antioxidant effects, as reported by Someya et al using mouse model of age-dependent sensorineural hearing loss. In response to CR, SIRT3 directly deacetylates and activates mitochondrial isocitrate dehydrogenase 2, leading to increased NADPH levels and an increased ratio of reduced-to-oxidized glutathione in mitochondria, thereby enhancing the mitochondrial glutathione antioxidant defense system [162]. Hence, 10 week CR or RP result in improved protein quality and decreased protein damage, with resulting longer protein half-lives and

reduced protein degradation. Indeed, CR substantially reduced p62 in OCR hearts, while the RP effect is modest. p62 has been shown to recognize ubiquitinated protein aggregates and target them to the autophagosome or proteasome for degradation [163,164]. The reduced protein damage in OCR may explain the reduced p62 levels without increased autophagy. These changes make sense in the context of reduced nutrients or nutrient sensing where the organism needs to cope with decreased amino acid substrate and energy availability.

It is noteworthy that the increased protein ubiquitination and trend towards increased carbonylation of proteins in untreated old hearts (Figure 2-6D, E) is not accompanied by increased protein turnover (shorter half–lives) in old hearts (in fact, it trends towards slower turnover, consistent with a prior report (Niedermuller, et al., 1986). This indicates that proteostasis is impaired in old hearts, a result that is consistent with previous reports in other tissues and organisms (reviewed in (Taylor, 2011 #583)).

The translational repressor 4E-BP, a downstream target of mTOR, has been shown to mediate the lifespan extension effect of dietary restriction in Drosophila by enhancement of mitochondrial activity [143]. Using translational state array analysis, Zid et al. further demonstrated a preferential translation of mitochondrial genes after CR and proposed that this was related to shorter and less complex 5'UTRs. In contrast, a recent study applying transcriptome-scale ribosome profiling demonstrate that mTOR inhibition by Torin 1 in MEFs globally suppressed mRNA translation with no preferential regulation of mRNA with complex 5'UTRs [165]. Our measurement of protein synthesis does not find any evidence of a preferential change in the dynamics of mitochondrial proteins in aged hearts after 10 weeks of CR or RP (Figure 2-5B); however, because the relative abundance of mitochondrial proteins is elevated at 10 weeks (Figure 2-5A), we cannot rule out the possibility of preferential synthesis at earlier times after CR or RP treatment.

In summary, treatment with either CR or RP for 10-weeks in old mice effectively reverse the pre-existing cardiac hypertrophy and diastolic dysfunction, attenuate age-dependent protein oxidative damage and ubiquitination, significantly decrease protein turnover rate, and ameliorate proteome remodeling in aging hearts.

2.5 MATERIALS AND METHODS

Supporting information and supplementary data can be accessed online: http://onlinelibrary.wiley.com/doi/10.1111/acel.12203/suppinfo.

2.5.1 Experimental diet, isotope labeling and echocardiography

Forty five C57BL/6 female mice (25 month-old) from the National Institute of Aging (Charles River) were handled according to the guidelines of the Institutional Animal Care Committee of the University of Washington. This single gender was used in order to eliminate gender differences in response, and because the National Institute of Aging Interventions Testing Program previously demonstrated a larger life-span extension by rapamycin in females (10). One week after arrival, mice were started on a synthetic diet (Harlan Teklad diet #TD.99366), nutritionally similar to the NIH-31 standard for rodents. Three weeks later, at 26 months of age, the mice were individually housed and randomly assigned to three diet regimens for 10 weeks (Figure 3-1): 1) *ad libitum* synthetic diet (CL, control group), 2) caloric restricted synthetic diet (CR), 3) *ad libitum* synthetic diet added with microencapsulated rapamycin (2.24mg / kg / day, purchased from the University of Texas Health Science Center, San Antonio). CR mice received a diet that was 10% less than CL in week 1, 25% less in week 2, and 40% less from week 3-10. Young mice at 4 months of age received the same *ad libitum* synthetic diet as young control (YCL). After 10 weeks treatment groups were maintained but all mice were switched to leucine-deficient synthetic diet (TD.09846, Harlan Teklad, Madison, WI) supplemented with 11.1 g/kg of [5,5,5 - $^{2}H_{3}$] - L - leucine (Cambridge Isotope Laboratory, MA), the same leucine content as diet # TD. 10943. Although we measured newly synthesized proteins by heavy label incorporation, as old mouse body weights were not significantly changed during the last 7 weeks of the experiment and young weights changed only 1% per week (Fig. S1), we believe that protein synthesis and degradation are essentially in equilibrium at this time. In addition, the abundance of all peptides identified remain unchanged over the labeling period (Fig. S7, regression slopes centered over zero), indicating that proteins were at steady-state at the time of labeling.

Echocardiography was performed at baseline and at the end of experiments (10 weeks) under 0.5% isoflurane, as described, using a Siemens Acuson CV-70 equipped with a 13MHz probe(9).

2.5.2 **Western blots and protein carbonyl assay**

Antibodies used for the Western blots were Beclin-1, LC3 (both from Novus Biologicals), p62, phospho-4EBP1, 4EBP1, phospho-EEF2, phospho-S6, S6 and ubiquitin (all from Cell Signaling). Cardiac tissue protein carbonyl was measured using OxiSelect protein carbonyl ELISA kit (Cell Biolabs, San Diego, CA).

2.5.3 **Sample Preparation and Analysis by Mass Spectrometry**

Three to four mice of each experimental group were euthanized by cervical dislocation at each of the four time points shown in Figure 3-1. The heart was removed immediately, then ventricular tissues were homogenized in cold buffer, processed and trypsin-digested, and loaded to LC-MS/MS, using a Waters nanoAcquity LC system and a Thermo Scientific LTQ-FT Ultra.

2.5.4 **Topograph analysis of peptides turnover and relative abundance**

The Topograph software program was developed for the deconvolution and measurement of peptide isotopologue abundances from LC-MS chromatograms, and the calculation of peptide turnover rates, as previously described [88] (http://proteome.gs.washington.edu/software/topograph/). After the % newly synthesized peptide was calculated, for each of the multiple peptides that uniquely mapped to one protein (mean 50.1, median 21.5) these values were plotted for each sample at each time point to generate an exponential curve following a first order kinetics (Fig. S3B). Using a logarithmic transformation the first order protein turnover rate (slope) is determined by linear regression. For detail see the statistical method below, the supplementary methods and [88].

For comparison of relative abundance between two experimental groups, we applied Topograph chromatogram alignment to correct chromatographic drift that may occur during the LC-MS/MS and allowing comparisons of low abundance analytes that may be detected in only one but not the other samples. A LOESS regression was used to find the best fit line through the data points (Fig. S8). For peptides that were identified in one sample, the regression of the identified peptide's MS/MS scan number

is used to estimate a window for the same peptide in the other samples and a matching chromatographic peak was identified within that time range.

2.5.5 **Metabolic profiling of cardiac tissue extract**

Pulverized cardiac tissues were resuspended in 80:20 methanol: water and soluble extracts were collected and dried by speed vac. Extracts were reconstituted in 5 mM ammonium acetate in 95% water/5% acetonitrile + 0.5% acetic acid and filtered prior to LC-MS analysis. The filtered samples were injected to the LC system, which was composed of two Agilent 1260 binary pumps, an Agilent 1260 auto-sampler and an Agilent 1290 column compartment containing a column-switching valve (Agilent Technologies, Santa Clara, CA). The chromatography was performed using Solvents A (5 mM ammonium acetate in water + 0.5% acetic acid + 0.5% acetonitrile) and B (acetonitrile + 0.5% acetic acid + 0.5% water), with 5% B for 2 min, 5% B to 80% B in 3 min, 80% B for 3 min, 80% B to 5% B in 3 min, and 5% B for 7 min.

After the chromatographic separation, MS ionization and data acquisition was performed using AB Sciex QTrap 5500 mass spectrometer (AB Sciex, Toronto, ON, Canada) equipped with electrospray ionization (ESI) source. Multiple-reaction-monitoring (MRM) mode was used for targeted data acquisition. The extracted MRM peaks were integrated using MultiQuant 2.1 software (AB Sciex, Toronto, ON, Canada).

2.5.6 **Statistical analysis**

Statistical analyses were performed using either Stata IC10, R or Bioconductor. Analyses used only peptides that mapped to a single protein. For the cases where a protein consisted of more than one peptide, statistical models were modified to appropriately account for the multiple peptides by using a blocking factor. For each protein we applied a non-linear regression fits of first order exponential curves to the % newly synthesized protein using: $y = 100 + \beta 1^{e\alpha t}$. To determine whether the slopes α were statistically significantly different between experimental group, we used ANCOVA. Half-lives were calculated according to first order kinetics: $t1/2 = \ln^{166}/$ slope. The equality of distribution of protein half-lives between two groups (Figure 3-3A) were compared by a Kolmogorov-Smirnov test. The equality of distribution of protein half-life ratios (Figure 3-3B) were examined using a test of proportions.

For proteomics relative abundance data, statistically significant changes of proteins between experimental groups were determined using a linear model of peptide abundance to calculate fold changes of proteins between experimental groups in the same manner as a two-sample t-test using the R/Bioconductor software. The linear model gave p-values that were adjusted for multiplicity with the Bioconductor package q-value, which allows for selecting statistically significant genes while controlling the estimated false discovery rate.

The networks and canonical pathways were generated with Ingenuity Pathway Analysis (IPA, Ingenuity Systems, www.ingenuity.com). A $q<0.05$ was set to identify molecules whose expression was significantly differentially regulated. Canonical pathway analysis identified the pathways from the IPA library of canonical pathways that were significant to the data set. The significance of the association between the data set and the canonical pathway was derived by taking a ratio of the number of molecules from the data set that map to the pathway divided by the total number of molecules present in the canonical pathway. The Fisher's exact test was used to calculate a p-value reflecting the probability that the association between the mapped proteins in the dataset and the canonical pathway is explained by chance alone.

SUBACUTE CALORIE RESTRICTION AND RAPAMYCIN DISCORDANTLY ALTER MOUSE LIVER PROTEOME HOMEOSTASIS AND REVERSE AGING EFFECTS

3.1 SUMMARY

Calorie restriction (CR) and rapamycin (RP) extend lifespan and improve health across model organisms. Both treatments inhibit mammalian target of rapamycin (mTOR) signaling, a conserved longevity pathway and a key regulator of protein homeostasis, yet their effects on proteome homeostasis are relatively unknown. To comprehensively study the effects of aging, CR and RP on protein homeostasis, we performed the first simultaneous measurement of mRNA translation, protein turnover and abundance in livers of young (3 month) and old (25 month) mice subjected to 10 week RP or 40% CR. Protein abundance and turnover were measured *in vivo* using $^{2}H_{3}$-leucine heavy isotope labeling followed by LC-MS/MS, and translation was assessed by polysome profiling. We observed 35-60% increased protein half-lives after CR and 15% increased half-lives after RP compared to age-matched controls. Surprisingly, the effects of RP and CR on protein turnover and abundance differed greatly between canonical pathways, with opposite effects in mitochondrial [167] dysfunction and eIF2 signaling pathways. CR most closely recapitulated the young phenotype in the top pathways. Polysome profiles indicated that CR reduced polysome loading while RP increased polysome loading in young and old mice, suggesting distinct mechanisms of reduced protein synthesis. CR and RP both attenuated protein oxidative damage. Our findings collectively suggest that CR and RP extend lifespan in part through the reduction of protein synthetic burden and damage and a concomitant increase in protein quality. However, these results challenge the notion that RP is a faithful CR mimetic and highlight mechanistic differences between the two interventions.

3.2 INTRODUCTION

Protein homeostasis is the equilibrium between protein synthesis, maintenance, and degradation. The dysregulation of this dynamic process has been implicated in aging and age-related diseases [168]. Converging evidence indicates that aging is accompanied by an increase in damaged proteins [169] caused by misfolding, translation errors, and post-translational modifications such as oxidation, as well as a decline in damage clearance pathways such as autophagy and proteasomal degradation [170].

Calorie restriction (CR) is the best characterized and most effective intervention known to extend lifespan across a spectrum of species [21], with up to 40% extension in mice [171] . In addition to increasing longevity, CR is capable of decreasing morbidity by retarding the occurrence of many chronic diseases such as cancer and diabetes [48]. The mammalian target of rapamycin (mTOR) pathway is widely regarded to be a central modulator of nutrient sensing and growth, which is known to adjust metabolism, increase autophagy, and reduce protein synthesis during CR [26]. In 2009, Harrison et al. reported increased longevity in mice fed with rapamycin (RP), a macrolide antibiotic that inhibits the mTOR kinase [25,172]. While the magnitude of longevity extension by RP at doses tested so far is only ~8-17%, considerably less than that of CR, RP has also been reported to improve functional ("healthspan") characteristics of aging mice [138,173] . While mTOR inhibition is a central theme in the research of CR and RP, decreased protein synthesis and increased autophagy are together not a sustainable cellular state, suggesting that cells may assume a new state of homeostatic balance over the course of treatment, and this is in need of further study.

In this report we examine protein turnover, abundance, and synthesis changes following sub-acute (10 week) CR and RP in young and old mice. Protein turnover was measured *in vivo* using LC MS/MS and calculated using Topograph, software that deconvolutes isotopologue distributions and calculates amino acid precursor pool enrichment levels; this permits the accurate determination of the proportion of newly synthesized protein [88]. To further investigate mRNA translation we examined ribosome loading by polysome profiling. These methods revealed the effects of the two treatments on liver protein dynamics and proteome remodeling.

3.3 RESULTS*

3.3.1 Liver total and mitochondrial proteome dynamics with aging and short-term CR and RP

To investigate the effects of CR and RP on hepatic protein turnover rates *in vivo*, we performed stable-isotope metabolic labeling in mice with a synthetic diet containing $^{3}H_{2}$-leucine (Figure 3-1A). CR was a 40% reduction in total calories introduced over 3 weeks and RP was delivered using the dose (14 ppm) and formulation previously shown to extend mouse lifespan [25] and healthspan [138]. Both CR and RP are known to inhibit mTORC1 [26], which is suspected to mediate much of their longevity and health span benefits. Immunoblotting showed that CR and RP both substantially decreased S6 ribosomal protein phosphorylation in both young and old livers (Fig. S1A, C), but only RP significantly increased eEF2 phosphorylation (Figure 3-4C, D) and only young RP showed a significant reduction in phosphorylation of 4ebp1 (Fig. S1B). The absence of a chronic effect of RP on 4ebp1 phosphorylation has been previously reported [174].

* Supporting information such as supplementary figures, tables, datasets, and methods can be found online: http://blogs.uw.edu/nbasisty/home/136-2/

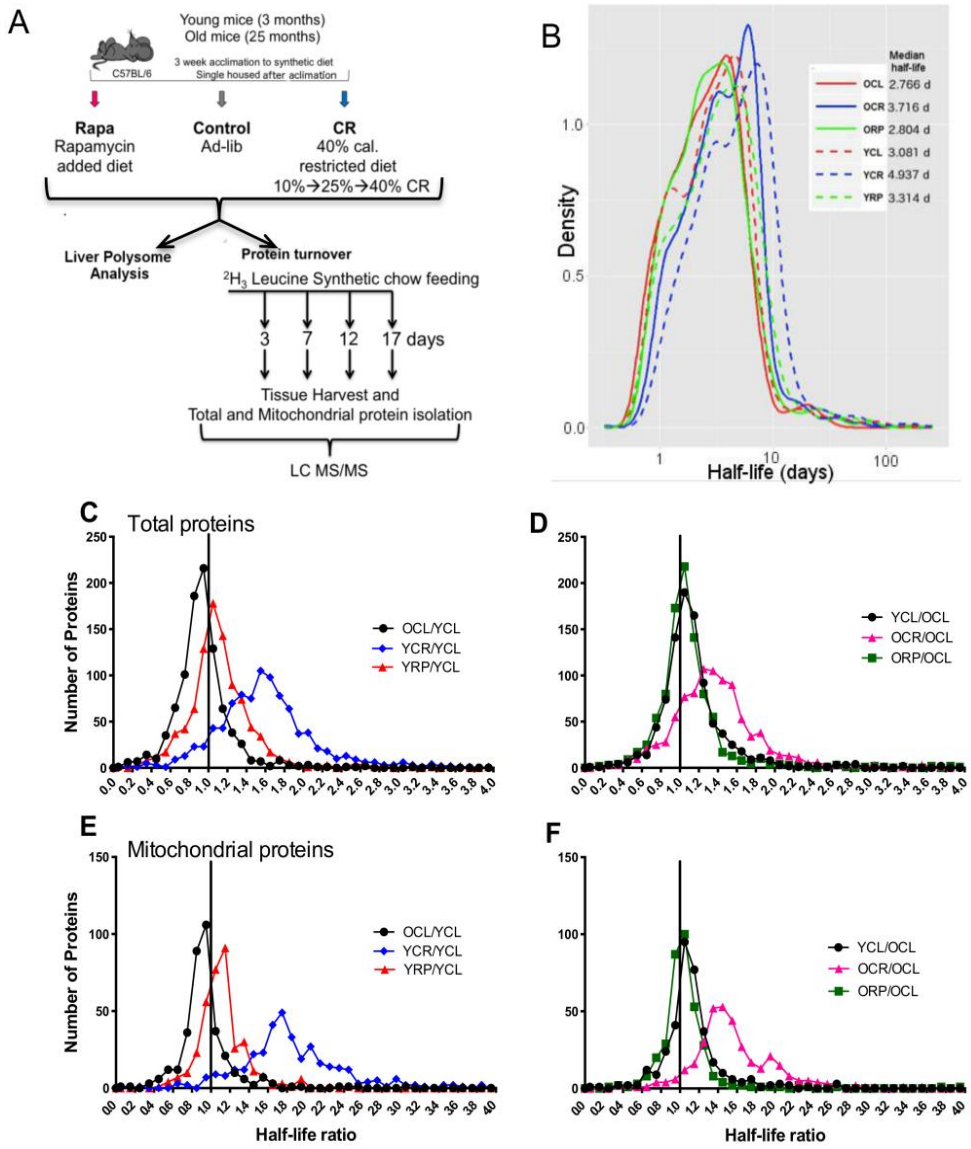

Figure 3-1 Subacute treatment of CR and RP prolong liver protein half-lives. (A) Summary of experimental design showing young (3 months at the start of treatment) and old (25 mo at the start of treatment) C57BL/6 female mice started on an ad libitum, encapsulated RP (14 ppm)-containing or CR (40% restricted) diet for 10 weeks. Livers were harvested and frozen for polysome analyses from five mice per cohort at the conclusion of 10 weeks, and the rest were switched to the same diets except that leucine was replaced with3H2–leucine. Mice were euthanized 3, 7, 12, and 17 days post-3H2–leucine diet feeding. Liver tissue was harvested and LC-MS/MS performed on tryptic peptides of total and mt proteins. Topograph software enabled the calculation of protein half-lives. (B) Protein half-life density plot illustrates the distribution of half-lives of young (dashed) and old 1 control (CL), calorie restricted (CR), and rapamycin (RP) cohorts. Median half-life in days is indicated on the right of the legend. Protein half-life ratio histograms for two group comparisons: (C,D) total protein half-lives as ratio to those same proteins in YCL (C) or OCL (D). (E,F) Mt protein half-lives as a ratio to YCL (E) and OCL (F). All comparison mean ratios were significantly different from 1.0 with a $P < 0.01$ by z-test for proportions. OCL/YCL < 1.0, $P < 0.001$, and all others > 1.0 $P < 0.01$.

Tissues harvested over time were analyzed by shotgun nLC/MS-MS followed by protein turnover and abundance measurements using the software Topograph [88]. We identified an average of 3,110 peptides per sample in total lysates that mapped uniquely to one of 950 proteins and an average of 4,001 peptides in purified mt fractions that uniquely mapped to 750 proteins. At each of 4 time points following the switch to heavy labeled diet the percent newly synthesized protein was determined. The rate of synthesis followed first order kinetics (Fig. S2A) and the turnover rate constant was calculated [88]. Old mouse weights were essentially constant during the time period of heavy labeling and young mouse weights varied by less than 1% per week (Fig. S3), suggesting a condition of steady-state where protein synthesis and degradation rates would be approximately equal. Furthermore, the abundance of all peptides identified did not change significantly over the labeling period (Fig. S4, regression slopes centered over zero), also confirming that proteins were at steady state. We therefore refer to the half-time of appearance of newly synthesized protein as the protein half-life (HL).

Protein HLs were seen to have a broad distribution, ranging over at least two $\log_{10}$ orders of magnitude, as shown in Figure 3-1B. While differences between groups are evident in these histograms, a more sensitive analysis is to compare HLs of the same protein in two groups (pairwise analysis of HL ratios, Figure 3-1C-F). Total proteome median HLs decreased from 3.1 (YCL) to 2.8 (OCL) days and the mean ratio of OCL/YCL is significantly less than 1.0 by approximately 20% ($p<0.0001$, Figure 3-1C), suggesting a small overall increase in hepatic protein turnover rates with age. CR induced an increase in both total and mt fraction protein HLs in both young (Figure 3-1C, E) and old (Figure 3-1D, F) livers. CR significantly increased young total proteome HLs by ~60% (to median of 4.9 days, $p < 0.0001$, Figure 3-1B, C) and old HLs by ~44% (to 3.7 days, $p < 0.0001$, Figure 3-1B, D) compared to their respective controls. Rapamycin treatment increased total proteome HLs modestly but significantly by 15% for young mice (to 3.3 days, $p < 0.0001$, Figure 3-1B, C) and 15% for old mice (2.8 days, $p < 0.0001$, Figure 3-1B, D).

HLs of mt proteins from purified mitochondria behaved similarly to total proteins, with median HLs decreasing significantly with age, from median 3.5 (YCL) to 3.3 (OCL) days ($p < 0.0001$, Figure 3-1 E). For proteins in common between total and mt extracts, the protein turnover rates were in high agreement

(Fig. S5, Spearman's $\rho > 0.65$ with $p<0.001$ for all slope comparisons), demonstrating the high reproducibility of the turnover rate measurements. Mt protein turnover was altered to a greater extent with CR than was that of total proteins, increasing HLs by ~85% to 6.4 days ($p < 0.0001$, Fig. 1E) in YCR and by 59% to 5.0 days in OCR ($p < 0.0001$, Figure 3-1F). RP increased young mt protein HLs by 12% (3.9 days, $p < 0.0026$) and old HLs by 7% (3.4 days, $p < 0.0001$, Figure 3-E, F). These changes indicate that the CR effect on protein HLs is considerably larger than that of RP at the 14 ppm dose and that the mt proteins have preferentially slower synthesis (longer HLs) after CR.

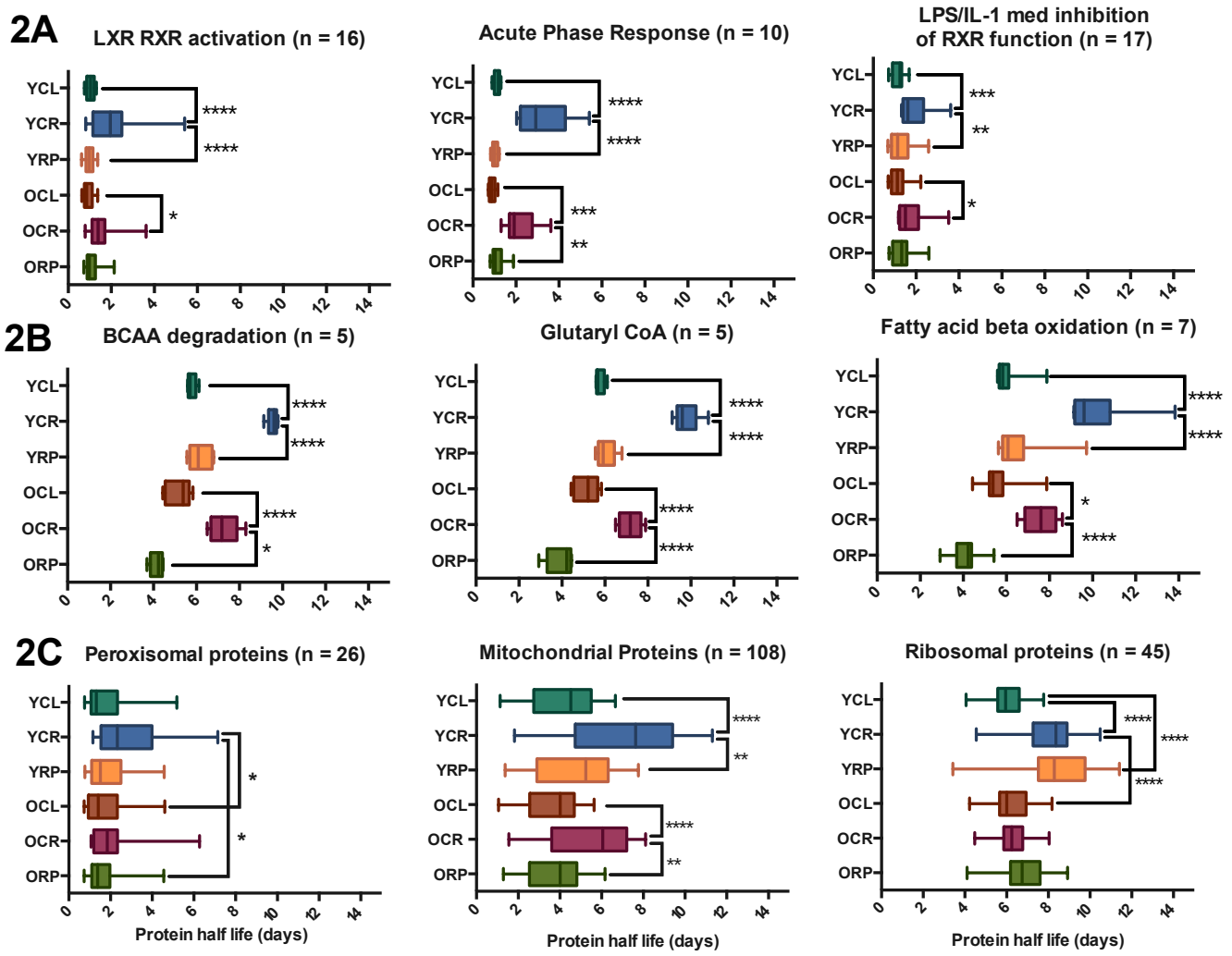

Figure 3-2 Box plots of liver protein half-lives of CR and RP by pathway and location. (A) Three representative IPA canonical pathways that are among the top fastest turning over (shortest half-lives). Boxes represent the inter-quartile range for protein HLs and whiskers extend from 5 to 95% of the data. (B) Three representative canonical pathways with the longest living proteins. Most pathways were metabolic indicating less turnover and higher stability of the metabolic proteins. BCAA, Branched-chain amino acid degradation. Old CR extended median HLs of all shortest and longest living pathways except the eIF2 signaling pathway that contains a majority of ribosomal proteins (ribosomal protein HLs shown in panel 2C). (C) Protein HLs by cellular compartment. Peroxisomal proteins were shortest lived while ribosomal proteins were longest lived. Statistical significance tested with one-way ANOVA, * p< 0.01, ** p<0.001. Detailed numerical detail and HLs for these pathways is in Table S1.

3.3.2 **Shortest and longest lived proteins, canonical pathways and subcellular locations**

The top 20% of shortest and longest-living proteins in the YCL cohort were analyzed for enrichment of canonical pathways, as defined by Ingenuity Pathway Analysis (IPA, Tables S1A and S1B). The shortest-lived protein pathways (Table S1A) had mean HLs of 0.894 to 1.524 days in YCL livers and were predominantly signaling pathways, including LXR/RXR activation, Acute Phase Response Signaling, and LPS/IL-1 mediated inhibition of RXR function; these three examples are illustrated in Figure 3-2A. CR extended the mean half-life of a majority of the short-lived protein pathways significantly (Table S1A). Even though YRP increased the mean half-life of most pathways, none of these changes was statistically significant (Table S1A, Figure 3-2A).

The protein pathways with the longest HLs are shown in Table S1B, ordered based on the YCL average half-life, which ranged from 5.55 to 11.89 days. The longest-lived proteins belonged to amino acid metabolism, intermediary metabolism, and energy (ketolysis, acetyl-CoA biosynthesis, fatty acid beta-oxidation) pathways. Pathways of these three categories are shown in Figure 3-2B. The average half-life of a majority of these pathways was significantly extended by CR in old mice ($p < 0.05$, Table S1B).

We also compared protein HLs in several cellular compartments as shown in Table S1C and Figure 3-2C. Of these, peroxisomal proteins had the shortest HLs (ranging from 1.8 to 3 days) and ribosomal proteins had the longest HLs (ranging from 6 to 8.4 days) that were extended by ~40% in young RP treated mice ($p < 0.0001$). RP did not have nearly as large nor as significant an effect on ribosomal protein half -lives in old mice (Figure 3-2C). Mt proteins were the second longest-lived category after ribosomal proteins and the only cellular compartment to have a significant increase in HLs with CR in both young and old groups (Table S1C, and Figure 3-2C).

3.3.3 **Pathway analysis of significant changes in hepatic proteome turnover**

In order to identify the pathways differentially affected by CR and RP, we categorized proteins whose half-lives were significantly altered ($q < 0.05$) by age or one or more intervention and assigned those to

canonical pathways using IPA. The top pathways most significantly altered by the treatments are shown in a heatmap (Figure 3-3A).

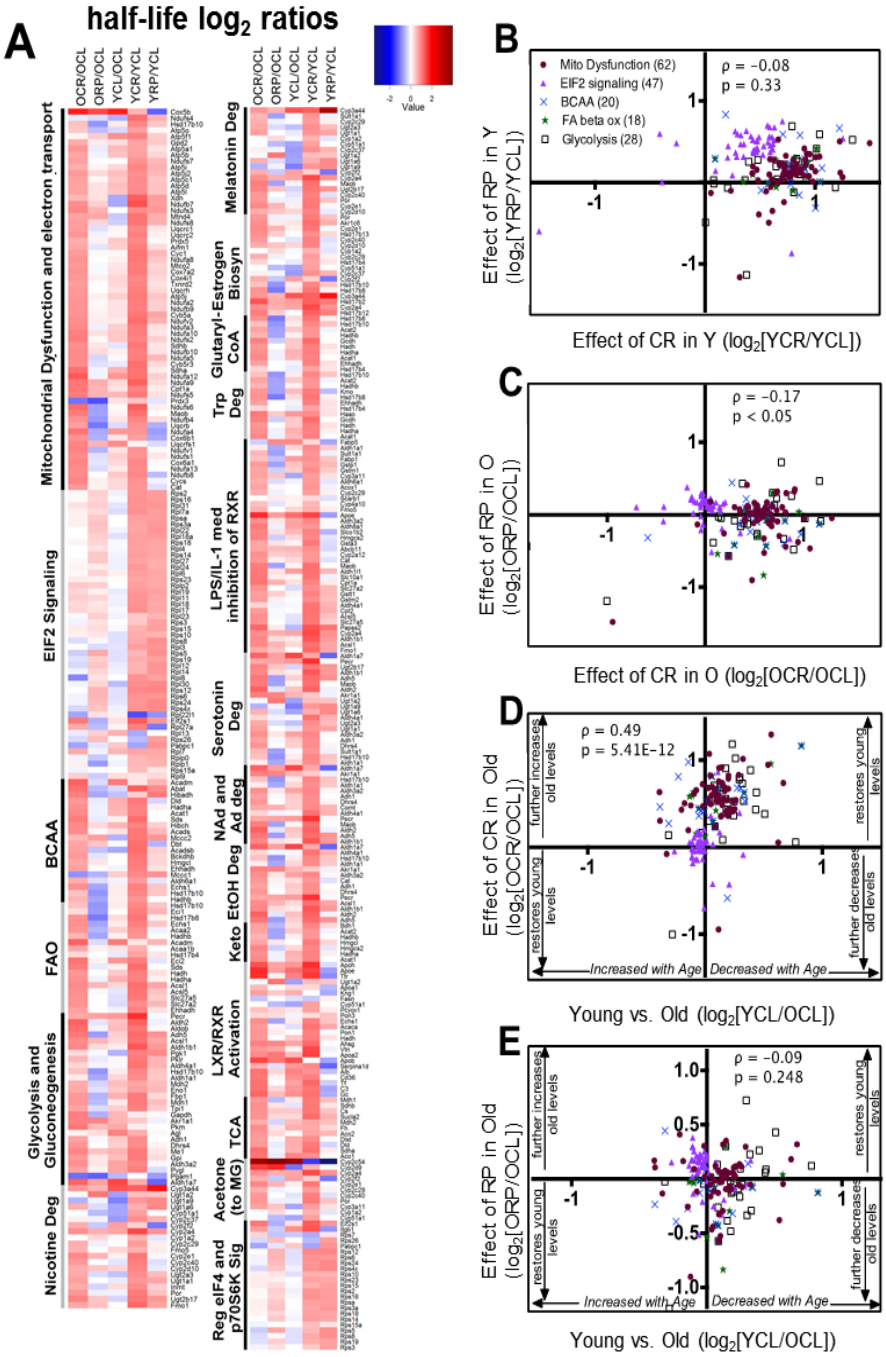

Figure 3-3 Heatmap of protein half-life differences and scatter plots of top pathway HL ratio comparisons. (A) Total proteins that were significantly altered (q<0.05) were categorized into the top 19 canonical pathways using IPA. Red indicates longer half-life in the numerator and blue indicates longer half-life in the denominator. Ratio values ranging from log2 -3 to +4 are depicted in a color gradient from blue to red. BCAA, branched chain amino acid degradation, FAO, fatty acid beta oxidation, Keto, ketogenesis, Acetone (to MG), acetone degradation to methylglyoxal. 3 Scatter plots of log2 ratio comparisons of top metabolic pathways for (B) YRP/YCL vs. YCR/YCL, (C) ORP/OCL vs. OCR/OCL, (D) OCR/OCL vs. YCL/OCL, (E) ORP/OCL vs. YCL/OCL. (D,E) If changes with aging are reversed, those proteins are located in the top right or bottom left quadrants of the scatter plots. The number of significantly changed proteins that mapped to each pathway is listed in parenthesis in panel (B). All heatmap proteins and their half-life log2 ratios are listed in Table S2.

Of the significantly changed protein HLs in the liver proteome, the majority (81%) belonged to metabolic pathways, including energy, amino acid, hormone, and intermediary metabolism. Other functional groups included signaling, transcriptional regulation (i.e., PXR/RXR activation), and biosynthetic pathways. Mitochondrial dysfunction (defined in the supplementary methods) is the top pathway significantly altered by the 10-week intervention. As noted above, HLs from total and mt fractions were highly concordant, and the mt fraction HL heatmap (Fig. S6) is very similar to the total protein heatmap.

In almost all pathways and both ages, CR globally extended protein HLs (decreased turnover) compared to controls, as demonstrated by consistent red colors (log_2 ratios>0) of the CR/CL ratios in the total (Figure 3-3A) and mt protein (Fig. S6) heatmaps. The only exceptions to this phenotype are eIF2 signaling and regulation of eIF4 and p70S6K signaling pathways (Figure 3-3A) where young, but not old HLs were increased by CR compared to controls. Notably, these are the pathways most directly downstream of mTORC1 and include many large and small ribosomal proteins. Although fewer than 12% of the total proteins included in the heatmap had HLs that were shorter in OCR than OCL (blue colors in Figure 3-3A), 45% of all observed ribosomal proteins in old livers had shorter HLs after CR. RP treatment increased mean HLs 5-15% in 9/19 pathways in young and old groups.

It is interesting to note that despite the similarities in lifespan and healthspan benefits of CR and RP, the effects on hepatic proteome dynamics are dramatically different between the two treatments. In young livers the magnitude of the change induced by RP is about 40% smaller than CR (Figure 3-1C, 3B) and in old livers the direction of change was often opposite to that of CR (Figure 3-3C; negative Spearman's $\rho = -0.17$, $p < 0.0505$). Moreover, whereas CR in old liver lysates had an effect that was generally toward making the HLs more similar to those of young livers (Figure 3-3D, significant positive correlation shown by Spearman's $\rho = 0.5$, $p < 0.0001$), RP produced effects that were highly variable, but often in an opposite direction to that of young control livers (Figure 3-3E, many proteins in the lower right and upper left quadrants). It is also apparent that while RP treatment in young and old mice visually resemble one another and correlate well in the heatmap (3A), the magnitude of the changes induced by RP in old mice is smaller than the response from young mice. Consistent with this, blood levels of rapamycin (Fig S11)

were found to be lower in old mice compared with the young cohort. Thus, diminished bioavailability of the drug in old mice likely explains part or all of the difference.

3.3.4 **Protein quality control: altered protein carbonylation, autophagy, and translational elongation by CR and RP**

Protein carbonylation can be used as a readout for oxidative stress and damage. We observed a significant decrease in protein carbonylation with CR and RP in both young and old animals after 10-weeks of treatment (Figure 3-4A). Autophagy is a major proteolytic system involved in protein quality control and degradation that is regulated by mTORC1. To examine the effects on autophagy, we measured the content of several autophagy markers with age and treatments. A significant decrease in p62 with aging was reversed by ORP ($p<0.01$, Figure 3-4B). Beclin-1 levels decreased with OCR ($p<0.01$, Figure 3-4B) and LC3 II/I ratios did not alter with aging or treatments. Collectively, these markers are consistent with a decline in autophagy in old mouse treatment groups, which is also consistent with reduced turnover (longer HLs) associated with OCR and ORP (Figure 3-1 C-F).

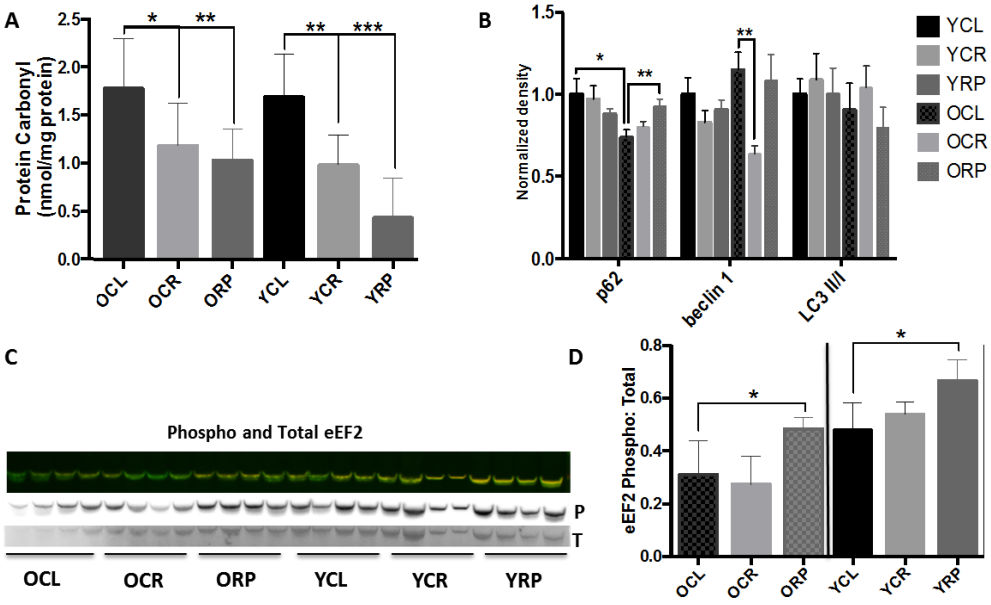

Figure 3-4 Protein carbonyl content, autophagic degradation, and translation elongation marker with treatment and aging. (A) Protein carbonyls are decreased with treatments. (B) Autophagic marker p62 show a decrease with aging and an increase with ORP while beclin-1 is decreased with OCR. LC3 II/I ratios did not change with age or treatments. (C) Representative fluorescent western blot of phospho-eEF2 and total eEF2. Phosphorylation of this elongation factor disrupts translational elongation. The ratio of phospho/total eEF2 is quantified in (D). Rapamycin treatment significantly increased this ratio in both young and old mice. n=4-6 per group., * $p<0.05$, ** $p<0.001$, *** $p<0.0001$

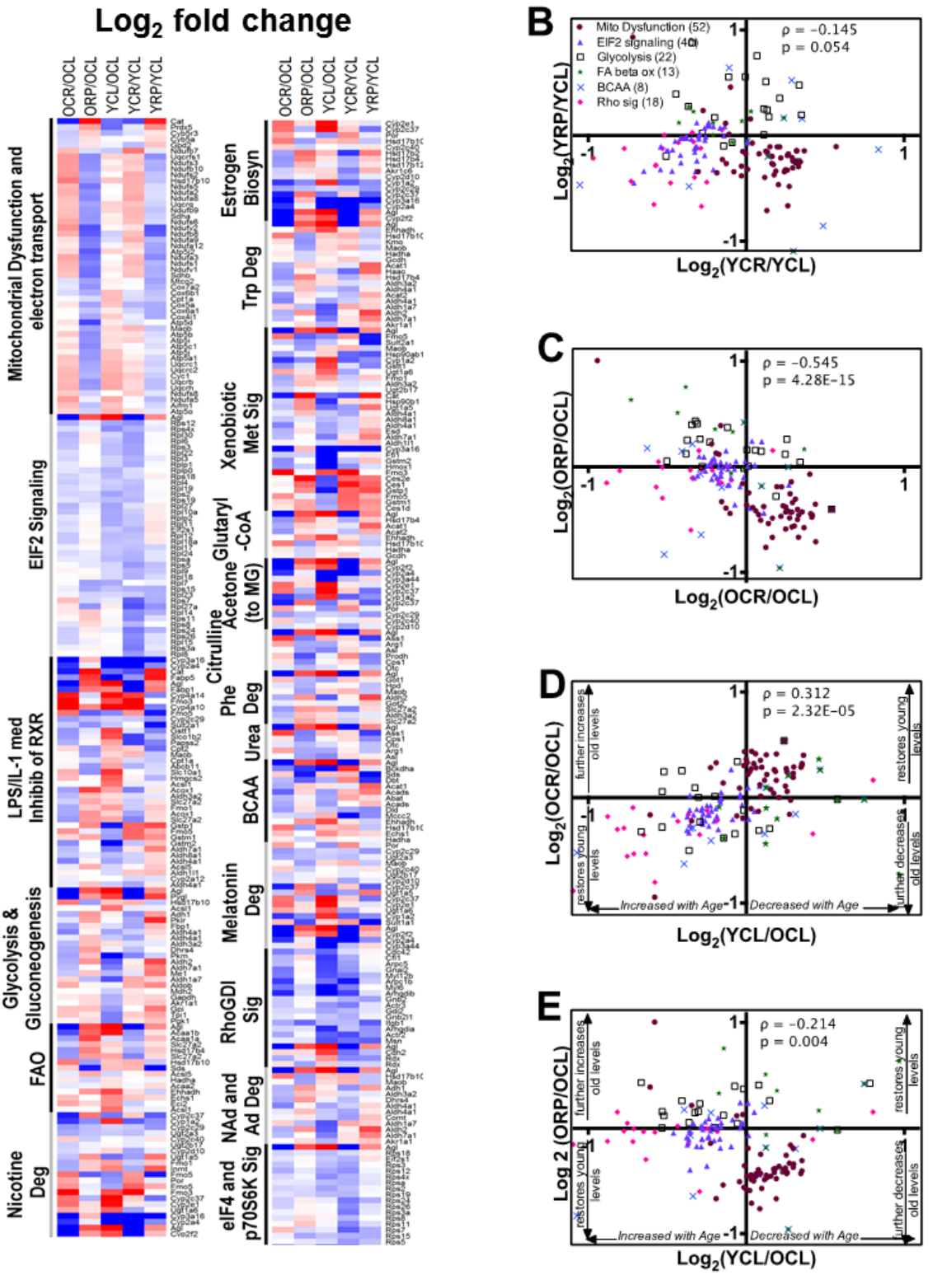

Figure 3-5 Heatmap of protein abundance differences and scatter plots of top pathway abundance comparisons. (A) Proteins that were significantly altered at q<0.05 were categorized into canonical pathways using IPA. The top 19 pathways are reported. Log2 fold changes ranging from -2 to +2 are gradually colored from blue to red. 3 Scatter plots of log2 fold change comparisons of the top metabolic pathway proteins of (B) YRP/YCL vs. YCR/YCL, (C) ORP/OCL vs. OCR/OCL (D) OCR/OCL vs. YCL/OCL, (E) ORP/OCL vs. YCL/OCL are shown. (D,E) If changes with aging are reversed, those proteins are located in the top right or bottom left quadrants of the scatter plots. The number of significantly changed proteins that mapped to each pathway is listed in parenthesis in panel (B). All heatmap proteins and their log2 fold-changes are listed in Table S3.

3.3.5 **IPA analysis of significant changes in protein abundance**

Topograph calculates peptide abundances by chromatographic peak areas under the curve (AUC), which includes the sum of the unlabeled and labeled peaks for each peptide. We found no systematic difference in the AUC estimates between samples from early heavy labeling times vs late (Fig. S4A) and the data from all 12 mice in each cohort were used in the analysis. From the 3110 unique peptides in the total protein fraction, protein abundances were calculated and the significantly altered proteins ($q < 0.05$, an average of 200 proteins in each pairwise comparison) were analyzed using IPA to define the canonical pathways affected by CR and RP.

This analysis revealed many contrasting changes between CR and RP (F Figure 3-5A). The most prominent example of this is the mt dysfunction pathway, where YRP/YCL and ORP/OCL comparisons showed a decrease in relative protein abundances, while YCR/YCL and OCR/OCL showed increases (Figure 3-5A mt dysfunction pathway, filled circles in Figure 3-5B, C in the lower right quadrants). Overall, this inverse correlation between CR and RP was stronger in old liver (Fig. 5C, Spearman's $\rho = -0.54$, $p < 0.0001$) than in young liver (Fig. 5B, Spearman's $\rho = -0.14$, not significant). This was recapitulated in the assay of aconitase activity, with a similar trend in citrate synthase activity (Fig S7). These apparent changes in mt protein content and activity by CR vs. RP are not likely to be explained by changes in total mt mass per cell as mtDNA copy number did not alter with treatments (S8A). Nor can they be explained by increased mt biogenesis, as mRNA levels of mt biogenesis markers Nrf1, Nrf2, and mt transcription factor A (TFAM) did not change with the treatments (Fig S8B-D).

In general, OCR restored protein abundances to young levels (significant positive correlation, Spearman's $\rho = 0.31$, $p < 0.0001$, Fig. 5D). Conversely, RP reduced most protein abundances (blue colors in ORP/OCL, Fig. 5A, significant negative correlation, Spearman's $\rho = -0.21$, $p = 0.004$ in Fig 5E), amplifying many of the changes that occurred with aging. Notable exceptions to this pattern were eIF2, eIF4 and p70S6K, and Rho GDI signaling pathways. These pathway components were almost all decreased by both CR and RP, and are comprised of many ribosomal and protein translation proteins regulated by mTORC1, as noted above. With the exception of these pathways, the striking difference between CR and

RP in old mice appears to create two very different metabolic profiles, suggesting that important parts of their mechanisms of action are distinct.

3.3.6 **Analysis of CR and Rapa effects on protein translation: polysome profiles and eEF2**

As initiation is usually the rate-limiting step of mRNA translation [175], we wished to gain insight into changes in global protein translation by examining polysome profiles of CR and RP treated livers. Figure 6A shows representative profiles of YCL, YCR and YRP liver polysome gradients. We quantified the areas under the curve of free subunits (40S, 60S), monosome (80S) and polysome peaks (Figure 3-6A); the ratios of these areas to the total area under the ribosome peaks are plotted in Figures 6B (young livers) and 6C (old livers). As expected, old CR showed a significant increase in free 40S and 60S subunits and a decrease in ribosome loading (5 ribosomes or higher, Figure 3-6C, $p < 0.001$) compared to control, indicating decreased translation. This was confirmed by a significant linear trend of decreased peak ratios vs. ribosome loading when the areas were analyzed as a percent of control values (Fig. S10B, $p<0.01$). Surprisingly, young RP livers showed an increase in polysomes consisting of 5 or more ribosomes and a decrease in 40S and 60S subunits (Figure 3-6B, $p < 0.0001$) and a significant linear trend of increased loading when the peak ratios were analyzed as a percent of control (Fig. S10A, $p<0.0001$). No significant differences were observed in individual old RP peaks (Figure 3-6C) but trend analysis showed significantly increased ribosome recruitment (Fig. S10B, $p< 0.0001$), just as was seen in young RP livers. This is contrary to the expected outcome of decreased translational activity by RP [176] and the net increase in protein half-lives seen in RP (Fig 1C-F), but it would be consistent with a reduction of elongation rates that would slow ribosome translocation on messages. In agreement with this, rapamycin significantly increased the proportion of phosphorylated eukaryotic elongation factor 2 (eEF2) in both young and old mice (Fig 4 C, D), which is consistent with reduced translation elongation rates [177].

The comparison of YCL to OCL polysome profiles (Figure 3-6D) showed significantly lower levels of 60S ribosomal subunits in OCL; this was confirmed by trend analysis (Fig S10C), which showed significantly ($p<0.001$) increased polysome loading in OCL livers compared to YCL. This result is consistent with the overall increase in protein synthesis rates (decreased half-lives) observed with aging (Fig. 1C).

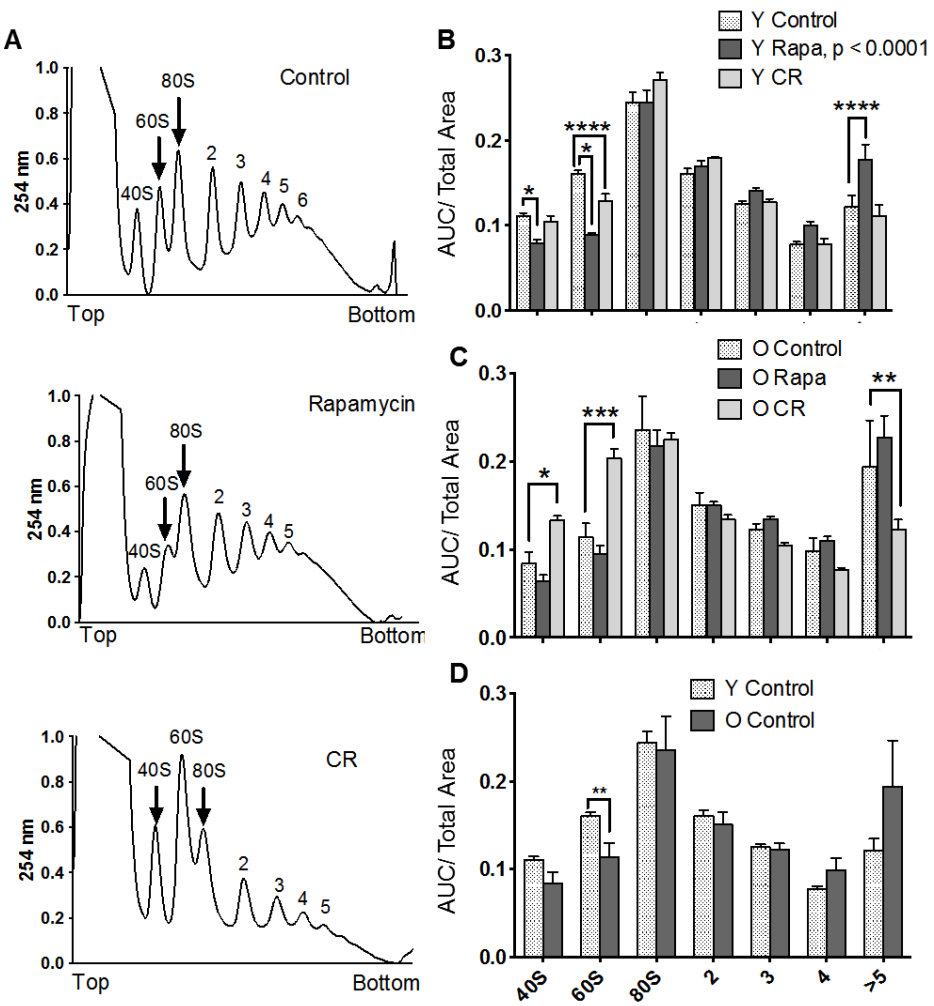

Figure 3-6 Global protein synthesis and elongation. Sub-acute CR decreases global protein translation while RP increases ribosome loading in the liver. (A) Representative polysome profiles of young control, RP, and CR groups. The "top" and "bottom" of the gradient are indicated on the x-axis. The peaks are labeled with the name of the ribosome subunit or number of ribosomes that they represent. (B, C) Area under the curve (AUC) measurements shown relative to the total AUC of the single subunits, monosome, and polysome peaks of control, CR, and RP livers of (B) young and (C) old mice. (D) Quantified relative polysome area of young and old livers. n=5 per group, $p<0.05$ ANOVA. * $p<0.05$, ** $p<0.01$, *** $p<0.001$, ****$p<0.0001$

3.4 DISCUSSION

In this study, we sought to investigate the hepatic proteome dynamics associated with two well-established longevity interventions, CR and RP, in young and old mice. To measure dynamic changes, we utilized whole-body stable isotope labeling and a new software tool to calculate protein turnover rates and relative protein abundances *in vivo*. While both CR and RP are lifespan-extending interventions with a mechanistic link in the mTOR pathway, our results provide insight into distinct differences (especially in protein abundances), as well as similarities (especially in protein HL changes) after subacute treatment. In particular, the highly opposing effects of these treatments on mt protein abundances (Fig. 5A) suggest that these interventions have a different effect on cellular energetics in liver. The effects of RP on protein half-lives, although positively correlated in many pathways, are generally much smaller than those of CR (Fig. 1C-F). While this might suggest that the ITP dose of RP is suboptimal as a CR mimetic, it is notable that the effects on altered protein abundance were qualitatively different, rather than just quantitatively different. We would not expect that a higher dose of RP would reverse the *direction* of abundance changes seen in Figure 5 A and D. Furthermore, RP was equally effective as CR in slowing turnover of ribosomal proteins in the eIF2, eIF4 and p70S6K pathways in young mice (Fig. 3A), in accord with the hypothesis that RP has a subset of specific overlapping targets with CR that are sufficient to promote health. These data are consistent with a recent study that suggests that 20 weeks of RP treatment inhibited pS6 but not 4EBP1, and thus there is little inhibitory effect on cap-dependent translation by RP [153]. This is in agreement with our observations (Fig. S1B,C) and another report that RP differentially inhibits S6Ks vs. 4EBP1 [153]. One may therefore speculate that the beneficial effects of RP track less with inhibition of cap-dependent initiation of translation and more closely with inhibition of ribosomal protein synthesis, reduced translation elongation and improved translational fidelity (see Fig S14 and discussion below).

Our approach to define proteome dynamics with CR and RP *in vivo* used novel software that is able to deconvolute complex isotopomer distributions and calculate amino acid precursor pool enrichment levels. This is key to accurate calculation of protein turnover rates; other heavy isotope labeling approaches require complex calculations to indirectly estimate and compensate for changes in precursor pool

enrichment [84,93,160]. With this novel platform we were able to determine the precursor pool-adjusted turnover rates of over 900 proteins in mouse liver. Previous reports on the effect of CR on protein turnover suggest an increase in protein synthesis and degradation [178-182]. In contrast, we observed a large global increase in HLs (decreased synthesis) following 10 weeks CR, a reversal from the slightly lower HLs seen in old control livers (Figure 1C OCL/YCL). Consistent with our data, Price *et al.* reported prolonged HLs in over 80% of liver proteins with chronic CR [160]. We believe an important part of this apparent contradiction with previously published turnover data relates to differences between acute, subacute, or chronic CR treatments.

The global decline in protein synthesis rates observed with subacute CR, and to a lesser extent with RP, is consistent with the hypothesis that with longer treatment times CR is switching cells to an energy-conservation state, decreasing the energetically expensive process of protein synthesis. After subacute or chronic treatment these longer-lived proteins may have higher quality and less damage; this is supported by our observation of lower levels of protein carbonyls (Fig. 4A) and a recent report that showed increased protein translation fidelity in RP-treated liver MEFs [161]. Consistent with this interpretation, acute RP treatment (1-2 wks) caused insulin resistance and lower glucose tolerance [152] while a longer treatment (20-wk) reversed the insulin resistance with better lipid profiles and increased oxygen consumption [153]. Our results are also disparate to two recent reports using metabolic-labeling that showed no change in overall protein synthesis in the liver, heart, or skeletal muscle with CR and RP [158,159]. We and Price *et al.* show substantially reduced global turnover with CR, and we observed a reduction in turnover after RP. A plausible explanation for the difference from Miller and colleagues is that they measured “bulk” protein synthesis that can be dominated by the synthesis rates of a few highly abundant structural proteins, while our and Price’s measurements of large numbers of individual proteins are not skewed by the most abundant proteins.

Whereas there is an abundance of evidence that acute CR and RP treatments increase autophagy [183,184], our data are contrary to this: LC3-II/I levels are unchanged and beclin-1 only decreased with OCR, while p62 only increased with ORP (Fig. 4B). Measurement of autophagic flux will be needed to conclusively determine the status of autophagy, however, this disparity may be due to the majority of prior studies reporting changes after acute CR and RP treatments. In order for protein turnover rates to have decreased after 10 weeks of CR and RP, as we observe, elevated rates of autophagy cannot be

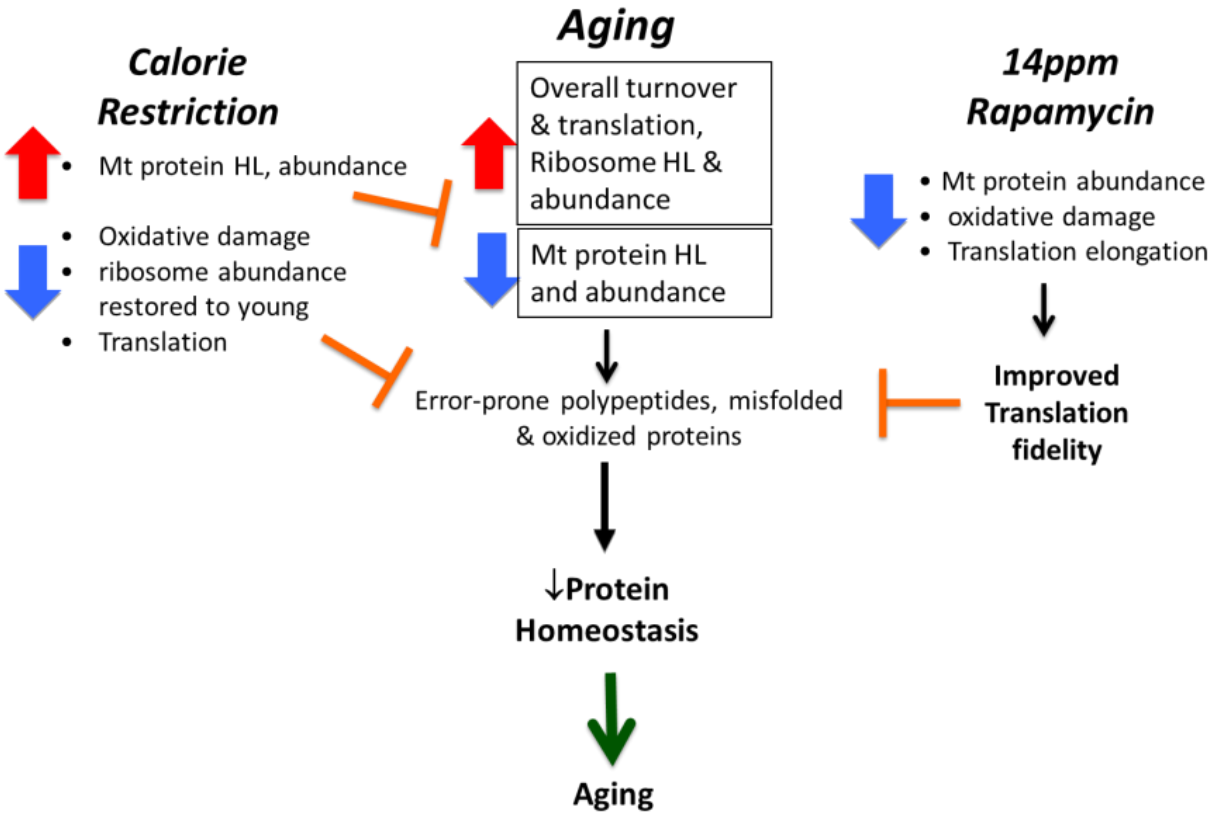

Figure 3-7 A summary model of the effects observed in this study. With aging, we observed an overall increase in turnover and translation with a concomitant decrease in mt protein HLs and abundance. In combination, these factors can result in increased ROS and the formation of error-prone polypeptides and oxidized proteins, thereby disrupting protein homeostasis. CR reversed these changes effectively recapitulating a more youthful proteome, while RP changes were more subtle but indicated decreased oxidative damage and changes that improved translational fidelity. Short-term CR and RP can both restore protein homeostasis to promote more healthy aging.

maintained.

An unanticipated finding of this study was the increased polysome loading observed with young and old RP treatments (Figure 3-6B, C; Fig. S10A, B). This might seem to be inconsistent with reduced protein

turnover and a previous report of a reduction in cap-dependent translation by RP [176]. This dichotomy is resolved by noting that RP treatment reduces eEF2 phosphorylation (Fig. 4C, D), which will lead to a reduced elongation rate of ribosomes; this can result in increased polysome loading, even if initiation is decreased. This condition has been shown to enhance translation fidelity [161], keeping proteins in good quality with longer half-lives [185]. Thus, our results are consistent with the hypothesis that reduced rates of translational elongation and reduced rates of protein synthesis after 10 weeks of RP facilitate production of error-free polypeptides that are longer lived.

In agreement with our observation of differential mt protein abundance (Fig. 5C), Zid and colleagues demonstrated preferential translation of mt proteins after CR in Drosophila [143] and CR has also been shown to increase mt gene expression and respiratory capacity in multiple murine tissues [186-188]. In contrast, acute RP has been shown to suppress mt biogenesis [189] and decrease mt respiration in cultured cells [100,190]. Surprisingly, carbonylation, an indication of oxidative protein damage, was significantly lower in RP compared to CR in both young and older livers (Fig. 4A). We believe this is best explained by our observation of differential mt respiratory dynamics, as indicated by increased protein abundances (Fig 5A) and higher levels of aconitase activity in CR compared to RP (Fig. S7A). Increased mt respiration with CR may be producing more carbonyl inducing ROS while decreased mt activity in RP results in less carbonylation. Interestingly, these differences in mt occurred without a change in mtDNA copy number and mt biogenesis (Fig. S8). The 10 week treatments also made no impact on the elevated mitochondrial deletion frequency seen in old mice (Fig S9).

Consistent with differences we observe in treatments, two recent reports have highlighted the distinctive effects of RP and CR in the liver after a 6 month treatment [191,192] CR had a larger and mostly opposite effect on the transcriptome compared to RP. Genes associated with mt function and antioxidants were among the top upregulated with CR while most transcripts changed with RP was down regulated. No significant change was observed in the liver metabolome by RP but CR had a larger effect changing metabolites associated with energy status. Compared to CR, RP showed no protective effect on fat mass, insulin sensitivity, redox status, or the fatty acid oxidation in liver. These results track with our

observations of distinctive differences in mt protein abundance (Fig. 5A,5B), polysome loading (Fig. S10 A,B), and ~40% lower effect on protein half-lives (Fig. 3A,C) by RP compared to CR.

A cautionary note is that the effects of CR and RP on the proteome appear to be different depending on the tissue examined. We have recently reported that short-term CR and RP in the heart produced similar proteome effects, both treatments restoring proteins involved in mitochondrial function, electron transport chain, fatty acid oxidation and TCA cycle into youthful levels. Furthermore, both treatments reversed age-dependent cardiac hypertrophy and diastolic dysfunction to the same extent [85]. The magnitude of change in protein HLs by OCR in the heart was similar to liver (~45% longer than OCL) but ORP induced a bigger change in the heart (27% longer compared to only 15% in the liver). Overall the changes in proteome turnover and abundance were highly similar in both treatments, including effects on mt proteins, in contrast to our observations in the liver. Therefore, these treatments, especially RP, appear to have much different effects on the proteome and physiology depending on the tissue type, with heart and liver perhaps lying at extremes, considering their disparate function and energetics.

In summary, we investigated the effect of CR and RP in parallel on young and aged mouse protein turnover, abundance, and polysome loading. Our findings provide compelling evidence supporting the idea that CR's beneficial effect on life span is mediated to a large extent by a restoration of a more youthful proteome: a majority of the metabolic pathways were significantly altered by aging and this was reversed in OCR. The effects of RP in liver are complex and in many cases dissimilar to those of CR, but nevertheless indicate a large impact on proteome dynamics. Ribosomal and mt proteins in particular behaved very differently in OCR and ORP (Fig. 3A,C-E, Fig. 5A,C-E). Increased HLs after RP and decreased relative protein abundance in many key metabolic pathways in old mice, coupled with increased polysome loading (most likely due to a reduction in elongation rate), suggests a slowing of protein synthesis with production of higher quality, longer lived proteins after RP. Overall, our data provide the first comprehensive analysis of proteome dynamics with aging and sub-acute CR and RP and underline a functional connection between protein homeostasis and longevity.

3.5 MATERIALS AND METHODS

Supporting information and supplementary data can be accessed online:

http://onlinelibrary.wiley.com/doi/10.1111/acel.12317/suppinfo

3.5.1 Animals

C57BL/6 female mice were purchased at 3 and 25 months of age (Figure 1A) from the NIA Charles River colony. Female mice were used as a past study showed that the effects of RP in murine aging were larger in this gender [25]. Mice were housed at 20ºC with a 12-hour light and dark cycle. All animals were handled according to the guidelines of the Institutional Animal Care Committee of the University of Washington and the National Institutes of Health. One week after arrival, all mice were started on a synthetic diet (Harlan Teklad diet #TD.99366) that was nutritionally similar to the NIH-31 standard for rodents. The use of this diet facilitated the subsequent substitution of heavy-labeled [5,5,5 – $^{2}H_{3}$] leucine for light leucine, which enabled the protein turnover measurements. Mouse weights and food intake were recorded weekly. The young and old mice were individually housed after three weeks of acclimation to the synthetic chow and were randomly assigned to three groups: 1) an *ad libitum* synthetic food regimen [9]; 2) rapamycin-containing synthetic diet (RP) and 3) calorie restricted (CR), as detailed in the supplemental methods.

3.5.2 Stable Isotope labeling

After 10 weeks of diet regimens, all mice received a synthetic diet (TD.09846, Harlan Teklad, Madison,WI) with the light leucine fully replaced by 11 g/kg of deuterated [5,5,5 – $^{2}H_{3}$] – L – leucine (Cambridge Isotope Laboratory, Tewksbury, MA), with CR and RP cohort conditions continued as above. Three mice were euthanized for tissue collections and proteomics analysis at four time points: days 3, 7, 12 and 17 after switching to $^{2}H_{3}$ – leucine diet.

3.5.3 Mass spectrometry and analysis

Whole liver tissue was homogenized or mt fractions were isolated as previously described [193]. Both were processed, trypsin digested, and LC-MS/MS analysis performed with a Waters nanoAcquity UPLC and a Thermo Scientific LTQ Orbitrap Velos, as previously described [88]. The raw data from MS/MS and extended supplementary files are available at https://chorusproject.org/pages/blog.html#/351.

The Topograph software program (http://proteome.gs.washington.edu/software/topograph/)(http://proteome.gs.washington.edu/software/topograph/) was developed for the measurement of peptide isotopologue abundances from LC-MS/MS chromatograms and the calculation of peptide turnover rates [88]. It allows the measurement of the proportion of the amino acid precursor pool that is labeled, which varied over time and condition (Figure S12A). This information allows the correct calculation of percent new synthesis for each peptide, which when plotted for 12 biological replicates over time (4 time points) generated an exponential curve following first order kinetics (Fig. S2A). Using a logarithmic transformation, the first order protein turnover rate (slope) was determined by linear regression (Fig S2B). Only peptides that uniquely mapped to a single protein were used for our measurements. See supplemental methods for details.

STABLE ISOTOPE LABELING REVEALS NOVEL INSIGHTS INTO POLY-UBIQUITINATED HOMEOSTASIS AND PROTEIN AGGREGATION WITH AGE, CALORIE RESTRICTION, AND RAPAMYCIN TREATMENT

4.1 SUMMARY

Background: Accumulation of protein aggregates with age, a symptom of declining proteostasis, was first described in aged human tissue over 150 years ago. Scientists have since described many forms of aggregates in virtually every human tissue. Poly-ubiquitin modifications are a canonical marker of insoluble protein aggregates, however, the composition of most age-related inclusions remains relatively unknown. **Methods/Principal Findings:** To examine the landscape of age-related protein aggregation *in vivo*, we performed an antibody-based pulldown of poly-ubiquitinated proteins coupled with metabolic labeling and mass spectrometry on young and old untreated, calorie restricted and rapamycin-fed mice. The abundances and percentages of newly synthesized protein in the poly-ubiquitinated proteome (poly-ubiquitinome) were estimated relative to the unmodified proteome. We show that in old mice there is an increase in the abundance of many poly-ubiquitinated proteins and a greater retention of pre-existing (unlabeled) poly-ubiquitinated proteins relative to their unmodified counterparts – fitting the expected profile of aggregating proteins. These candidate proteins were refined to include only proteins that increasingly appeared in insoluble protein fractions with age. Finally, we confirm the aggregation of several of the top candidate proteins by confocal microscopy. **Conclusions/Significance:** Stable-isotope labeling can be a powerful tool to gain novel insights into proteostasis mechanisms, such as the aggregation of proteins. Understanding the composition of protein aggregates and the cellular machinery that targets them offers new insights into aggregation mechanisms and may identify novel targets for intervention.

4.2 INTRODUCTION

Maintenance of proper protein homeostasis (proteostasis) is essential to cellular and organismal health. A wealth of research has shown that age-related diseases and conditions are associated with the inability of the cell to maintain healthy proteins or get rid of defective proteins[11], including: neurodegenerative disease[12], cardiac dysfunction[13,14], cataracts[15], and sarcopenia[16]. Loss of proteostasis can manifest on the cellular level in a number of ways: protein aggregation[194], unfolding[195], oxidative damage[196,197], post-translational modification[40,198-200], as well as altered rates of synthesis and degradation[91,92,201].

The age-dependent accumulation of proteins and other macromolecular "junk" was first described over a hundred years ago[202], and has since been reported to accumulate in virtually all human tissues with age[11,34,203,204]. Insoluble inclusions have been extensively cataloged based on histological appearance, macromolecular structure or origin, described by various names such as lipofuscin[205], amyloid[15], aggresome-like induced structures [206,207], advanced glycation end products (AGE)[208], plaques [209], dendritic cell aggresomes-like induced structures (DALIS)[210], particle-rich cytoplasmic structure (PaCS)[211], inclusion bodies[212], ceroid[202], aggresomes[203], etc. In some disease-associated inclusions, particularly in neurodegenerative diseases, the one or few primary protein constituents involved are well known, such as amyloid beta and alpha-synuclein in Alzheimer's disease and Parkinson's disease, respectively[120,213]. Most other protein inclusions, however, are identified by histological or biochemical features, but the identities of the protein components are not known.

The Ubiquitin-Proteasome System (UPS) is a robust and highly precise system of maintaining proteome homeostasis by the recognition and degradation of damaged, unfolded, overly abundant, or otherwise dysfunctional proteins by the proteasome. In addition to a well-known association with proteosomal degradation, poly-ubiquitination is closely associated with insoluble protein inclusions characteristic of aged tissue [39], signals protein turnover through autophagy [42], localizes to viral stress granules [214], and decorates pathogen containing vacuoles to facilitate host-cell defense [43].

Using a combination of stable isotope labeling and proteomics, we recently reported that a large number of age-related changes in protein abundances, quality, *in vivo* turnover rates, and total protein ubiquitination could be mitigated or reversed in mice treated with short-term calorie restriction (CR) or rapamycin (RP) [91,201]. To examine how poly-ubiquitin mediated proteostasis may underlie these changes, we perform a similar stable isotope approach on several sub-proteome fractions: the poly-ubiquitin mediated proteome (poly-ubiquitinome) and the urea-soluble and insoluble proteomes. We demonstrate that aging and treatment have widespread effects on the landscape of poly-ubiquitin modified and insoluble proteins. With age, there is an accumulation of pre-existing ubiquitin-modified proteins relative to their unmodified counterparts. Additionally, a number of proteins become increasingly insoluble with age. We show that this data can verifiably predict *in vivo* protein aggregates, and demonstrate the utility of combining protein abundances and turnover kinetics, as well as sub-proteomic fractions, in uncovering novel mechanistic insights on a large scale.

4.3 RESULTS

4.3.1 Experimental Workflow

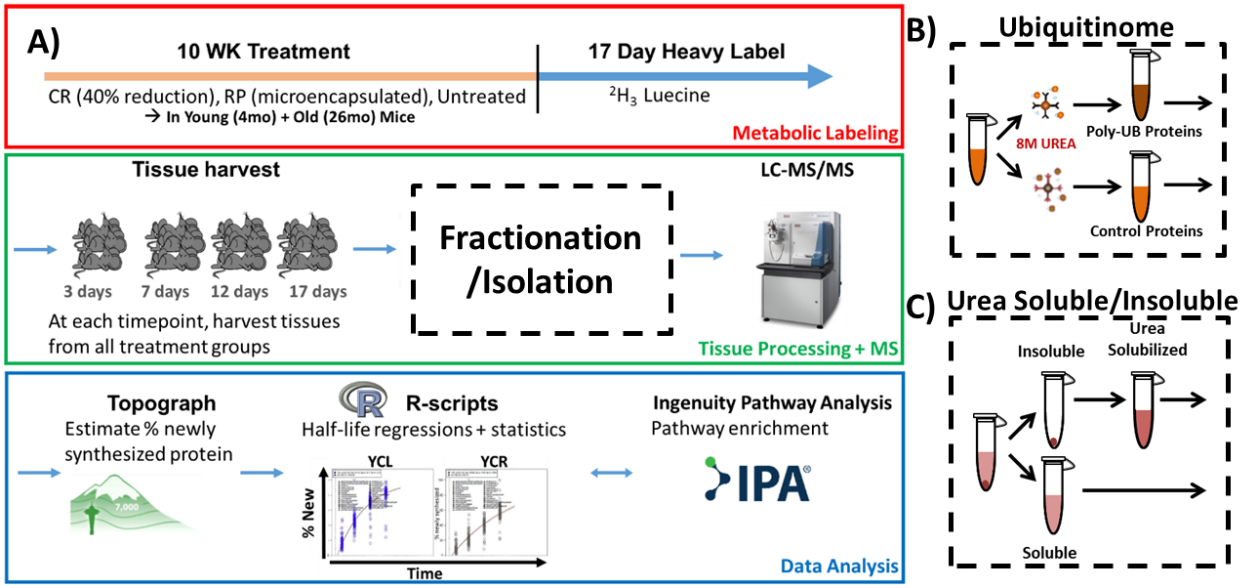

Figure 4-1 Workflow A) Young and old mice are treated for 10 weeks with CR, RP, or ad libitum diet, then dietary leucine is replaced with deuterated "heavy" leucine for 17 days while mice remain on treatments. Tissues are harvested from each treatment group over 4 timepoint over the 17 day labeling period, followed by processing of livers into protein fractions and analysis by nLC-MS/MS. Topograph software is used to calculate precursor-pool corrected estimates of percentage of newly synthesized protein as well as perform peak area integration. Statistical analysis and visualizations are performed by in-house R-scripts. Pathway enrichments are performed using commercially available Ingenuity Pathway Analysis (IPA) software.

The experimental workflow, summarized in Figure 4-1, utilizes a previously described metabolic labeling proteomic workflow [88,201] in combination with an antibody-based enrichment of the poly-ubiquitin-modified proteome. Briefly, 4 and 26 mo old mice were subjected to one of three treatments for 10 weeks (6 groups total): *ad libitum* synthetic chow control diet (CL), caloric restricted (CR) or *ad libitum* plus rapamycin (RP). RP was used at the concentration and formulation previously shown by the NIA Interventions Testing Program to extend mouse lifespan [25]. Following 10 weeks of treatment, deuterated "heavy" leucine was substituted into the diet and maintained along with treatments for 3, 7, 12, or 17 days before tissues were harvested and frozen. In order to enrich the poly-ubiquitinated proteome, we performed an antibody enrichment of proteins from liver lysates using the FK2 multi-ubiquitin (ub) antibody in highly denaturing buffer containing 8M urea to avoid non-specific binding (Figure 4-1B). This antibody has been previously shown to be effective in performing pulldowns under these conditions, which we were able to confirm (Supplementary Figure 4-1B). To further control for non-specific binding, a

portion of each lysate was subjected to a pulldown under the same conditions with an isotype control antibody. All ub-enriched and control samples were analyzed by nLC-MS/MS followed by an analysis of abundances and percentage of newly synthesized proteins in Topograph similarly to previously described [88], although additional steps were taken to estimate the proportion of newly synthesized ubiquitin modified proteins (described below). Importantly, the resulting data from ubiquitin-enriched fractions were corrected to isotype control pulldowns to omit any possible non-specifically enriched proteins from further analysis. For isolation of the urea soluble and insoluble proteome (Figure 4--1C), a low speed spin was performed and the supernatant was prepared as the soluble portion. The insoluble pellet was solubilized in 8M urea.

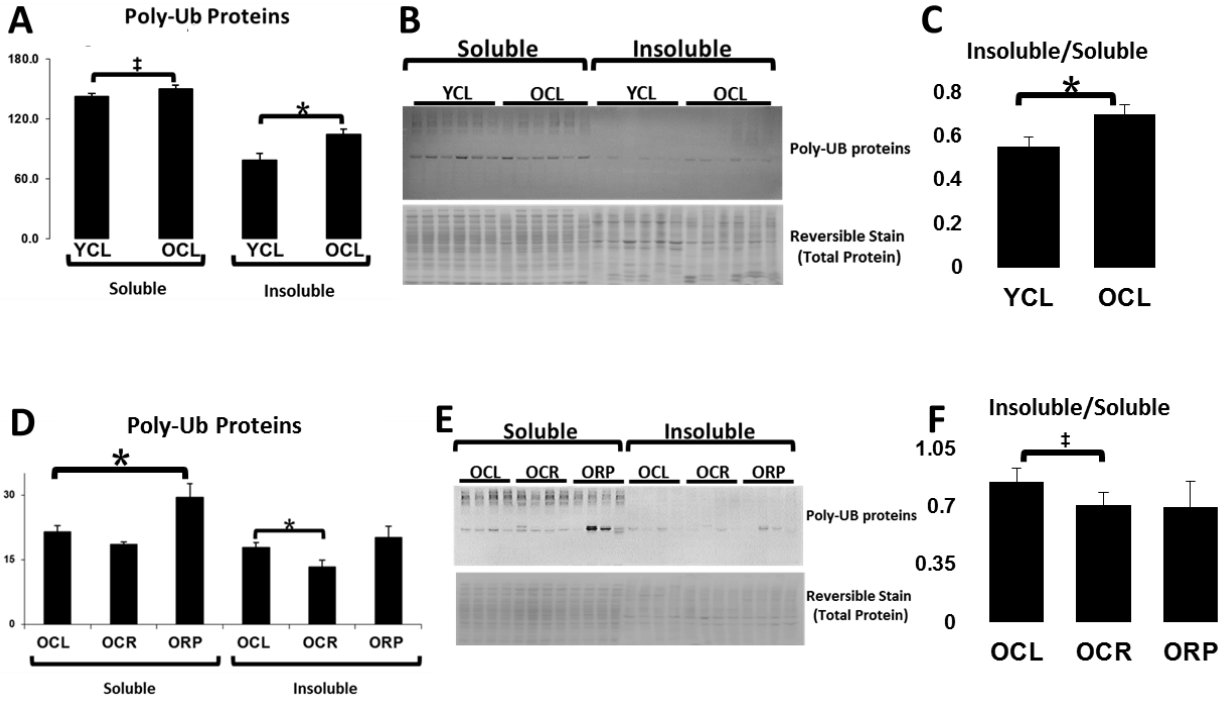

Figure 4-2 increasingly insoluble poly-ub modified proteins with age. A) Significant increase in poly-ubiquitinated proteins in the insoluble fraction with age and a trending increase in the soluble fraction. B) Representative western blot and total protein reversible stain. C) The ratio of insoluble/soluble protein increases with age. D) Increased soluble poly-ub modified proteins in old RP treated mice compared to untreated and a decrease in insoluble poly-ub proteins in mice on CR compared to controls. E) Representative western blot and total protein reversible stain. F) The proportion of insoluble/soluble proteins significantly decreases with CR, and appears to move in the same direction despite seemingly opposite changes in panel D.

4.3.2 **Accumulation of increasingly insoluble poly-ubiquitinated proteins with age**

To assess whether the age-dependent increase in ubiquitinated (UB) proteins we previously reported [201] could be due to accumulation and retention of insoluble protein aggregates, we performed western blotting of poly-UB proteins in the soluble and insoluble proteomes with age (Figure 4-2A-C). There was a significant increase in insoluble UB proteins with age, as well as a trending increase in insoluble UB proteins (Figure 4-2A). Due to differences in buffer conditions insoluble and soluble UB proteins cannot be compared directly, however, quantification of the insoluble/soluble ratios in young and old mice suggest there is an increasing proportion of insoluble proteins in the aged poly-ubiquitinome (Figure 4-2C). We also assessed whether these changes were reversed by CR and RP treatment, as previously observed in total protein ubiquitination (Figure 4-2D-F). A significant reduction was seen in insoluble ubiquitinated proteins in old mice on calorie restriction. Interestingly, aged mice fed rapamycin showed a significant increase in soluble poly-ubiquitinated proteins (Figure 4-2D). However, when taking the ratio of insoluble/soluble proteins in each treatment, both CR and RP show a decreased proportion of insoluble UB-proteins on average, though this is only statistically significant with CR (Figure 4-2F).

4.3.3 **Abundance changes in the poly-ubiquitinome**

To identify the poly-ubiquitinated proteins that are altered by aging, CR, and RP, we performed mass spec analysis of the antibody-enriched poly-ubiquitinome as described above (Figure 4-1A-B). To account for the possibility that an increase in a given poly-ub protein is a reflection of a general increase in the abundance of the unmodified protein, areas of poly-UB proteins were normalized to their unmodified signals in a total (non-enriched) fraction. All poly-ubiquitinated proteins that significantly increased or decreased in abundance with age (after normalization) were analyzed using Ingenuity Pathway Analysis (IPA) software to determine canonical pathways that were most significantly enriched. These results were visualized on a heatmap for the top 10 enriched pathways (Figure 4-3A). An increase (red) indicates a greater accumulation of a poly-ub protein than is seen in the protein overall, while blue represents a decrease in poly-ubiquitination. It is interesting to note the similarity in pathways enriched here and in our previously reported abundance and turnover analysis in liver [201]. Young mice showed clearly lower levels of poly-ub protein compared to aged control mice or aged mice treated with CR or RP.

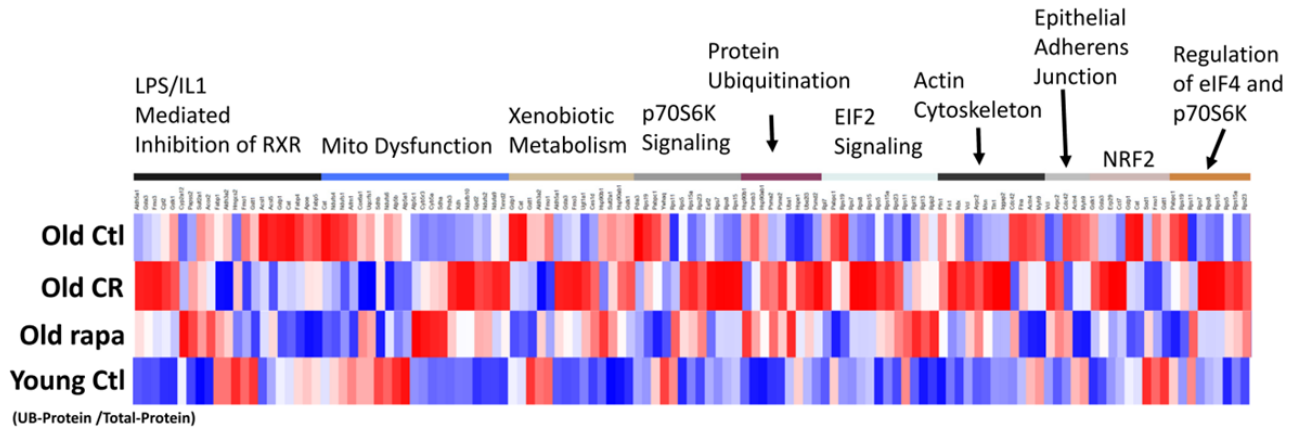

Figure 4-3 Heatmap of top pathways altered in poly-ubiquitination.

4.3.4 Turnover changes in the poly-ubiquitinome

One of the characteristics of typical poly-ub protein aggregates and insoluble proteins in general is that they are difficult to degrade. We therefore estimated the percentage of newly synthesized protein within the ubiquitinome to build a list of candidates that we believe to be likely be aggregating proteins. To calculate these values in Topograph we manually indicated the precursor pool percentages for each sample based on the precursor enrichments that were calculated from the total fraction. We compared the proportion of newly synthesized and pre-existing proteins in the poly-ub-modified fraction to the unmodified fraction and plotted results on a heatmap. Interestingly, old untreated mice were heavily composed of pre-existing poly-ub proteins, while both treatments were improved in comparison.

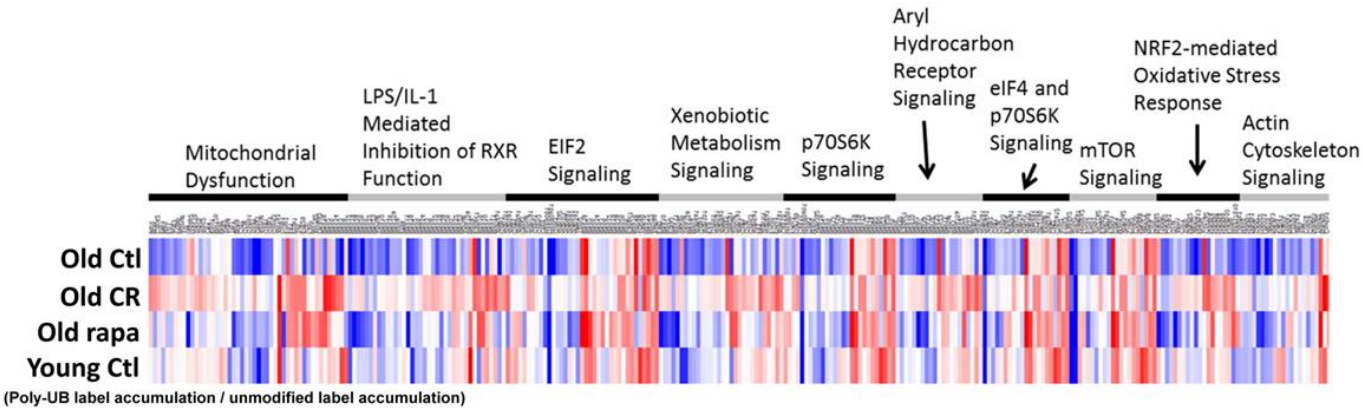

Figure 4-4 Heatmap of top poly-ub protein pathways with an altered proportion of old and new proteins.

4.3.5 Urea soluble and insoluble –"omes"

On average, across the top pathways, old mice had the greatest abundance of poly-ubiquitinated proteins, and the greatest proportion of poly-ub proteins were pre-existing "old" proteins, suggesting the accumulation of poly-ub proteins was in part due to an inability to degrade proteins. We hypothesized proteins following this pattern are likely to be forming insoluble aggregates, as aggregates are less efficiently degraded and removed from cells, if at all. The poly-ub proteins that were increasing in abundance with age were filtered for those that retained a high proportion of pre-existing proteins To test results against current knowledge of liver

aggregates we looked among top candidates, proteins showing the highest significance and magnitude of change, for proteins which are well established to aggregate in the liver in current literature.

Mallory Bodies (MBDs) are a highly studied and characterized aggregate in the liver associated with fatty liver disease [215]. These aggregates are known to be highly modified with poly-ubiquitin [216] and are composed primarily of a single protein of known identity - keratin 8 [215]. There is also an increased risk of having MBDs with age in both mice and humans [217,218]. Interestingly, keratin 8 was among the proteins showing the largest abundance increases in the ubiquitinated fraction in addition to being highly composed of pre-existing proteins (Table 1). In addition, western blotting for Keratin 8 in the insoluble and soluble fractions showed that Keratin 8 became increasingly insoluble with age (Figure 4-5), further suggesting heavy-label MS may be an effective method of uncovering the identities of novel aggregate-prone proteins.

Keratin 8	Old CR	Old RP	Old Ctl	
Δ Abundance	-1.82	-2.95	3.01	UB-modified (positive) or unmodified (negative)
% New Protein	9.08	0.6	-6.26	Newly synthesized (positive) or pre-existing (negative)

*Log2 Fold Change Scale

Table 4-1 Changes in poly-ubiquitinated Keratin 8 abundance and proportion of pre-existing protein

While the data provided by the poly-ubiquitinome provides evidence of accumulation of a protein as well as retention of the pre-existing copies, this does not conclusively indicate that a protein is forming an insoluble aggregate – a protein could just as easily be accumulating in solution. In order to further refine our list of possible candidates to account for this, we performed another round of MS analysis on the lysates from the same mice, however, for each mouse we prepared the insoluble fraction in addition to the soluble fraction. As the earlier ubiquitin pulldowns had already been done in 8M Urea, we prepared the insoluble pellets from a low-speed spin of remaining whole-lysates followed by a solublization of the pellet with an 8M Urea-containing buffer.

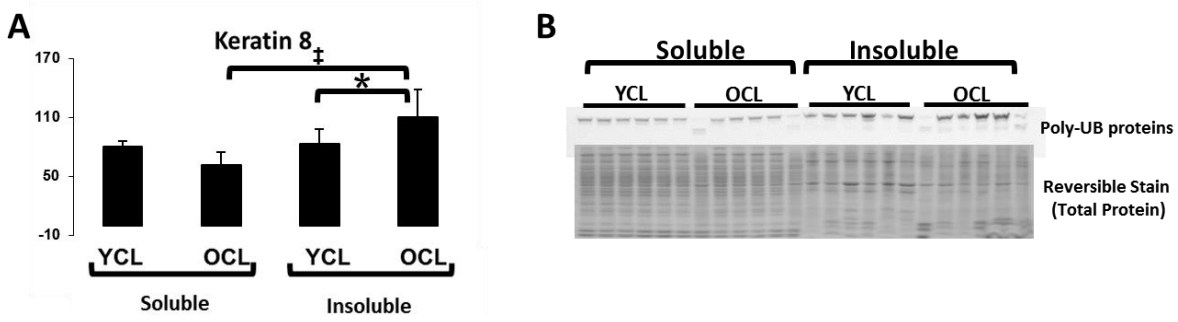

Figure 4-5 Keratin 8 increases and become increasingly insoluble with age. A) Increased insoluble Keratin 8 with age by B) western blotting (normalized to total protein reversible stain).

To get a visual confirmation of the aggregation of Keratin 8, we performed confocal microscopy imaging on Keratin 8 and poly-ubiquitin, both highly associated with Mallory Bodies, in order to get a visual confirmation of the presence of insoluble aggregates within these mice. Indeed, we confirmed an accumulation of Keratin 8 formed poly-ubiquitinated accumulations in old mouse tissue. Interestingly, both CR and RP mice were protected from the effect seen in old WT mice (Figure 4-6). Ongoing studies are investigating the remaining list of candidate “aggregator” proteins, as shown in Table 2.

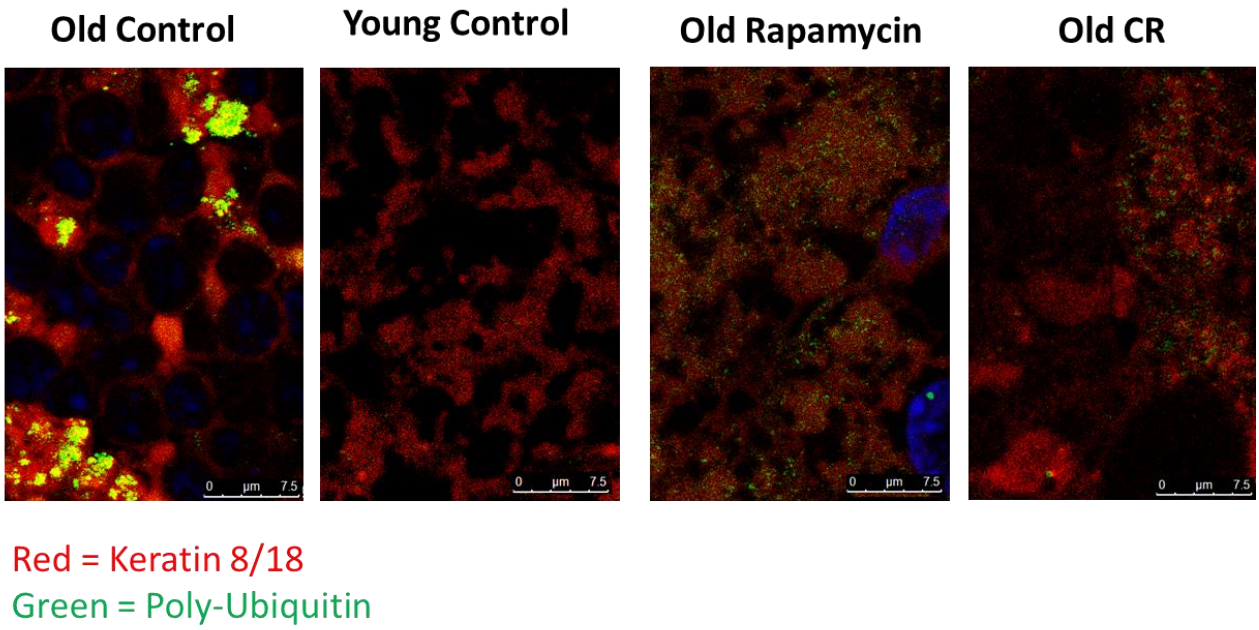

Figure 4-6 Confocal microscopy of Keratin 8 and Poly-Ubiquitin.

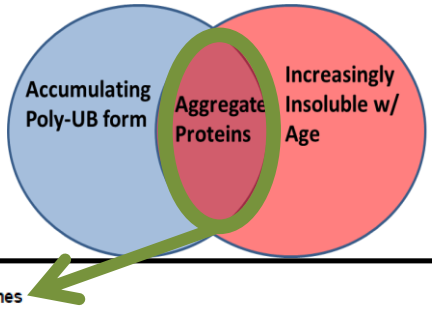

Entry	Entry name	Protein names	Gene names
P41216	ACSL1_MOUSE	Long-chain-fatty-acid--CoA ligase 1 (EC 6.2.1.3) (Long-chain acyl-CoA synthetase 1) (LACS 1)	Acsl1 Acsl2 Facl2
P57780	ACTN4_MOUSE	Alpha-actinin-4 (Non-muscle alpha-actinin 4)	Actn4
Q9Z0X1	AIFM1_MOUSE	Apoptosis-inducing factor 1, mitochondrial (EC 1.1.1.-) (Programmed cell death protein 8)	Aifm1 Aif Pdcd8
P47740	AL3A2_MOUSE	Fatty aldehyde dehydrogenase (EC 1.2.1.3) (Aldehyde dehydrogenase 3) (Aldehyde dehydrogenase family 3 member A2)	Aldh3a2 Ahd-3 Ahd3 Aldh3 Aldh4
Q8BWF0	SSDH_MOUSE	Succinate-semialdehyde dehydrogenase, mitochondrial (EC 1.2.1.24) (Aldehyde dehydrogenase family 5 member A1)	Aldh5a1
Q03265	ATPA_MOUSE	ATP synthase subunit alpha, mitochondrial	Atp5a1
P56480	ATPB_MOUSE	ATP synthase subunit beta, mitochondrial (EC 3.6.3.14)	Atp5b
P24270	CATA_MOUSE	Catalase (EC 1.11.1.6)	Cat Cas-1 Cas1
P58252	EF2_MOUSE	Elongation factor 2 (EF-2)	Eef2
P11276	FINC_MOUSE	Fibronectin (FN) [Cleaved into: Anastellin]	Fn1
P08113	ENPL_MOUSE	Endoplasmin (94 kDa glucose-regulated protein) (GRP-94) (Endoplasmic reticulum resident protein 99)	Hsp90b1 Grp94 Tra-1 Tra1
P26041	MOES_MOUSE	Moesin (Membrane-organizing extension spike protein)	Msn
Q8VDD5	MYH9_MOUSE	Myosin-9 (Cellular myosin heavy chain, type A) (Myosin heavy chain 9) (Myosin heavy chain, non-muscle IIa)	Myh9
O88428	PAPS2_MOUSE	Bifunctional 3'-phosphoadenosine 5'-phosphosulfate synthase 2 (PAPS synthase 2) (PAPSS 2) (Sulfurylase kinase 2)	Papss2 Atpsk2
P62962	PROF1_MOUSE	Profilin-1 (Profilin I)	Pfn1
P26039	TLN1_MOUSE	Talin-1	Tln1 Tln

Table 4-2 Top candidate "aggregator" proteins

4.4 MATERIALS AND METHODS

4.4.1 Animals

C57BL/6 female mice were purchased at 3 and 25 months of age (Figure 4-1A) from the NIA Charles River colony. Female mice were used as a past study showed that the effects of RP in murine aging were larger in this gender [219]. Mice were housed at 20ºC with a 12-hour light and dark cycle. All animals were handled according to the guidelines of the Institutional Animal Care Committee of the University of Washington and the National Institutes of Health. One week after arrival, all mice were started on a synthetic diet (Harlan Teklad diet #TD.99366) that was nutritionally similar to the NIH-31 standard for rodents. The use of this diet facilitated the subsequent substitution of heavy-labeled [5,5,5 – $^{2}H_{3}$] leucine for light leucine, which enabled the protein turnover measurements. Mouse weights and food intake were recorded weekly. The young and old mice were individually housed after three weeks of acclimation to the synthetic chow and were randomly assigned to three groups: 1) an *ad libitum* synthetic food regimen [9]; 2) rapamycin-containing synthetic diet (RP) and 3) calorie restricted (CR), as detailed in the supplemental methods.

4.4.2 Mass spectrometry

Portions of harvested mouse livers were used for MS analysis to determine abundance and proportion of newly synthesized and pre-existing poly-ubiquitin-modified proteins. In order to purify poly-ubiquitinated proteins, liver lysates were immuno-purified with a previously described poly-ubiquitin specific FK2 antibody [220]. Each liver lysate was split into two samples for incubation on filtration columns with either the FK2 antibody or an isotype control antibody. To prevent enrichment of interacting proteins, lysates contain highly denaturing 8M urea which does not affect the FK2 antibody binding. Columns are washed several times and eluted with 100mM Glycine, pH 2.8. Protein from each sample will be methanol-chloroform precipitated and re-suspended into a trypsin compatible buffer followed by trypsin digestion, neutral ion removal, and MS analysis as described earlier.

Using the software Topograph (described earlier), we measured abundance and the proportion of new and existing proteins within poly-ubiquitinated proteins. To further control for non-specific contaminants,

the values obtained in the FK2 enrichments are later corrected to the control enrichments (protein by protein).

4.4.3 **Data Repository**

The raw data from MS/MS and extended supplementary files are available at https://chorusproject.org/pages/blog.html#/961In order to view the data, a free account must be obtained by following the instructions on the Chorus Project website. For R-scripts, spreadsheets, and other data please contact the corresponding author.

4.4.4 **MS Data Analysis**

MS data were processed with the Hardklor (v1.33) and Bullseye (v1.25) algorithms to refine precursor mass measurements(20,21), followed by database search against all mouse entries of the UniProt database (UniProt release 2013_02) with the SEQUEST algorithm (vUW2012.01.7) – searching a total of 74,888 protein entries that were designated Mus musculus (Mouse). A dynamic modification of 3.0188325 for leucine was set to account for [5,5,5-2H3]-leucine and a static modification of 57.021461 for cysteine was set for carbamidomethyl modifications. The precursor monoisotopic mass tolerance was set to ± 10 ppm and the fragment mass tolerance window was set to 0.36 m/z. Enzyme specificity was set to semi-tryptic, allowing for up to 2 missed cleavage sites per peptide. The false discovery rate for spectrum matches was determined by the Percolator algorithm (v2.04) using a reversed copy of the UniProt database as a decoy [221]. Only results with a q-value less than 0.01 were kept for further analysis. This filter was used as it allows a small number (1%) of false positives to the next portion of analysis while providing enough data for categorization and statistical analysis of subsets of proteins. In addition, less than 5% of accepted false positives are expected to pass a subsequent turnover score filter, described below.

Topograph (v1.1.0.297) software performs estimation of peptide turnover rates in stable-isotope labeling experiments. It was designed with the unique ability to calculate the enrichment of amino acid precursor pool, allowing an accurate estimation of peptide turnover rates when the amino acid precursor pool is not

fully labeled [88]. (http://proteome.gs.washington.edu/software/topograph/). Determining precursor relative isotope abundance (RIA) is a critical step in accurately estimating the fraction of newly synthesized and pre-existing peptides.

Prior to analysis of abundance and turnover, peptides with a turnover score less than 0.98 were filtered out of the data. Turnover score is a metric internal to Topograph, ranging from 0 to 1, which describes the closeness of each observed isotopologue distribution with its closest matching theoretical distribution. A cutoff score of 0.98 was derived by plotting a receiver operator curve of true positive results versus true negative results (not shown), where true positive was defined as any peptide measurement that fell within 2 standard deviations of the mean label enrichment for all peptides, and true negatives were results that did not meet these criteria.

Relative peptide abundances were determined by integrating MS1 peaks. For peptides that were identified in one sample, the regression of the identified peptide's MS/MS scan number is used to estimate a window for the same peptide in the other samples and a matching chromatographic peak was identified within that time range. This method allows peaks areas to be measured even in samples in which they are low and otherwise difficult to identify [222].

Only peptides that uniquely mapped to a single UniProt protein accession for Mus Musculus (UniProt release 2013_02), consisting of 74,888 entries from UniProtKB/Swiss-Prot and UniProtKB/TrEMBL, were used for quantification of abundance and turnover. First, sequences were searched against Swiss-Prot (reviewed) entries and accepted in a unique match is found. If no match was found, a second search was performed on TrEMBL (unreviewed) entries and the unique matches were retained. All remaining peptides, consisting of peptides with either no matching proteins or greater than 1 matching protein, were filtered out. For the cases where a protein consisted of more than one peptide, statistical models were modified to account for the multiple peptides by using a blocking factor. For each protein we applied non-linear regression fits of first order exponential curves to the percent newly synthesized protein using: $y = 100 + \beta 1 e \alpha t$. To determine whether the rates of turnover (slopes, α) were statistically different between

experimental groups, ANCOVA was used. Half-lives are calculated directly from slopes, where t1/2 = $\ln^{223}$/ slope. For details see the methods supplement of Hsieh et al. 2012 [88].

4.4.5 Pathway analysis

Top pathways were determined using QIAGEN'S® Ingenuity Pathway Analysis (IPA®, QIAGEN Redwood City, www.qiagen.com/ingenuity) on all proteins which were significantly changed (p-value < 0.05) in abundance or half-life by aging (OWT vs YWT) or mCAT (YmCAT vs YWT and OmCAT vs OWT) expression. IPA determines the p-values of enrichment into canonical pathways by Fischer exact test.

All significantly changed proteins were then grouped by IPA canonical pathway and z-scores were visualized on a heatmap created in R using the gplots package. Values within each pathway category were clustered by Ward's method.

4.4.6 Immunoblotting and ELISA

A portion of each tissue was aliquotted into separate tubes containing cold isolation buffer (250 mM sucrose, 1 mM EGTA, 10 mM HEPES, 10 mM Tris-HCl pH7.4) as well as protease and phosphatase inhibitors (Pierce #87786 and #78420, Waltham, MA, USA) at the time of harvest, and stored at -80 degrees Celsius to be used for immunoblotting and other bench assays as necessary. Western blotting was done on the NuPAGE® Bis-Tris gel system (Life Technologies #WG1403BOX, Carlsbad, CA, USA) according to the manufacturer protocols with primary antibody concentrations of 1,000X and secondary antibody concentrations of 10,000X. The following primary antibodies were used: multi-ubiquitin FK2 (D058-3, MBL), agarose conjugated multi-ubiquitin FK2 (D058-3, MBL), FK2 isotype control (M075-3), agarose conjugated FK2 isotype control (M075-8), Secondary antibodies: Donkey anti Rabbit (42PI31458, Waltham, MA, USA), Goat anti Mouse (42PI31432, Waltham, MA, USA), and Rabbit anti Goat (42AP106P, Waltham, MA, USA), Qdot 705 (Q-11061MP. Thermo Fisher), Qdot 585 (Q-11011MP, Thermo Fisher)

RESPIRATORY CHAIN PROTEIN TURNOVER RATES IN MICE ARE HIGHLY HETEROGENEOUS BUT STRIKINGLY CONSERVED ACROSS TISSUES, AGES AND TREATMENTS

5.1 SUMMARY

The mitochondrial respiratory chain (RC) produces the vast majority of cellular ATP and requires strict quality control mechanisms to sustain metabolic homeostasis. To examine RC subunit proteostasis *in vivo*, we measured RC protein half-lives (HL) in mice by LC-MS/MS using metabolic $^{2}H_{3}$-leucine heavy isotope labeling under divergent conditions. We studied seven tissues/ fractions of young and old mice, under control diet, or one of two diet regimens (caloric restriction or diet with rapamycin) that alter protein turnover (42 conditions in total) with up to a 11.5 -fold difference in mean HL. Normalization to the mean HL of each treatment/condition showed that relative HLs were conserved across conditions (Rho=0.57, p<10-4), but were highly heterogeneous between subunits, with a 7.3-fold mean range overall, and a 4.6-fold range within complex I alone. To identify factors regulating this conserved distribution, statistical analyses were performed to study the correlation of HLs to properties of subunits. HLs significantly correlated with localization within the mitochondria, evolutionary origin, location of protein-encoding, and ubiquitination levels. These findings challenge the notion that all subunits in a complex turnover at comparable rates and suggest that there are common rules governing the differential proteolysis of RC protein subunits under divergent cellular conditions.

5.2 INTRODUCTION

A primary function of the mitochondrion is to maintain the four electron transfer complexes (ETC) I-IV and an ATP Synthase, complex V, which generates the currency of cellular energetics ATP. Together these complexes form the mitochondrial respiratory chain (RC). Due to electron leakage from the ETC during oxidative phosphorylation, mitochondria are also the major source of reactive oxygen species (ROS) in the cell [224] and therefore require a network of quality control systems to maintain protein homeostasis. Continuous fission and fusion serves to protect the integrity of the mitochondrial [225] network, with damaged mt regions being subject to mitophagy, a bulk removal process [226]. Additionally, proteases and chaperones within each mt compartment oversee proper folding or degradation of damaged proteins [227]. Accumulating evidence indicate that the ubiquitin proteasome system (UPS) also plays a role in mt protein degradation [228]. However, in the event of mt protein damage exceeding the organelle's quality control capacity, a collective cellular response termed mt unfolded protein response (mtUPR) is initiated; a mitochondria-to-nucleus signal transduction pathway that up-regulates genes encoding mt chaperones and proteases [229]. Even though these multiple quality control mechanisms limit mt damage, failure to maintain mt protein quality control is believed to underlie many pathological events and aging [230]. Understanding mt proteome dynamics can provide a framework for the investigation of protein quality control in the mitochondria [11]. In spite of this, there is a paucity of understanding of the mechanisms of mt dynamics and quality control in the study of mt pathologies and aging. In addition, no studies have attempted to identify common underlying components of mt protein dynamics across varying tissues and metabolic conditions.

Early studies investigating mt protein turnover reported that it is a unitary process involving the whole organelle, suggesting that all mt proteins turn over at similar rates [77,231,232]. Consistent with this view, several recent reports show that proteins localized to specific organelles or belonging to complexes often have similar turnover rates [93,233]. In particular, it has been suggested that RC complexes and supercomplexes are maintained in unitary solid states [234,235]. However, other investigators have found less homogeneity in mt turnover rates within respiratory complexes and challenge the notion of unitary turnover. Kim and colleagues reported wide differences in mt protein half-lives within heart and liver tissues, suggesting a complexity in regulation of the mt RC proteome [84]. In contrast to previous reports,

these authors also showed that subunits of RC complexes turn over with different kinetics, albeit over a narrow range. A recent study of Arabidopsis mt proteins also reported a wide (30-fold) range of degradation rates within the RC [236], supporting a more protein-specific turnover process rather than a unitary one.

Using a newly developed mass spectrometry method that accounts for precursor pool enrichment [88], we examined the *in vivo* turnover rates of over 250 mt proteins including 84 individual RC proteins in mouse heart, liver, skeletal muscle, and the brain cortex. To examine conditions that modify cellular homeostasis, we investigated the effect of aging, caloric restriction (CR) and the "CR mimetic" rapamycin (RP) [25,138] on mt proteome dynamics. CR and RP target the mTORC1 complex to alter protein synthesis and degradation rates [21], making them useful modulators of cellular proteostasis.

5.3 RESULTS*

5.3.1 Experimental design and protein half-lives of RC proteins

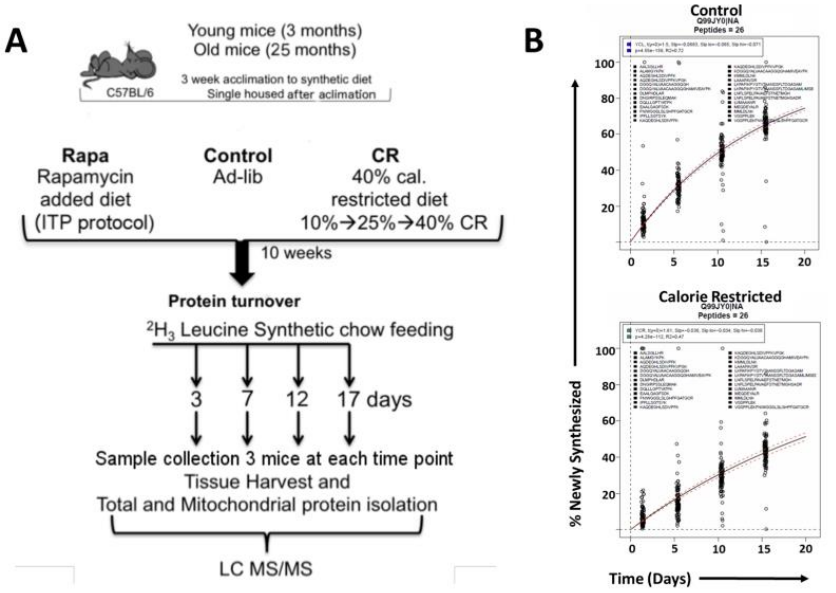

Figure 5-1 Summary of the experimental design showing young (3 mo) and old (25 mo) C57BL/6 female mice maintained on a control diet or fed ad libitum, an encapsulated RP (14 ppm)-containing diet, or a CR (40% restricted) diet for 10 wk. Mice were subsequently switched to the same basic diet but with leucine replaced with [3H2]-leucine and euthanized 3, 7, 12, or 17 d thereafter. Heart, liver, brain cortex, and the skeletal muscles EDL and soleus were harvested, and LC-MS/MS was performed on tryptic peptides of total lysates or purified mt. B) The protein turnover rate was determined by fitting the fractional syntheses of peptide isotopomers of a protein into an exponential curve of first-order kinetics over the labeling period. Individual data points represent all peptide isotopomers that matched a single protein.

The experimental design is summarized in Figure 5-1A. All mice were maintained on three diet regimens for 10 weeks and their stabilized weights varied less than 1.1% in the final 5 weeks. Total proteins were extracted from liver, heart and brain. Mitochondria were also purified from heart and liver and two skeletal muscles, extensor digitorum longus (EDL) and soleus, prior to protein extraction. Trypsin-digested peptides from lysates were analyzed by shotgun nLC/MS-MS followed by protein synthesis measurements using the software Topograph [88]. We measured turnover rates for up to 84 proteins of the RC (out of 90 known RC proteins) for each of six age/treatment groups in each of seven tissues or tissue fractions. This is the highest coverage for RC protein HL measurement to date. Average HLs of the RC proteins in each tissue and age or treatment group are shown in Table 1. Mean HL in different tissues ranged from 5.2 days (liver) to 33.9 days (EDL), a 6.5-fold difference. In comparison to heart, the two muscle types had 5-10% longer average HLs, while the liver proteins had about 80% shorter HLs (Table 1). There was no significant change in HLs with age except after CR. Both the CR and RP treatments resulted in significantly altered half-lives ($p< 10^{-5}$), with CR having the largest effect -- 38-60% longer HLs than young controls, compared

* Supporting information such as supplementary figures, tables, datasets, and methods can be found online: http://blogs.uw.edu/nbasisty/home/136-2/

to 16-19% longer half-lives after RP. The substantial shifts in distribution of HLs between tissues are further illustrated by histograms shown in Supplementary Figure 5-1A. All RC protein HL values are listed in Supplementary Dataset 1.

5.3.2 RC protein HL relative differences are broadly conserved across tissues and treatments

To compare the relative distribution of RC HLs within each condition we normalized individual HLs in all tissues and treatments to their mean HLs, as displayed in Figure 5-2A. The mean value for each protein (in rows) across all conditions (in columns) is shown in the right-most column. With the tissue/treatment differences accounted for in this way, the RC proteins span a 7.3-fold range between longest and shortest mean HLs. Complex I (CI) proteins had the broadest range of normalized HLs, ranging 4.6-fold (n= 42), while complex V (CV) had the smallest range, 2.2-fold (n=13). In spite of the substantial differences in tissue and treatment half-lives (Table 1), the normalized heatmap shows broad conservation of HLs across tissues and conditions. Subsets of proteins with relatively homogenous normalized HLs within complexes can be appreciated by the horizontal color bands. This effect, measured as the average correlation between mouse groups, was highly statistically significant (Spearman's rho = 0.57, $p < 10^{-4}$), illustrating that the relative (normalized) differences in RC protein HLs are highly consistent across tissues and treatment groups, in spite of the large differences in average HLs that we observed between tissues and treatments (Table 1). The average normalized HL across all tissues, ages and treatments is shown as a separate column to the right of the tissue groups on the heat map and this same color is plotted onto schematics of the RC complexes and proteins (Figure 5-2B), based on known location information [237-244]. All mean normalized $\log_2$ HLs are listed in Supplementary Dataset 2.

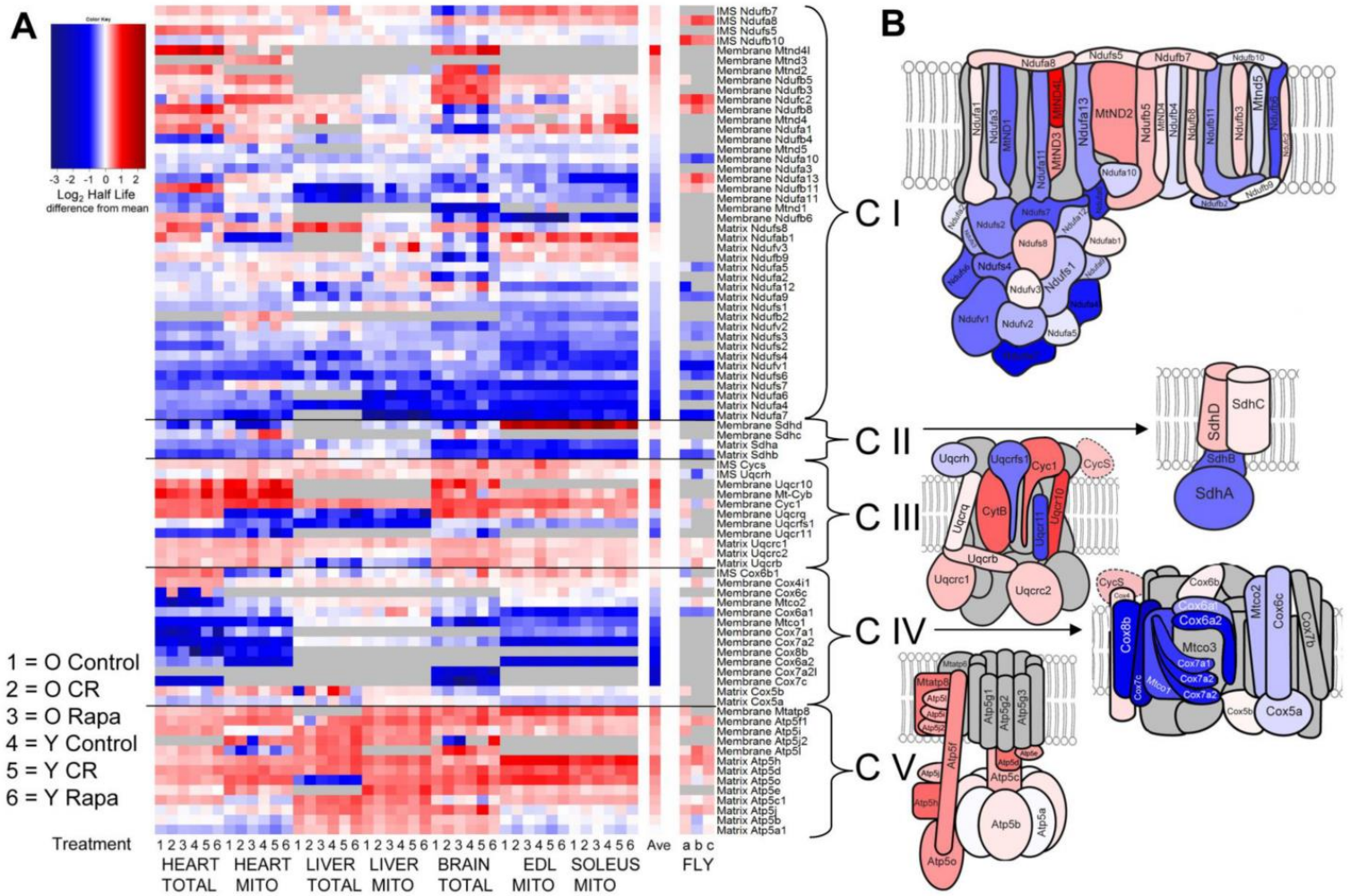

Figure 5-2 Heat map of RC protein relative HLs shown for 6 experimental groups in 7 tissue types. A) All protein HLs are normalized to the mean HL of their respective tissue and treatment group (columns). The 6 age-treatment groups are numbered (see key). Protein subunits in each complex are grouped according to their location in the mitochondrion IMS, membrane, and matrix. The relative log2 HLs, ranging from 23.4 to +2.5 (58-fold) around the mean, are depicted in a color gradient from dark blue to dark red (see color key). Gray: values missing in the MS data. The rightmost 3 columns depict mean-adjusted HLs of orthologous proteins from fly heads (columns a, WT; b, parkin and c, Atg7 mutant flies) from Vincow et al. (39). B) The RC complexes showing the subunit topology within each complex. The proteins are colored according to their average relative HL across all mouse treatments and tissues (the rightmost column of the mouse heat map).

5.3.3 **Mouse RC protein turnover is evolutionarily conserved**

The heterogeneity in RC protein relative HLs maybe evolutionarily conserved in lower organisms, as suggested by the conserved colors in 43 orthologous proteins from fly data previously published by Vincow et al. [245]. Data sets from wild type and *parkin* and *Atg7* mutants are shown in the three rightmost columns of Figure 5-2A. The mouse protein average HLs correlated significantly with the fly protein average HLs (Spearman's rho = 0.58, $p = 9.2 \times 10^{-5}$, Supplementary Figure 5-2 B, C).

5.3.4 **RC protein HLs are correlated with cellular location**

Proteins localized in the matrix of CI had 16% shorter HLs on average (faster turnover) than the CI membrane proteins, a difference that was highly significant after adjusting for tissue and treatment effects ($p = 1x10^{-19}$, Figure 5-3A). A similar pattern was previously reported for *Arabidopsis thaliana* RC proteins, with exceptions of carbonic anhydrase (CA) and CA-like subunits which are unique to plants [236]. In our study, this association of shorter HLs in matrix proteins was also statistically significant for complexes II and V l ($p = 1x10^{-19}$ and 0.027, respectively), with an average 41% and 5% shorter HLs in the matrix than their corresponding inner membrane proteins, respectively. However, this relationship was opposite in CIII (9% longer HLs in the matrix, p=0.03) and CIV (44% longer HLs in the matrix, p<0.00001), with CIII having generally longer HLs (21% longer, p<0.049) and CIV having shorter HLs (29% shorter, p<0.01) than other complexes (Figure 5-3A).

The average HLs of each of the 5 RC complexes, after adjustment for differences in subunit location, tissue and treatment, were significantly different for all pairwise comparisons ($p < 10^{-6}$, Figure 5-3B) except between CII and CIV, demonstrating complex-specific differences in turnover rates.

5.3.5 **Ancestral origin is highly correlated with RC protein HLs**

To determine whether evolutionary origin of RC subunits have an effect on protein turnover rates, we tested for correlation between HLs and ancestral age using a linear regression model. Each protein's origin was assigned to one of six ancestral ages including the ancestral bacterium, last eukaryotic common ancestor (LECA), unikonts, opisthokonts, metazoa, and vertebrata [246] (Supplementary Figure 5-2A). Complex II represents only a single ancestral group and was therefore removed from the linear analysis. The analysis was also restricted to ancestral groups that were present in all 4 remaining

complexes, i.e., bacteria (group 0), LECA (group 1) and Opisthokonts (group 3). The analysis was also restricted to ancestral groups that were present in all 4 remaining complexes, i.e., bacteria (group 0), LECA (group 1) and Opisthokonts (group 3). There was linear correlation of half-lives with ancestry groups 0, 1, and 3 ($p = 0.013$) and this improved further upon adjusting for the complex-differences noted above (Figure 5-3C, $p = 2x10^{-5}$). This data suggests that RC proteins with the earliest evolutionary origins, bacterium, likely have shorter HLs (faster turnover). Bacterial ancestry proteins were 4% shorter lived compared to LECA and 11% shorter lived compared to those more recently evolved, the opisthokonts (Figure 5-3C). One explanation for this could be their close proximity to electron transport and the catalytic core.

5.3.6 The order of assembly does not correlate with complex I turnover

We assigned complex I subunits into three sequential stages of assembly as previously reported [244,247]. We hypothesized that early assembled subunits might be less likely to turn over faster because they would be more stably associated with or internal to the complex structure. However, there was no significant (linear) correlation between assembly order and CI HLs ($p = 0.635$, CI [0.98, 1.04] for ratio of HLs between groups). This result is inconsistent with the view that subunits that are incorporated last turn over faster compared to subunits that are incorporated at early stages and become "protected" by their internalization as suggested by Kim et al. [84]. It also suggests that subunits that are incorporated last are not subject to appreciably greater proteolysis in the free environment.

5.3.7 The origin of protein encoding correlate with RC protein HLs

Mitochondria contain multiple copies of a 16.5-kb circular genome that encodes 13 essential subunits of four of the five RC complexes (I, III, IV, and V). All 13 proteins are hydrophobic integral proteins located in the inner membrane. The rest of the ETC proteins are encoded by the nuclear genome and are imported into the mitochondria by the TIM/TOM "translocase" proteins [248]. To determine if the location of protein synthesis has an effect on protein turnover, we compared nuclear DNA (nDNA) encoded protein HLs with mitochondrial DNA (mtDNA) encoded proteins, adjusting for tissue, age, treatment, and complex. Proteins encoded by the nuclear genome had 14% shorter HLs on average compared to mtDNA-encoded ETC proteins ($p = 1x10^{-10}$). Since all mtDNA-encoded proteins reside in the membrane-spanning region, we also compared their HLs to HLs of only the membrane integral RC proteins encoded by the nDNA. The

difference was maintained with 16% shorter HLs in nDNA-encoded membrane subunits compared to mtDNA-encoded proteins ($p = 9x10^{-10}$). Our data suggest that even within the same sub mitochondrial location, nDNA-encoded proteins turnover faster than mtDNA-encoded proteins. This may be due to additional proteostatic process(es) during the transit of nDNA-encoded proteins to the RC, however, the faster turnover that we observed of the nDNA-encoded RC subunits did not differ between total and mt fractions (ratio of HLs 0.999, CI [0.88 - 1.13], p = 0.99) and this would not be as supportive of the concept that degradation of subunits before entry into mitochondria is appreciably affecting turnover rates. Thus, RC proteins synthesized in the cytoplasm might instead be subject to additional proteostatic process(es) during their transit through the mitochondrial intermembrane space.

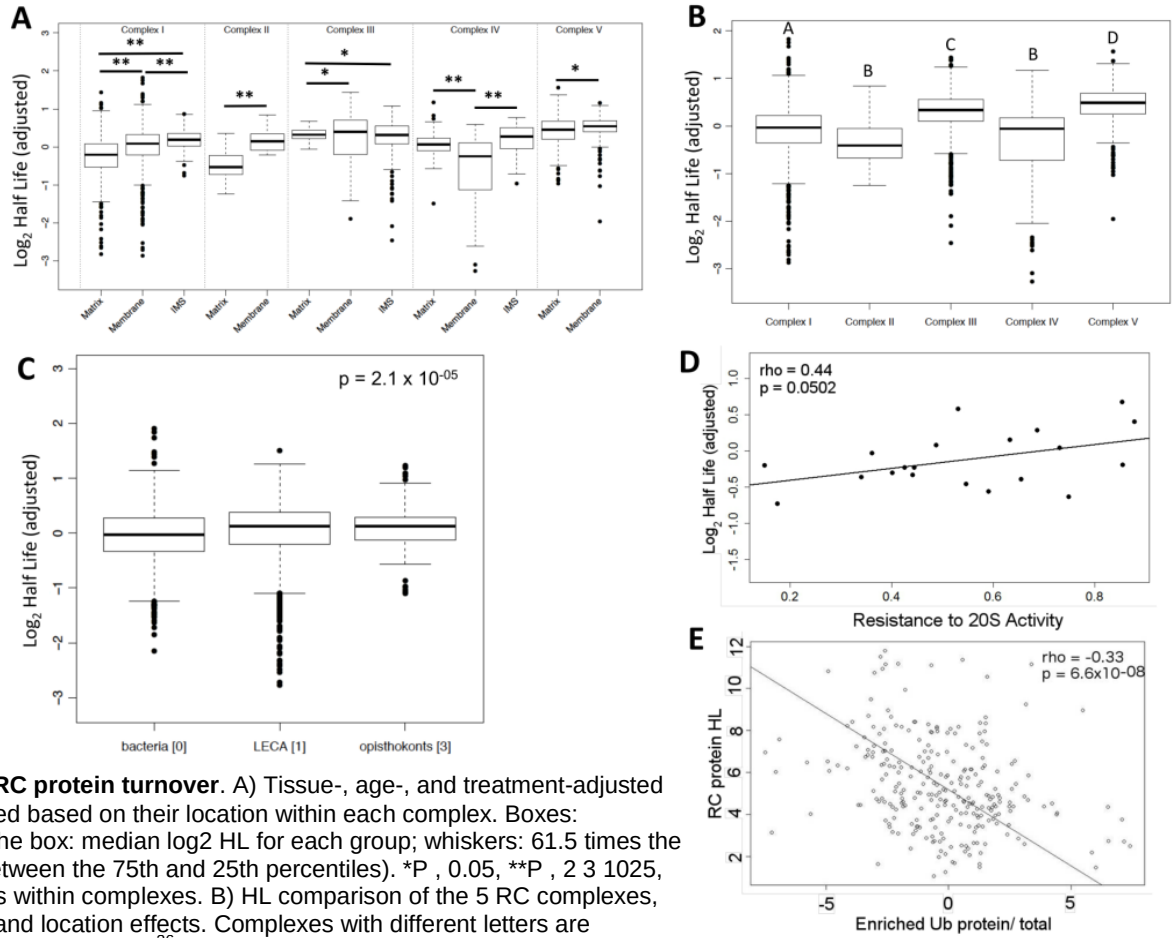

Figure 5-3 Factors affecting RC protein turnover. A) Tissue-, age-, and treatment-adjusted (log2) HLs of RC proteins plotted based on their location within each complex. Boxes: interquartile range; line within the box: median log2 HL for each group; whiskers: 61.5 times the interquartile range (distance between the 75th and 25th percentiles). *P , 0.05, **P , 2 3 1025, differences between 2 locations within complexes. B) HL comparison of the 5 RC complexes, adjusted for tissue, treatment, and location effects. Complexes with different letters are significantly different from each other ($P < 10^{-26}$). C) Log2 HLs of CI, -III, -IV, and –V adjusted for tissue, treatment, and complex effects correlated with ancestral levels of bacterium, LECA, and opisthokonts. D) Correlation of normalized log2 HLs of RC proteins with their resistance to degradation by the 20S proteasome. The degradation values are from Lau et al. (43). E) Correlation of RC protein HL and ubiquitin enrichment of the same proteins, as determined by poly-ubiquitinated protein antibody pulldown and LC-MS/MS.

5.3.8 **RC protein ubiquitination correlate with HLs**

To investigate the involvement of proteosomal degradation systems in RC protein turnover we utilized recently reported measurements of cardiac proteome susceptibility to proteolytic degradation [249]. The linear correlation between our HL measurements and 20s proteasome degradation susceptibility of RC proteins was statistically significant (Figure 5-3D, rho = 0.44, p = 0.05). In contrast, correlation between HLs and the reported susceptibility to degradation by the endogenous mitochondrial proteases did not reach significance, although it was trending (p = 0.089). These results are consistent with the observation of Lau et al. [249] that the 20s proteasome has a selective effect on the turnover of specific mitochondrial proteins, including RC subunits.

We extended these observations by measuring the abundance of ubiquitinated RC proteins from the liver, using an anti-polyubiquitin pulldown assay corrected for non-specific binding and comparing this to the total abundance of each protein. RC protein HL showed a significant negative correlation with ubiquitin enrichment (Figure 5-3E, rho = -0.33, $p = 6x10^{-8}$). Both these measures indicate a significant contribution by the 20S proteasome on RC protein dynamics. In fact, recent data highlight the involvement of the 20s proteasome in modulating mt proteome dynamics under oxidative stress conditions [249].

5.4 DISCUSSION

Knowledge of proteome dynamics is essential to understand how cellular systems maintain quality and integrity under varying biological conditions and in different molecular niches. By using a whole-animal metabolic labeling strategy, we examined the *in vivo* mitochondrial proteome dynamics in five different tissues each under the effects of aging, CR, and RP. We used a novel software tool that allowed the accurate determination of fractional protein synthesis and protein half-life, independent of variation in the precursor pool relative isotope abundance [88].

We observed a 7.3-fold range in normalized RC protein turnover rates, with up to 4.6-fold range within a complex. Protein HLs in different tissues vary greatly and CR and RP are known to affect protein synthesis [84,160,174]. Examination of HLs in different tissues and with these interventions allow us to deduce whether the observed diversity in RC turnover is tissue specific and if it is affected differentially by changes in overall turnover rates. Our findings reveal that in spite of the large differences in HL between tissues and age/treatments (Table 1), the pattern of diversity in turnover dynamics is conserved across the tissues/age/treatment groups (Figure 5-2A). The great heterogeneity in mt HLs cannot be readily explained by a macro degradation process such as mitophagy [250]. The evidence instead supports a process of individually targeted protein recycling of RC subunits, such as proteolysis by intra-mitochondrial proteases or the ubiquitin proteasome system. Several lines of evidence support the presence of a pathway that retro-translocates damaged mt proteins to the outer mitochondrial membrane (OMM) for ubiquitination and targeting to the proteasome [251,252]. For example, proteasome inhibition was shown to lead to a significant accumulation of key respiratory chain proteins, both mtDNA and nDNA-encoded [253], some by retrotranslocation to the OMM where ubiquitination and degradation occurred [249]. Consistent with this, we observed a significant positive correlation between our HL measurements and the reported susceptibility to 20s proteasome degradation (Figure 5-3D) and a highly significant correlation between HL and the relative ubiquitination levels of RC proteins (Figure 5-3E). These results indicate a role for the UPS in RC protein turnover in mice.

The broad variation in mitochondrial protein HLs that we observed (Figure 5-2A) is consistent with previous data from Arabidopsis[236], Drosophila[245] and mice [84], and the large differences seen between tissues (especially liver vs. others) is dramatic but consistent with previous data. However, our observation that a specific pattern of heterogeneity is maintained within the RC, both within and between individual complexes, and is broadly conserved across tissue and treatments is unexpected. The possibility that this finding is evolutionarily highly conserved is suggested by the strong correlation observed between mouse RC HLs and the average of the orthologous fly protein HLs that have been previously reported [245] (Supplementary Figure 5-2B, C). Our data support previous studies that have shown that mt protein quality control mechanisms [254], are highly conserved but add to the understanding that to a large extent, common mechanisms govern RC protein quality control.

Multiprotein complexes are often responsible for major functional processes in the cell such as protein translation (ribosome), degradation (proteasome), and oxidative phosphorylation (RC). A range of prior studies have suggested that the constituents of these protein complexes turn over at similar rates in a coordinated fashion [84,93,233,255,256]. However, exceptions to this have also being reported, showing variability in turnover within well-defined complexes [84,257]. In our data, we detected a wide range of turnover rates between and within RC complexes. This variability was in part correlated with protein localization in the mitochondria. For instance, proteins located in the matrix generally had faster turnover than their respective membrane or IMS proteins (Figure 5-3A). One explanation for this could be increased oxidative damage and faster turnover in the high-ROS matrix owing mostly to complexes I and III, which produce the majority of ROS created by the RC [224,258]. Interestingly, assembly factors in all complexes displayed faster turnover rates compared to other localization groups (e.g., in CI 20% faster vs. matrix subunits, $p<0.0001$; CIII 54-58% faster vs. matrix and membrane subunits, $p<0.0001$), concordant with recent reports that showed faster turnover kinetics for mitochondrial assembly factors or chaperones [84,236]. Overall, this data suggest that proteins within RC protein complexes appear to turnover in a heterogeneous fashion and that turnover correlates with subunit localization. In contrast, there was no significant correlation in HLs with stages of CI assembly, inconsistent with the view that exposed

subunits that are incorporated last would turn over faster compared to subunits that are incorporated at early stages, becoming “protected” by their internalization.

Interestingly, our data also show that the location of RC protein synthesis, i.e., the cytoplasm for the nDNA-encoded subunits vs. mitochondrial matrix for the mtDNA-encoded proteins, has a small, but significant effect on protein turnover: RC proteins synthesized in the cytoplasm turnover 14-16% faster, but this was observed equally in both total and mitochondrial purified fractions, seemingly at odds with the concept that additional proteolysis in the cytoplasm explains the HL difference in coding origins. Current literature on mitochondrial protein import suggest, however, that most nDNA-encoded proteins are translated on the OMM, tethered by the nascent polypeptide or the polysome-bound mRNA [248]. If these are tethered in a way that they are co-purified with mitochondria, it would explain our observation. Alternatively, RC proteins synthesized in the cytoplasm may be subject to additional proteostatic process(es) during their transit through the mitochondrial intermembrane space.

If RC proteins are recycled before they are incorporated into complexes, the 7.3-fold range of mean normalized HL’s that we observe would require at least 86% of some proteins to be degraded before entry into complexes. It would also require that this process be specific to the mitochondrion, since there is a very modest HL difference between proteins encoded by n-DNA vs. mt-DNA. Understandings of mechanisms of mitochondrial protein turnover and the contribution from various proteolytic systems is still evolving. Mitochondria contain proteases in each mt compartment that sustain a stoichiometric balance between nuclear DNA and mtDNA-encoded subunits, removing excess subunits, dysfunctional, oxidatively modified or otherwise damaged [259]. These proteases are found within mitochondria and play important roles in clearing proteins. Lon and ClpXp are two AAA+ proteases (AAA is ATPase Associated with various cellular Activities) residing in the matrix, while two other AAA metalloproteases, m-AAA (matrix AAA) and i-AAA (intermembrane AAA), embedded in the inner membrane performs quality control in their respective compartments [227,228]. As noted above, this contrasts to mitophagy, a process that degrades whole mitochondria or mitochondrial fragments [250], although autophagy has occasionally be

suggested to play a role in the selective turnover of some mitochondrial proteins [260], including RC proteins, possibly involving the ubiquitin proteasome system [245].

The alternative model of dynamic RC protein exchange in which intermediate subunits and proteins can be readily exchanged or recycled when damaged/unfolded seems equally implausible, as the observed heterogeneity in turnover would require that damaged or misfolded proteins would be released from complexes, followed by reassembly with new protein. This would be inconsistent with the current understanding of a highly structured order of complex assembly [261], and would require a view that allows for reassembly of complexes to continue from "checkpoints" in assembly rather than starting over completely, or perhaps in an order that is not well fixed at all. Such a theory would also need to account for the large variation seen in turnover rates for RC complexes I, III, and IV, which exist as supercomplexes [261,262]. It has been assumed that the formation of these supercomplexes prevent destabilization and degradation while enhancing electron transport efficiency. Is it possible that, even within supercomplexes, protein components are in a state of fluidity where they can be ejected and replaced as needed? A recent report supports a "plasticity model" of RC organization where supercomplexes exist as dynamic aggregates, a state that allows adaptability to varying substrates and specific cellular requirements [262]. This would challenge the "solid state" model of rigid high order assembly [261]. \

In conclusion, this study demonstrates for the first time that the relative turnover of respiratory chain proteins is highly conserved across tissues and conditions that substantially differ in overall homeostasis. The high inter-protein heterogeneity in turnover between and within RC complexes, as well as in non-RC proteins of the mitochondria supports a dynamic, non-unitary mechanism of protein quality control. The high degree of conservation of heterogeneity between tissues and treatments suggests that mechanisms and rules of protein turnover are uniform regardless of tissue-type and relative long or short HLs of tissues or treatments. The similarity to previously reported Drosophila turnover rates suggests that these rules are evolutionarily conserved. The contrasting hypotheses of dynamic RC protein exchange vs. highly heterogeneous degradation of RC proteins in mitochondria *prior* to RC complex assembly are in

need of further study. Regardless of mechanism, the very high relative turnover rates of some proteins indicates that mitochondria impose very stringent quality control, in spite of the very high energetic cost of protein synthesis, and that understanding the rules that govern heterogeneity in turnover should provide new insights into mitochondrial dynamics.

5.5 MATERIALS AND METHODS

Supporting information and supplementary data can be accessed online:

http://onlinelibrary.wiley.com/doi/10.1111/acel.12317/suppinfo

5.5.1 Animals

C57BL/6 female mice at 3 and 25 months of age (Figure 5-1A) were obtained from the National Institute of Aging Charles River colony. Female mice were used, as the effects of rapamycin in murine aging were much larger in this gender [25]. Mice were housed at 20ºC with a 12-hour light and dark cycle in an AAALAC accredited facility under Institutional Animal Care Committee supervision.

5.5.2 Diet Regimens and Feeding

One week after arrival, all mice were started on a synthetic diet (Harlan Teklad diet #TD.99366) to facilitate the subsequent substitution of heavy-labeled leucine diet to enable protein turnover measurements. After three weeks mice were individually housed and randomly assigned to three groups: 1) maintained on an *ad libitum* synthetic food regimen [9]; 2) administered rapamycin-containing synthetic diet (RP); 3) calorie restricted (CR), as detailed below. Mice were maintained on these three regimens for 10 weeks. There was an average of 7.4% body weight loss on the synthetic diet that stabilized a week after start of feeding.

Mice in the CR group received a vitamin and mineral adjusted diet (Harlan diet # TD. 10943) providing the same essential nutrient levels as the control group. CR rations per mouse were calculated based on the age-matched *ad libitum* mouse intake normalized to each restricted animal's starting body weight. Restricted mice received 10% less than control mouse consumption in week 1, 25% less on the second week, and 40% less in the 3rd week onwards. The young CR cohort lost on average ~20% from their stabilized body weights over the 3 week progressive diet restriction. The weight loss of the old CR mice averaged ~25%. After this initial loss, CR mice maintained a stable weight. If any CR mouse lost 30% or more of their stabilized body weight, food rations were increased by 5-10% until they stabilized at 70% of their initial body weight, a limit set by the animal care committee. The old control and Rapa mice

maintained a stable weight over the study period. For details on body weights see the supplementary information of Karunadharma et al. 2015 [201]. Microencapsulated rapamycin was purchased from the University of Texas Health Science Center at San Antonio and administered at 14 mg per kg of food (2.24 mg of rapamycin/kg body weight/day). RP blood levels were measured at 4 weeks and at the time of euthanasia; the mean concentration of RP in young and old mice was 76 ± 8 ng/ml and 44± 4 ng/ml, respectively [201].

5.5.3 **Stable Isotope labeling**

After 10 weeks of diet regimens, all mice were started on a leucine-deficient synthetic diet (TD.09846, Harlan Teklad, Madison, WI) with the light leucine fully replaced by 11 g/kg of deuterated [5,5,5 – $^{2}H_{3}$] – L – leucine (Cambridge Isotope Laboratory, MA), with CR and RP cohort conditions continued as above. Four mice per cohort were euthanized by cervical dislocation at four time points: days 3, 7, 12 and 17 after switching to $^{2}H_{3}$-leucine diet. (Figure 5-1A).

5.5.4 **Mass spectrometry**

Tissues were removed immediately, rinsed in cold saline and homogenized in cold isolation buffer (250 mM sucrose, 1 mM EGTA, 10 mM HEPES, 10 mM Tris-HCl pH7.4). Lysates were centrifuged at 800 x g for 10 minutes to get rid of the debris. A portion of liver, muscle and heart tissue was processed for mitochondrial fractions as previously described [193]. All samples were trypsin digested and LC-MS/MS analysis performed with a Waters nanoAcquity UPLC and a Thermo Scientific LTQ Orbitrap Velos, as previously described [88].

MS data was processed with the Hardklor (v1.33) and Bullseye (v1.25) algorithms to refine precursor mass measurements (45, 46), followed by database search against all mouse entries of the UniProt database (UniProt release 2013_02) with the SEQUEST algorithm (vUW2012.01.7), searching a total of 74,888 protein entries that were designated Mus musculus. A dynamic modification of 3.0188325 for leucine was set to account for [5,5,5-$^{2}H_{3}$]-leucine and a static modification of 57.021461 for cysteine was set for carbamidomethyl modifications. The precursor monoisotopic mass tolerance was set to ± 10 ppm

and the fragment mass tolerance window was set to 0.36 m/z. Enzyme specificity was set to semi-tryptic, allowing for up to 2 missed cleavage sites per peptide. The false discovery rate for spectrum matches was determined by the Percolator algorithm (v2.04) using a reversed copy of the UniProt database was used as a decoy (47). Only results with a q-value less than 0.01 were kept for further analysis

5.5.5 **MS analysis**

Topograph (v1.1.0.297) software was used for the deconvolution and measurement of peptide isotopologue abundances from LC-MS chromatograms and the calculation of peptide turnover rates, as previously described [88]. (http://proteome.gs.washington.edu/software/topograph/). Relative peptide abundances were determined by integrating MS1 peaks. For peptides that were identified in one sample, the regression of the identified peptide's MS/MS scan number was used to estimate a window for the same peptide in the other samples and a matching chromatographic peak was identified within that time range. This method allows peaks areas to be measured even in samples in which they are low and otherwise difficult to identify [263]. For two given LC-MS/MS chromatograms, the MS/MS scan number for peptides identified in both samples were plotted against each other in a scatter plot. A LOESS regression was used to find the best-fit line through the data points [75,201].

Topograph allows the measurement of the proportion of the amino acid precursor pool that is labeled, which varied over time and condition. This information allows the correct calculation of the percentage of each peptide that is newly synthesized, which when plotted for 12 biological replicates over 4 time points generated an exponential curve following first order kinetics. Using a logarithmic transformation, the first order protein turnover rate (slope) was determined by linear regression.

Only peptides that uniquely mapped to a single UniProt protein accession were used for quantification of abundance and turnover. For the cases where a protein consisted of more than one peptide, statistical models were modified to appropriately account for the multiple peptides by using a blocking factor. For each protein we applied non-linear regression fits of first order exponential curves to the % newly synthesized protein using: $y = 100 + \beta 1^{eqt}$. ANCOVA was used to identify statistically significantly different

turnover (slopes, α) between experimental groups. For details see the methods supplement of Hsieh et al. 2012 [88].

This turnover calculation relies on the assumption that proteins existed in a condition of steady state at the time of sampling, in which protein synthesis and degradation rates were approximately equal. To reasonably account for steady-state, mice were acclimated to experimental diets until reaching stable weights, which remained stable over the course of heavy labeling. Furthermore, the abundance of all peptides identified did not change significantly over the labeling period (regression slopes centered over zero), confirming that proteins were at steady-state at the time of labeling. To reduce the complexity of each regression we derived a single x-intercept (time of first appearance of heavy label) as an average for each age/treatment group and subsequently fixed the x-intercept for regression of individual proteins within each group to this value. These intercepts for liver and heart have been published in Supplementary information of Karunadharma et al. 2015 and Dai et al. 2014, respectively [91,201].

As previously shown, relative standard errors (RSE) of the HL estimates are small (<2.5%) as shown for liver and heart in. There is an increase in the RSE's at the short (<3 days) or very long (> 12 days in liver, >45 days in heart) HL ranges in both tissues, possibly due to the reduced precision in HL estimates that are beyond our chosen span of harvest times (3-17 days) [91,201].

Between the total and mitochondrial fractions, liver HLs differed 6% ($p<0.0001$) and heart HLs differed by 16% ($p<0.0001$) on average among the age//treatment groups (Table 1); we tentatively ascribe these differences to non-representative extraction or survival of mitochondria during purification or contamination by microsomal fractions.

5.5.6 **Ubiquitin enrichment and analysis**

A portion of liver tissues was enriched for poly-ubiquitinated proteins using an antibody pulldown, as previously described [220]. In order to purify poly-ubiquitinated proteins, total liver lysates were prepared in a simple 50mM ammonium bicarbonate buffer containing 8M Urea and then split into 2 fractions. The first

fraction was immuno-purified using the agarose-conjugated poly-ubiquitin specific antibody “FK2” (D058-8, MBL, Nagoya, Japan) and the second fraction from each portion of liver was enriched using an agarose-conjugated isotype negative control antibody (M194-3, MLB, Nagoya, Japan). Using low molecular weight exclusion filter spin columns, all samples were washed 2x with an 8M Urea wash buffer, followed by 2x wash with 50mM ammonium bicarbonate. Antibody-bound proteins were eluted with 100mM Glycine, pH 2.8 and precipitated using a standard methanol chloroform extraction. The insoluble proteins were then pelleted, decanted, and resuspended in a mass-spec-compatible mitochondrial isolation buffer, then prepared for mass spectrometry identically to whole-cell extracts, as above. Isotype-control enriched abundances were subtracted from FK2-enriched sample abundances to remove nonspecific contamination.

5.5.7 **Statistical Analysis**

Tissue (HT, HM, LT, LM, BT, EM, SM), age-treatment (OCL, OCR, ORP, YCL, YCR, YRP), complex (CI to CV) and localization (membrane, matrix, IMS) log-HLs interaction were examined by least squares regression, while ancestral age, assembly order, 20s proteome degradation susceptibility and ubiquitin enrichment were fitted as continuous linear variables. RC protein subunits with membrane-spanning domains were assigned “membrane” as their location for statistical purposes. Factors for each protein also were fitted as precision variables for tests of tissue, age-treatment and complex; these protein effects did not appreciably alter the estimated effects but do result in greater statistical power. A likelihood ratio test was used to test overall effects of tissue, age-treatment and complex as well as linear trend tests for the continuous variables. The Wald test was used for the pairwise comparisons reported in the Results. A pairwise comparison to test for a non-zero difference in the mean log HL between two groups is equivalent to testing that the geometric mean of the HL ratios between the two groups is different from one. After establishing large and highly significant tissue and age-treatment group effects, all other tests were adjusted for these two variables. Because of imbalances on ancestral group across the different complexes that precludes proper adjustment for confounding by complex, a second test for ancestral group effect was performed on a balanced subset of the data and adjusted for complex effects. The subset was restricted to ancestral groups that were present in all complexes, resulting in restriction to

bacteria (group 0), LECA (group 1) and Opisthokonts (group 3) in complexes I, III, IV and V. Eighty-four different respiratory proteins (RC) were used in the analyses. Protein SDHD was excluded from statistical and turnover analyses due to high variability and inconsistency across tissues. Statistical significance was set at level 0.05. Statistical computations were done in R.

5.5.8 **Raw Data Repository and Other Files**

Raw files and datasets from the MS analysis can be viewed and downloaded online on the Chorus Project data repository - https://chorusproject.org/pages/blog.html#/352. For R-scripts and other data, please contact the corresponding author to receive copies.

OVEREXPRESSION OF MITOCHONDRIAL-TARGETED CATALASE IS GOOD FOR THE OLD MOUSE PROTEOME BUT NOT FOR THE YOUNG: REVERSE ANTAGONISTIC PLEIOTROPY

6.1 SUMMARY

Aims: Reactive oxygen species (ROS) are highly reactive oxygen-containing molecules associated with aging and a broad spectrum of pathologies. We have previously shown that transgenic expression of the antioxidant enzyme catalase targeted to the mitochondria (mCAT) in mice reduces ROS, attenuates age-related disease, and increases lifespan. However, it has been increasingly recognized that ROS also has beneficial roles in signaling, hormesis, stress response, and immunity. We therefore hypothesized that mCAT might be beneficial only when ROS approaches pathological levels in older age and might not be advantageous at a younger age when basal ROS is low. **Results**: We analyzed abundance and turnover of the global proteome in hearts and livers of young (4 mo.) and old (20 mo.) mCAT and wild type (WT) mice. In old hearts and livers of WT mice, protein half-lives were reduced compared to young, while in mCAT mice the reverse was observed; the longest half-lives were seen in old mCAT mice and the shortest in young mCAT, Protein abundance of old mCAT hearts recapitulated a more youthful proteomic expression profile (p-value < 0.01). However, young mCAT mice partially phenocopied the older wild-type proteome (p-value < 0.01). **Innovation**: Age strongly interacts with mCAT, providing an example of antagonistic pleiotropy in the reverse of the typical direction. **Conclusion**: These findings underscore the contrasting roles of ROS in young vs. old mice and indicate the need for better understanding of the interaction of dose and age in assessing the efficacy of therapeutic interventions in aging, including mitochondrial antioxidants.

6.2 INTRODUCTION

Reactive oxygen species (ROS) are associated with the progression of a broad spectrum of pathologies including aging[51], neurodegeneration , metabolic syndrome [53-55], heart disease [56,57,94], cancer , and others [59]. Mechanistically, this has largely been attributed to oxidative modification of cellular macromolecules, including lipids [60], DNA [61] and proteins [62]. While ROS have been widely regarded as a major component of aging since the "Free Radical Theory of Aging" was proposed in the 1950s [51], there is an increasing appreciation that ROS also serve important physiological signaling roles. It is therefore important to closely examine both negative as well as positive consequences of therapeutic interventions that target ROS.

Given that oxidative modifications can impair the activity of macromolecules, and the well documented correlation between oxidative damage and aging reported in almost all models studied, it has been tempting to conclude that this is a likely mechanism for aging [264]. However, there are many observations at odds with this theory of aging. Clinical trials of dietary antioxidants to reduce cancer [63], gastrointestinal [265], neurological [266], rheumatoid [267], endocrine [64], and cardiovascular diseases [65] have thus far shown little to no efficacy. Some have shown adverse outcomes [66]. In mice, deletion of many antioxidant enzymes has little effect on lifespan and, importantly, overexpression of several antioxidants including superoxide dismutase and peroxisomal catalase has failed to extend lifespan [70,268]. Compared to mice with a median lifespan just over 2 years, the naked mole rat shows remarkable longevity, living 10-30 years, in spite of similar rates of ROS production and more extensive oxidative damage to its tissues over its lifetime [269], suggesting that ROS may not necessarily play a causative role in aging. Additionally, while mtDNA mutations increase with age, the characteristic mutations created by ROS are not among those most seen by the new method of duplex sequencing, suggesting that ROS may not be a driver of somatic mutations in aging [270]. In C *elegans*, an invertebrate model of aging, several strains deficient in respiratory proteins which produce excess reactive oxygen species are in fact longer lived than WT controls [69].

Our group has previously shown that mice overexpressing mitochondrial-targeted catalase (mCAT), but not nuclear or peroxisomal catalase, have an approximately 20% increased median and maximal lifespan

[18], suggesting that reducing ROS specifically in the mitochondria is key to achieving a beneficial effect on aging. mCAT has been shown to reduce oxidative modification of DNA and proteins, and delays the progression of multiple pathologies [71]. We have also demonstrated that mCAT is protective against cardiac aging [73] as well as models of cardiac hypertrophy and failure in young mice [75], [76]. Other laboratories have demonstrated that mCAT mice have additional benefits, such as improved amyloid precursor protein processing [72], reduced loss of bone after estrogen withdrawal [271], reduced insulin resistance [61], and protection against radiation exposure [74]. Similar benefits have been seen in mice treated pharmacologically with the mitochondrial targeted tetra peptide SS-31[56] (d-Arg-2′, 6′-dimethyltyrosine-Lys-Phe-NH_2), also known as Bendavia, which targets mitochondrial inner membrane cardiolipin, enhance electron transfer efficiency and thereby reduce ROS production [272]. This report describes an analysis of global proteomic changes resulting from mCAT overexpression in the context of aging, measuring both protein abundances and turnover rates. We report changes in the hepatic and cardiac proteomes with age,

6.3 RESULTS*

6.3.1 mCAT has opposite effects on hepatic and cardiac protein turnover in young versus old

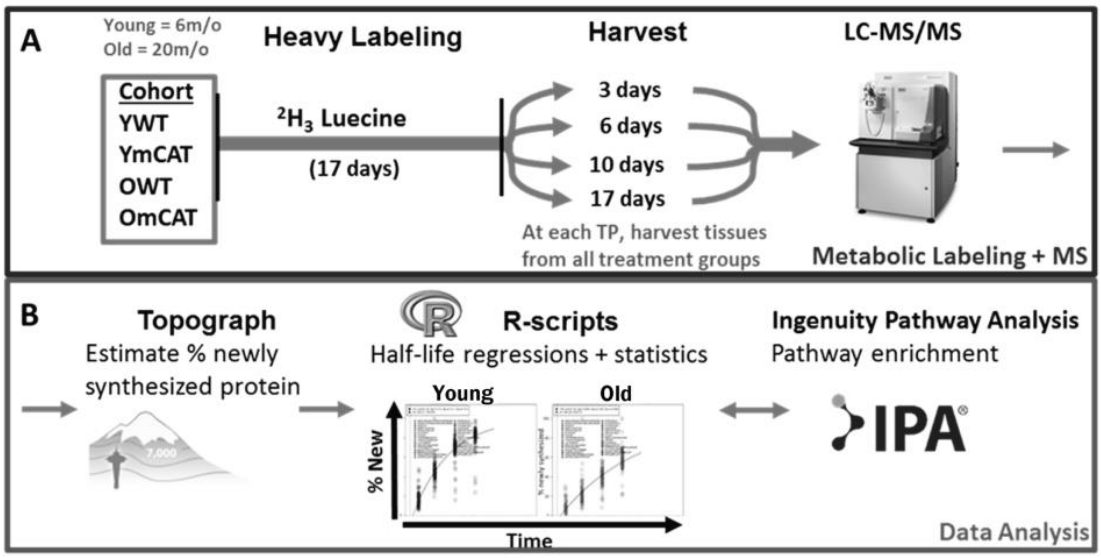

Figure 6-1 Experimental workflow for metabolic labeling and proteomic analysis. A) YWT, YmCAT, OWT, and OmCAT mice were placed on a diet in which leucine was substituted for deuterated leucine for up to 17 days. At each of four time points – 3, 7, 12, and 17 days – mice from each of the four groups were sacrificed, tissues harvested, and flash frozen until used to prepare total lysates. Total lysates from hearts and livers were subject to shotgun (data-dependent) mass spectrometry analysis. B) Topograph software was used to estimate the percentage of newly synthesized protein for every protein at each timepoint, as well as area under the curve for each peptide. First-order exponential regressions of the percentage of newly synthesized protein over time were performed in R to determine half-lives. Abundances, as determined by peptide peak areas, and half-lives for each experimental group underwent statistical comparisons and visualization in R. Ingenuity Pathway Analysis software was used to perform pathway enrichments into top canonical pathways.

mice

In order to comprehensively quantify *in vivo* changes in global proteome half-lives (HLs), we performed stable-isotope metabolic labeling of mice by administering a synthetic diet containing $^3H_2$-leucine over a period of 17 days, as previously described [201] (Figure 6-1). Hearts and livers were collected at four subsequent time points from each of four experimental groups: young WT (YWT) and young mCAT (YmCAT) at 3-4 months of age, old WT (OWT) and old mCAT (OmCAT) at 18-21 months of age. All samples were analyzed by nLC-MS/MS. Topograph software was used to estimate the proportion of newly synthesized protein at each time point, corrected for enrichment of heavy leucine in the amino acid precursor pool [88], and HLs were calculated based on first order regressions of percentage of newly

* Supporting information such as supplementary figures, tables, datasets, and methods can be found online: http://blogs.uw.edu/nbasisty/home/136-2/

synthesized protein over time. In heart we identified 11,240 unique peptides mapping to 2570 proteins and in liver we identified 11, 461 unique peptides mapping to 3145 proteins.

There were no significant protein abundance changes over the 17-day labeling period in either the hearts or livers of mCAT and WT mice at either age (SFigure 6-1). This indicates that 1) the presence of multiple peptide isotopic peaks, which arise from the combination of heavy and light leucine in the diet, does not seriously alter the integration of peak area by Topograph to quantitate protein abundance; 2) unchanging protein abundances suggest that the rates of protein synthesis and degradation are at steady states, as expected in adult animals.

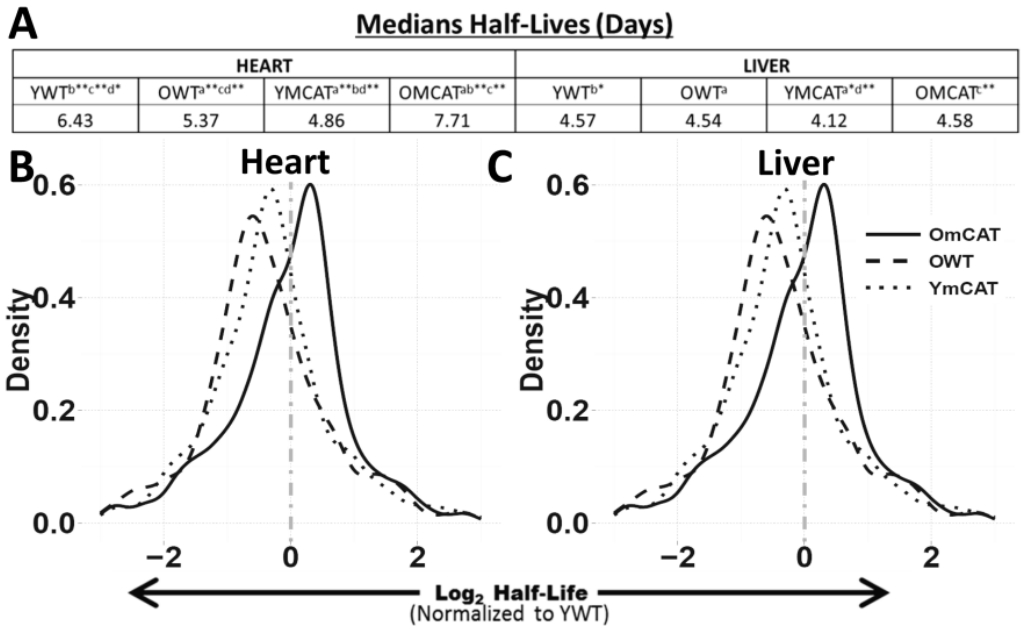

Figure 6-2 Medians and distributions of protein half-lives in hearts and livers of whole cell lysates in each experimental group. A) Table of median half-lives for each experimental group. Only proteins in common to both tissues and all experimental groups were considered in these calculations. Distributions of the changes in proteome half-life in B) heart and C) liver tissues by treatment - OWT, YmCAT, and OmCAT – each relative to young WT controls. Dotted lines mark the location of a ratio equal to one (YWT). One tailed t-tests: * p-value < 0.001 for the ratio being less than zero, **p-value < 0.001 for the ratio being greater than zero.

Median protein half-lives are longer in heart than liver; even among proteins common to both. The protein HLs in YWT hearts were 1.4 times longer (6.4 days) than in the liver (4.57 days) (Figure 6-2A). In the heart there was a significant difference in median half-life between any two age/treatment groups; the longest half-life was seen in OmCAT (7.71 days) followed by YWT (6.43 days), OWT (5.37 days), and YmCAT (4.86 days). The liver followed this same order over a smaller range, with half-lives of 4.58, 4.57,

4.54, and 4.12 days in OmCAT, YWT, OWT, and YmCAT respectively. Histograms of the distribution of half-lives in each experimental group in heart and liver are shown in supplementary Figure 6-2 (SFigure 6-2A, B). A more sensitive analysis was performed by normalizing HLs of each protein in each treatment group to the corresponding protein's YWT HL This paired analysis of the protein by protein fold change in HL in each group versus YWT is visualized in histograms for heart (Figure 6-2B) and liver (Figure 6-2C). A positive number indicates an increase in half-life versus YWT (in units of $\log_2$ fold change) while a negative number indicates a reduced HL relative to YWT. As previously reported [91,201], old WT mice had significantly decreased HLs compared to young WT mice; however, old mCAT HLs were longer than old WT and thus more similar to young WT, consistent with restoring a more youthful proteome. Interestingly, the young mCAT had *shorter* HLs than YWT, and the effect of aging on mCAT protein half-life *is thus a complete reversal of the change seen in WT mice*.

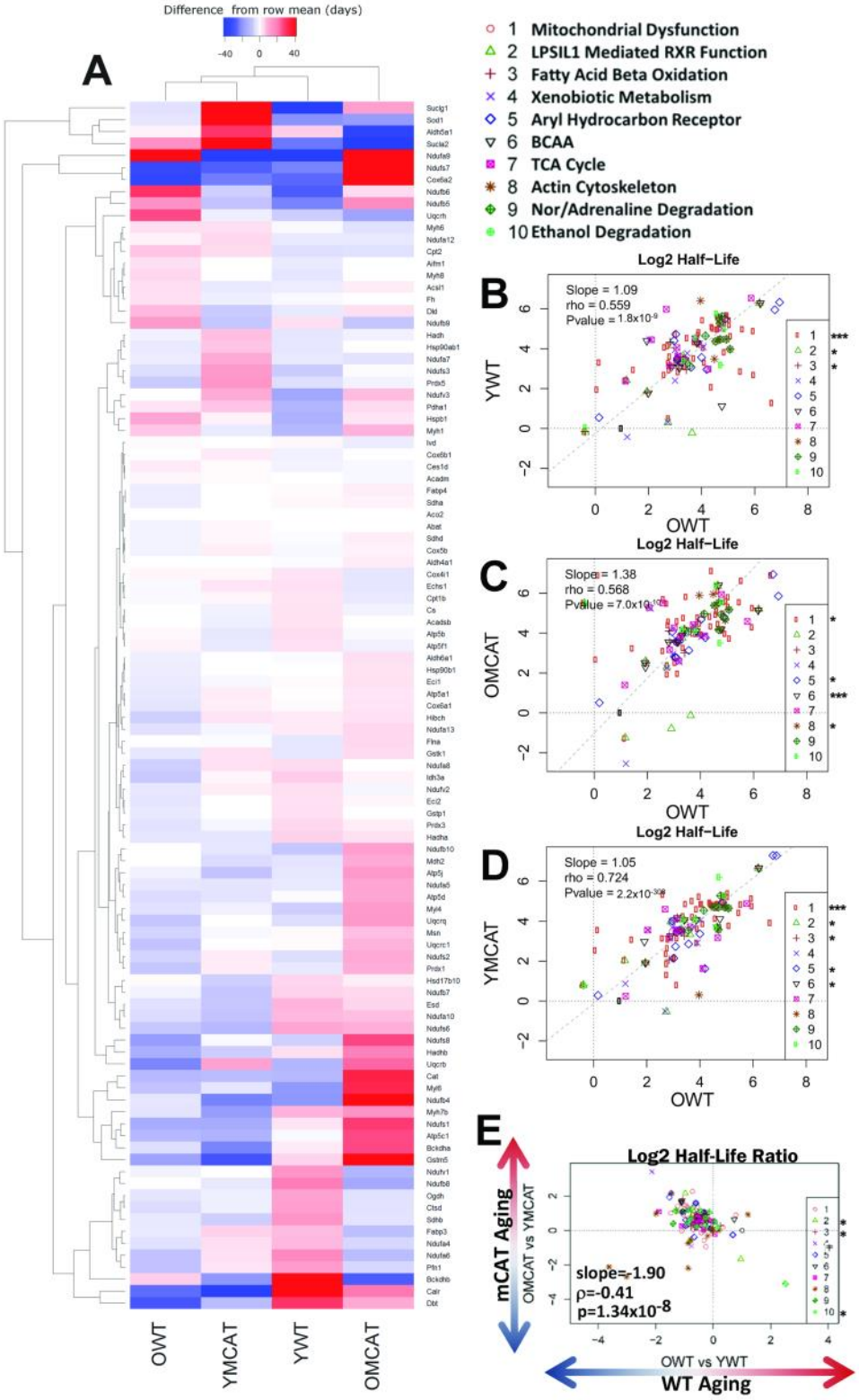

Figure 6-3 Heatmap of all cardiac proteins significantly changed in half-life during aging and correlation plots of cardiac proteins that significantly changed with age. A) Heatmap depicting all proteins with significantly altered (p-value < 0.05) in the statistical comparison of YWT and OWT proteome half-lives. The four columns correspond to the treatment groups used in this study: YWT, OWT, YmCAT, and OmCAT. Colors in the heatmap represent the half-life of a protein relative to its mean half-life (in days) across all treatment groups (difference from row mean). Correlations were performed between OWT half-lives versus each treatment group– B) YWT, C) OmCAT, and D) YmCAT. E) A correlation of WT aging (OWT/YWT) versus mCAT aging (OmCAT/YmCAT).

* p-value < 0.05, ** p-value < 0.001 for Spearman correlation of the individual pathways in the regressions.

6.3.2 **Analysis of cardiac proteome changes in half-life**

Proteins that showed a significant age or mCAT-dependent change in HL (p-value < 0.05) were plotted on a heatmap with hierarchical clustering in both rows and columns (Figure 6-3A). The first two columns, showing mostly decreases (blue) in half-life of OWT and YmCAT compared to the row means, illustrate the visual similarity between aged WT and young mCAT mice. This is in contrast to the increasing half-lives (red) seen in a higher proportion of proteins in the third and fourth columns, which include old mCAT and young WT mice.

The effects of mCAT overexpression on protein HLs were correlated with WT aging changes by bivariate plots for proteins in the top 10 Ingenuity Pathway Analysis [147] pathways, ranked by significance of half-life changes in WT aging (OWT vs. YWT) (Figure 6-3B-D). The majority of the "top" pathways were metabolic pathways (including mitochondrial dysfunction, xenobiotic metabolism, fatty acid oxidation, and TCA cycle) or signaling pathways (aryl hydrocarbon receptor signaling), and a few other notable pathways, such as actin cytoskeleton, which are closely tied to heart function. The regression in all top pathways combined confirms that the half-lives of these top pathway proteins in young mCAT mice is more similar to those of old WT mice (slope =1.05, r = 0.724, p-value<$2.2x10^{-308}$, Figure 6-3D) than to young WT (slope = 1.09, r=0.559, p-value = $1.8x10^{-9}$, Figure 6-3B) or old mCAT (slope = 1.38, r = 0.568, p-value = $7.0x10^{-10}$, Figure 6-3C). A direct comparison of WT aging (OWT vs. YWT) to mCAT aging (OmCAT vs. YmCAT) also showed a strong negative correlation (Figure 6-3D), highlighting the opposing effects of mCAT in young versus old mice. All proteins and corresponding heatmap values can be found in Supplementary Dataset 1. Pathway categorizations for the top 20 pathways can be found in Supplementary Dataset 2.

6.3.3 **Analysis of hepatic proteome changes in half-life**

Hepatic proteome turnover partially recapitulated the effects seen in the heart (Figure 6-4A), and the list of top affected pathways was highly overlapping in the two tissues (Figure 6-4B-D). All treatment groups showed a highly significant degree of correlation with OWT in all 10 top pathways combined, and this correlation remained significant for every individual pathway in YWT and YmCAT (Figure 6-4B,D) as well

as 8 out of 10 of the pathways in OmCAT (Figure 6-4C), This high degree of similarity between treatment groups in liver suggests that both aging and mCAT changes in half-life are modest. Even so, the apparent visual differences between groups in the heatmap are consistent with the differences in the strength of these correlations. For example, OmCAT is the most divergent group in both cases (Figure 6-4A, C). Additionally, mCAT aging did not show a significant correlation with WT aging (Figure 6-4D).

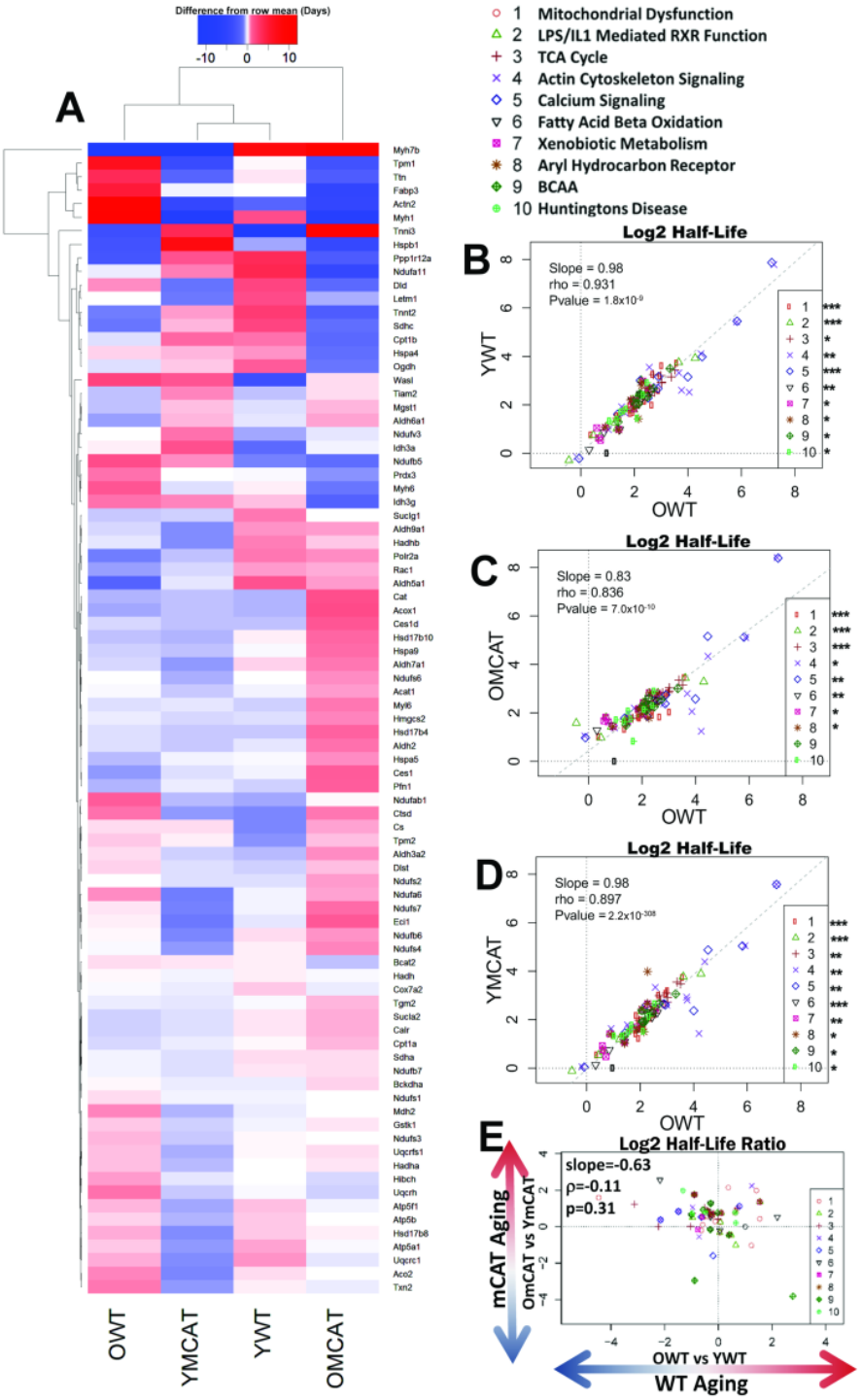

Figure 6-4 Heatmap and correlation plots of hepatic protein half-lives that significantly changed with age. A) Heatmap depicting all significantly changed (p-value < 0.05) protein HLs during aging (OWT vs YWT). The heatmap colors represent the half-life of a protein relative to its mean half-life (in days) across all treatment groups (difference from row mean). B-D) Correlations of OWT half-lives versus B) YWT, C) OmCAT, and D) YmCAT half-lives. E) A correlation of WT aging (OWT/YWT) versus mCAT aging (OmCAT/YmCAT).

‡ p-value < 0.10, * p-value < 0.05, ** p-value < 0.001 for Spearman correlation of the individual pathways in the regressions.

6.3.4 **Protein Abundance changes in the cardiac and hepatic proteomes**

MS1 peak areas were calculated in Topograph, and used to perform relative quantification of protein abundances (see methods). An inherent limitation to MS quantitation is that the intensity of peak areas is highly dependent on peptide ionization efficiency, which is very variable across peptides, and therefore provides no information about the absolute quantity of a peptide or protein. It is common to instead to measure the relative change in any given peptide across samples. To compare the effects of mCAT and aging on protein abundance we therefore examined relative differences in peak area by examining the ratios of treatment groups: OWT/YWT (WT aging), OmCAT/YmCAT (mCAT aging), YmCAT/YWT, and OmCAT/OWT (the effects of mCAT expression in young and old mice).. Our results show, similarly to the trend seen in half-lives, the effects of mCAT in young mice (YmCAT vs. YWT, column 1) are clustered with WT aging effects (OWT vs. YWT, column 2), while mCAT aging changes (OmCAT vs. YmCAT, column 3) and mCAT effects in old mice (OmCAT vs. OWT, column 4) cluster with each other and often show an opposite pattern of expression to the first two columns (Figure 6-5A). Because comparisons between sets of ratios with common terms (i.e. OWT/YWT vs YmCAT/YWT and OWT/YWT vs OmCAT/OWT) can introduce 'spurious correlation [273], we performed statistical analysis using partial correlations controlling for the common terms [274]. Notably, mCAT expression levels in young mice tend to be in the same direction as OWT, as can be seen from the positive correlation in Figure 5B (p-value < 0.05). In contrast, mCAT effects in old mice (OmCAT vs OWT) were not correlated with WT aging changes, while mCAT aging (OmCAT vs YmCAT) was correlated with WT aging changes (Figure 6-5D, p-value=1.57×10^{-14}). Among the top 20 pathways most significantly changed in the heart abundance proteome (Figure 6-3B-D, Figure 6-5B-D, Supplementary Dataset 2) 8 were in common with pathways most changed in the turnover data set. Three of these top 20 pathways are protein turnover mechanisms: protein ubiquitination, p70s6K, and clathrin mediated endocytosis (Supplementary Dataset 2).

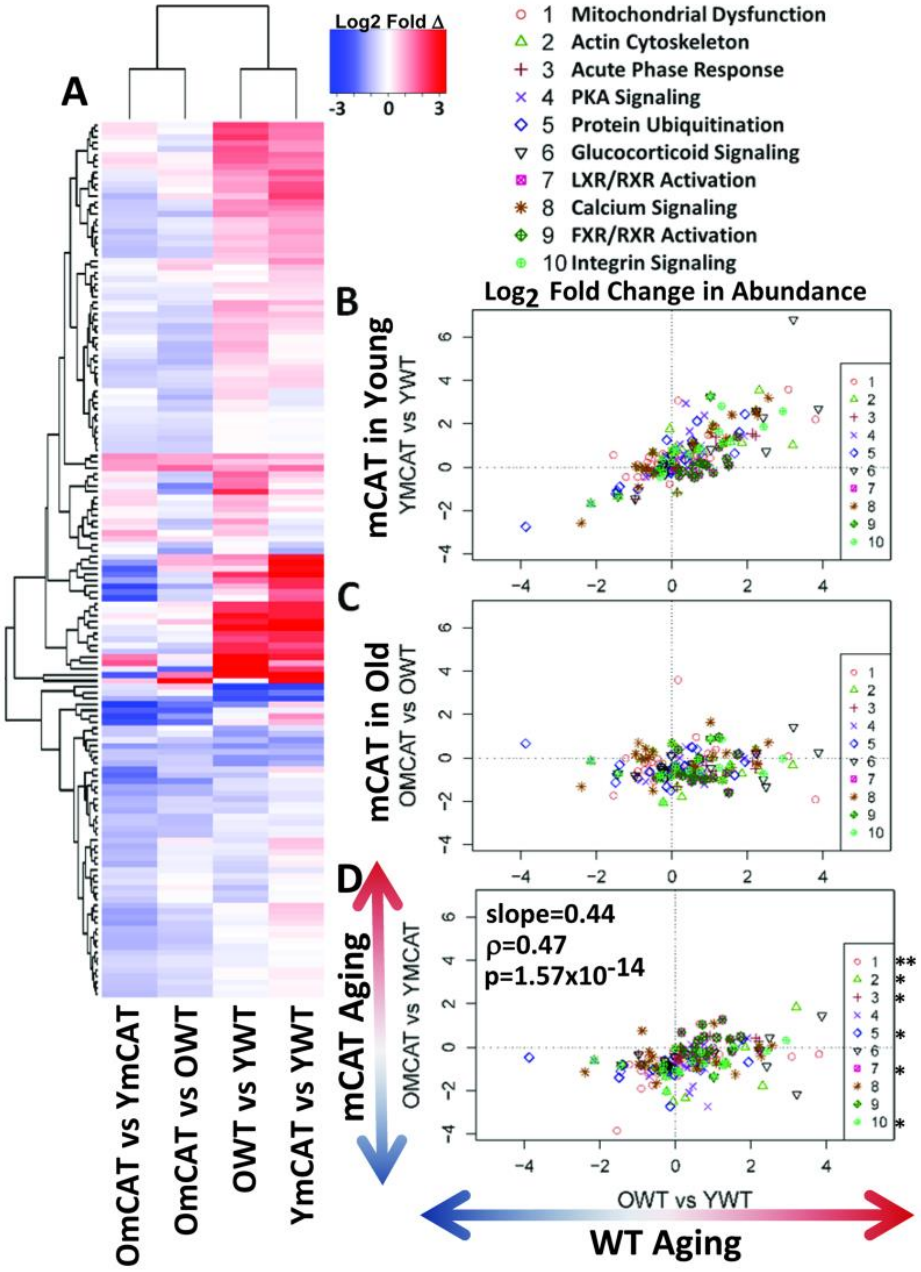

Figure 6-5 Heatmap of all significant cardiac protein abundance changes with age and correlations of WT aging to mCAT aging. A) The heatmap shows the direction and magnitude of abundance changes between the groups noted in the column labels. B-D) Correlation plots of changes in HL of proteins in the top 10 IPA pathways, B) The effect of mCAT in young mice (YmCAT vs YWT) positively correlates with WT aging (OWT vs YWT, p-value < 0.05). C) The effect of mCAT in old mice (OmCAT vs OWT) had little to no correlation with WT aging. D) The effect of aging in mCAT (OmCAT vs YmCAT) versus WT aging (OWT vs YWT) shows a significant negative correlation, with a correlation coefficient of -0.5.

* p-value < 0.05, ** p-value < 0.001 for Spearman correlation of the individual pathway between the x and y-axis groups.

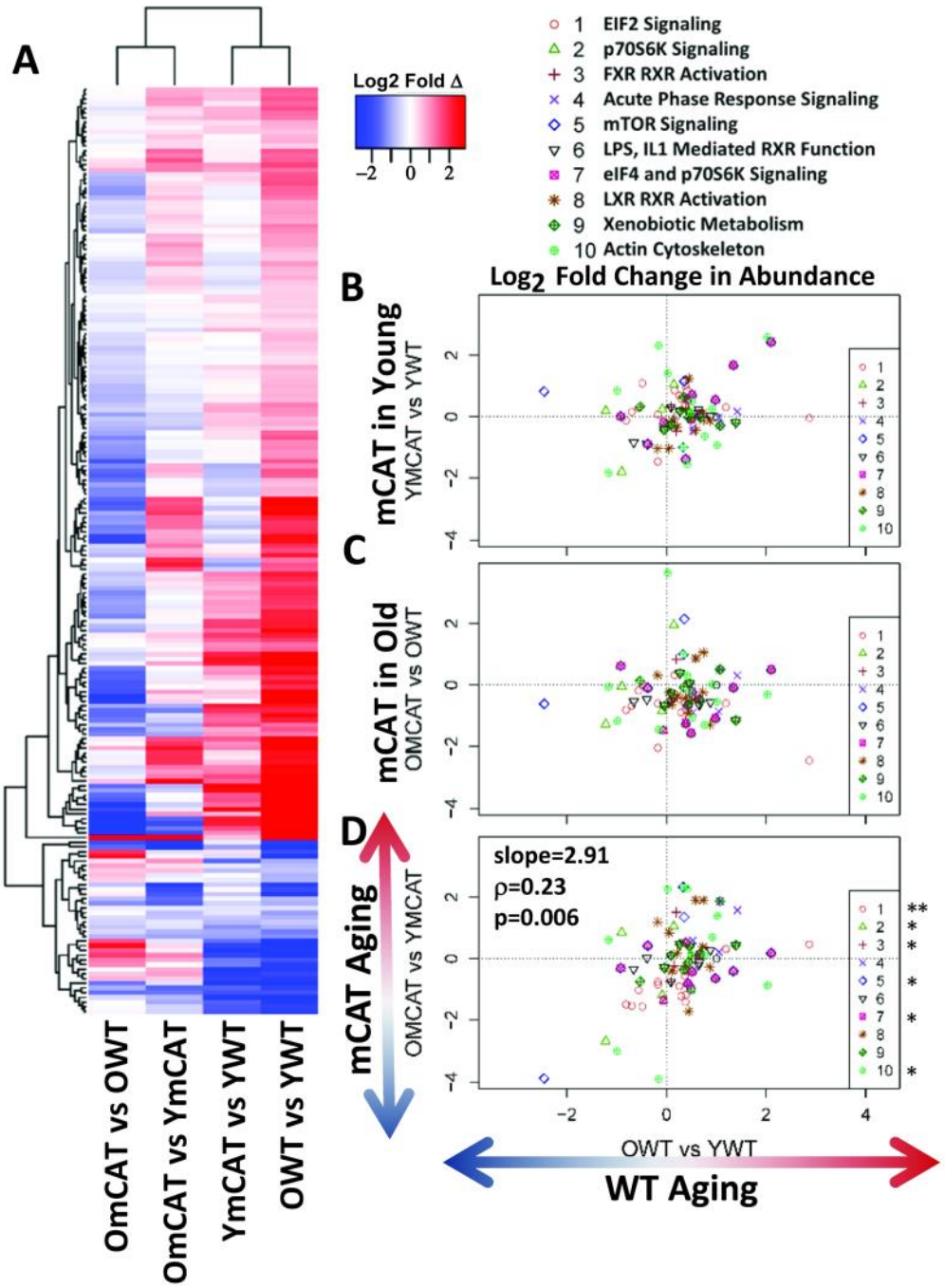

Figure 6-6 Heatmap containing hepatic protein abundance changes enriched into proteins significantly altered by aging (p-value< 0.05) and correlation plots of mCAT versus WT aging effects. A) The heatmap shows the direction and magnitude of abundance changes between the groups written in the column labels. B-D) Correlations were done on the top 10 pathways to compare the effects of mCAT to the effects of WT aging (OWT vs YWT). B) The effect of mCAT in young mice (YmCAT vs YWT) is significantly correlated with WT aging changes, but to a lesser extent than heart tissue. C) The effect of mCAT in old mice (OmCAT vs OWT) has no relationship with WT aging (OWT vs YWT), D) mCAT aging (OmCAT vs YmCAT) is significantly but weakly correlated with normal aging (OWT vs YWT). * p- value < 0.05,

** p- value < 0.001 for Spearman correlation of the individual pathway between the x and y-axis groups.

The effects of mCAT and aging on liver abundances appear to share many trends with heart changes, but to a much lesser extent (Figure 6-7A-D). Again, aging effects (OWT vs. YWT) and the effects of mCAT in young mice (YmCAT vs. YWT) clustered as a pair in the heatmap, while mCAT aging (OmCAT vs YmCAT) and the effects of mCAT in old mice (OmCAT vs OWT) were paired in another cluster (Figure 6-7A). Young mCAT effects were significantly correlated with aging effects, albeit much more weakly than in heart (p-value < 0.05). Among the top 10 IPA pathways, the three that showed individually significant correlations were protein turnover pathways: EIF2 signaling, p70S6K signaling, and eiF4/p70S6K signaling. The effects of mCAT expression in old livers did not have a significant negative correlation with aging changes (Figure 6-7C). However, the comparison of WT aging and mCAT aging effects (Figure 6-7D) did show a small negative correlation (p-value < 0.01).

The significantly weaker mCAT effects in liver seen for both half-lives and abundances are likely due to the much lower levels of liver mCAT expression from the chick beta actin promoted transgene. In contrast to highly expressed mCAT in heart, skeletal muscle and brain, we have previously reported no difference from littermate controls in mCAT liver expression [18]. To verify these previous observations, we measured protein levels of mCAT by western blot (Fig 7A) and mRNA expression by qPCR (SFigure 6-3A); the results confirmed that mCAT protein and mRNA expressions are essentially undetectable in liver. This suggests either that undetectably small levels of mCAT expression in livers are sufficient to produce modest and partial effects in proteome abundance and turnover, or that that the changes in liver are a non-cell autonomous effect of mCAT expression in other tissues.

6.3.5 **mCAT aging exhibits reverse antagonistic pleiotropy**

In order to compare the trajectories of wild type aging and mCAT aging, we condensed the proteomic changes into an index of aging change by taking the average absolute magnitude of the fold changes in protein abundance from YWT to OWT over all significantly altered (q-value<0.05) proteins in WT aging. By this metric, WT aging is an average 5.66 fold change in heart proteome abundance. For each of the same proteins the YWT vs. YmCAT or YWT vs. OmCAT was similarly calculated and the average absolute change expressed as a percentage of the WT aging effect (Figure 6-8). Consistent with the

abundance correlations noted above, mCAT mice have a striking reversal of the WT aging trajectory; the YmCAT proteome index for these same proteins is nearly 100% of OWT in magnitude, but declines to YWT levels in the old mCAT proteome. This surprising result was initially seen in a separate "pilot" experiment without heavy leucine labeling (Figure 6-8B, dotted line, heatmap summary in SFigure 6-4). Some of these trends in significantly changed proteins in the aging cardiac proteome were further validated by western blot (SFigure 6-5A, B). A similar analysis of the liver proteome (Figure 6-7B) showed a trajectory in mCAT aging that was similar to that of WT aging, although the slope was slightly lower. As noted earlier, this smaller effect is likely explained by the lack of detectable mCAT expression in liver

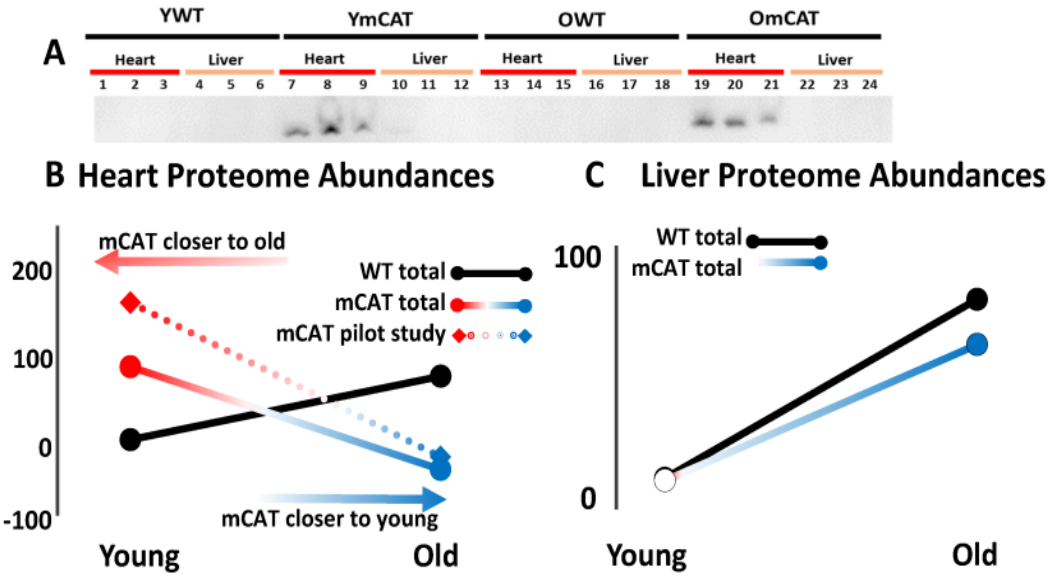

Figure 6-7 Reverse antagonistic pleiotropy in the proteome as a result of mCAT. We condensed proteomic changes into simple line plots depicting the trajectory of WT aging (black line) and mCAT aging (colored line). (See the methods for more detail.) A) The heart proteome demonstrates reverse antagonistic pleiotropy: the YmCAT proteome more closely resembles old mice, while the OmCAT mouse is shifted toward a younger proteome compared to their OWT counterparts. B) This effect was not seen in liver tissue, which C) did not express mCAT protein, as measured by western blotting and confirmed by qPCR (SFig 3).

tissues.

6.3.6 Changes in major proteostasis pathways

As described in Figure 6-2A and shown for reference as bar plots in Figure 6-8A and B, median proteome turnover rates of each experimental group in liver (Figure 6-8A) and heart(Figure 6-8B, suggest that global turnover may be highest in YmCAT and OWT and lowest in YWT and OmCAT mice. To explore some of the mechanisms by which abundance and turnover might be affected by mCAT and aging, we

measured markers of autophagy, oxidation, the ubiquitin proteasome, mitochondrial biogenesis, and protein translation (Figure 6-8C-H, SFigure 6-5C-F, SFigure 6-7A-H). Oxidation of proteins, as measured by protein carbonylation, was increased with age in WT hearts (Figure 6-8C) and liver (Figure 6-8D), as expected. This increase was not seen [65] or was smaller [275] in old mCAT mice and carbonylation remained unchanged in young mCAT mice. In concordance with faster protein turnover in YmCAT tissues, lamp2a levels, a marker of chaperone-mediated autophagy, were increased in YmCAT hearts and livers to levels similar to that seen in old WT tissues (Figure 6-8E, F). Levels of poly-ubiquitinated proteins were increased in OWT hearts and in all groups of liver relative to YWT (Figure 6-8G, H). This is consistent with the increases seen in the "Protein Ubiquitination" pathway of the proteomic data set (Supplementary Dataset 2).

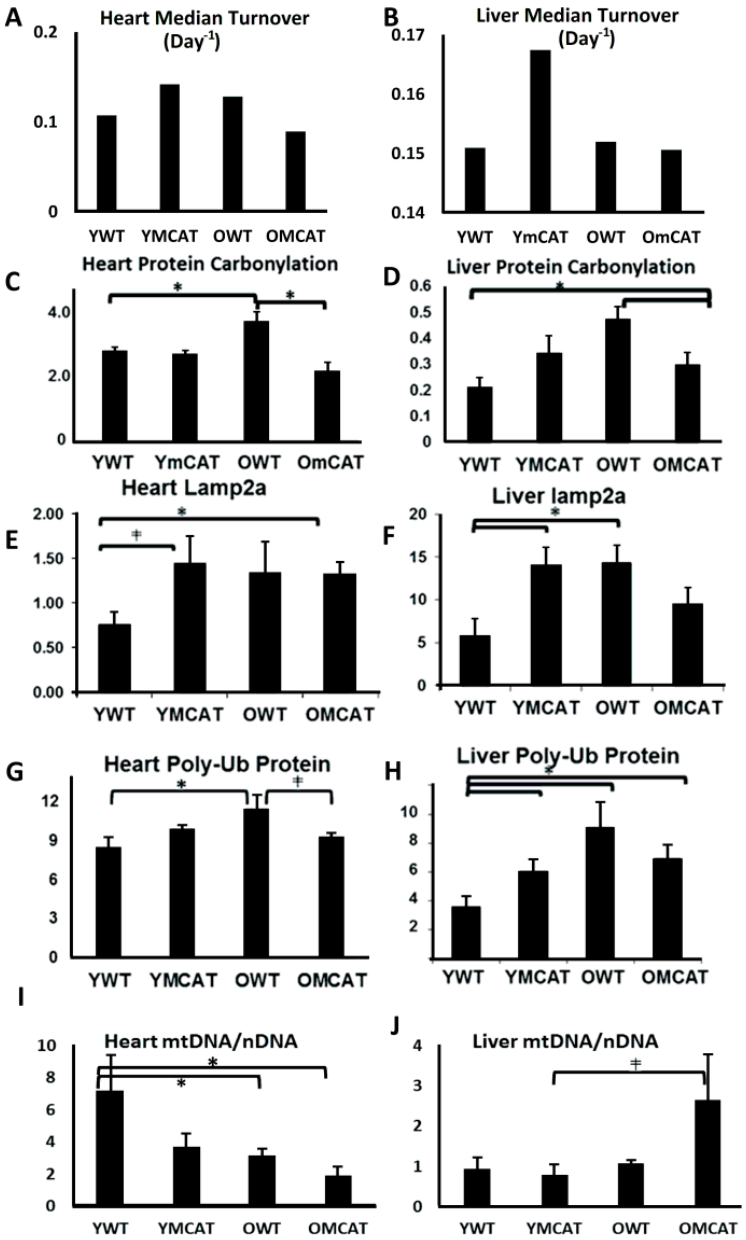

Figure 6-8 Protein turnover markers. mCAT and aging significantly alter markers of several protein turnover mechanisms. Western blotting was done on various markers of turnover pathways and compared to the median global protein turnover rates determined by mass spectrometry in A) heart and B) liver. C) Protein carbonylation increased with age and was attenuated in old mCAT in heart. D) Liver tissue similarly increased in carbonylation with age and this was attenuated in old mCAT mice. E) Chaperone mediated autophagy, as measured by lamp2a, was increased by both young and old mCAT hearts. F) Lamp2a was elevated in YmCAT as well as OWT mouse liver. G) Levels of poly-ubiquitinated proteins significantly increased with age in the heart, and this effect was attenuated in old mCAT. H) Levels of poly-ubiquitinated proteins in the liver were increased by both mCAT and aging. *p-value < 0.05

The p70s6k signaling pathway, consisting of ribosomal proteins, elongation factors, and initiation factors, all of which positively regulate protein translation, showed significantly increased protein expression in old WT and young mCAT mice in the pathway analysis, a pattern consistent with the increased global protein turnover rates seen in these groups. We confirmed these increases in eEF2 by western blot (SFigure 6-7A,

B). Macroautophagy was measured by the ratio of LC3II/I and Beclin1 (SFigure 6-7C, D). The LC3II/I ratio was not significantly altered in any group. However, these markers cannot determine flux through the lysosomal pathway, and therefore this would require further study.

To determine if mitochondrial biogenesis was significantly altered we performed analysis of mitochondrial DNA copy number (Figure 6-8I, J) and western blotting for PGC1 and COXIV (SFigure 6-5C-F). There was a significant decrease in mitochondrial DNA copy per cell in old WT and old mCAT hearts (Figure 6-8I), but a trend toward increased mito copy number in the OmCAT liver (Figure 6-8J), suggesting mitochondrial copy number may account for some of the protein abundance differences. There were no differences in PGC1α in either tissue.

6.4 DISCUSSION

This study presents a comprehensive characterization of proteome dynamics during aging in wild-type and long-lived mCAT mouse hearts and livers. In order to determine *in vivo* proteome turnover kinetics and protein abundances we utilized a metabolic labeling strategy in combination with LC-MS/MS and Topograph software. We were surprised to find that mCAT has very different effects in young compared with old mouse hearts, with YmCAT mice resembling OWT, in addition to OmCAT hearts having a more "youthful" proteome. This effect was observed in two independent data sets.

Globally, protein half-lives are decreased with age in both heart and liver, similarly to our previously reported observations [91,201]. Changes in HL in WT aging in both heart and liver within individual pathways were also concordant with these prior observations, including the pathways mitochondrial dysfunction, branch chain amino acid metabolism, actin cytoskeleton, oxidative stress response, ethanol degradation, and aryl hydrocarbon receptor signaling. Likewise, changes in protein abundances during WT aging were significant in most of the same pathways as previously reported. In heart this included mitochondrial dysfunction, actin cytoskeleton, calcium signaling, and LXR/RXR activation [91]. In liver abundances this included EIF2 signaling, p70S6K, and LPS & IL1 mediated RXR function [201]. A consistent finding in the present study and our previous reports [91,201] is the observation of an age-related decrease in protein half-

lives, and a lengthening of half-lives by the addition of an aging-intervention. We have observed this trend in three separate life-span extending interventions including calorie restriction (CR), rapamycin (RP), and now mCAT. This raises the question of whether enhanced protein quality and reduced protein turnover is a common underlying longevity mechanism in these and perhaps other interventions. The close connection between CR and rapamycin is expected based on their common effect in mTOR signaling, however, commonality with mCAT is less expected and strengthens the generality of this observation. One possibility may be that reduction of mtROS is a common component of all of these interventions - ROS is a powerful signal for cellular energy status and is very closely tied to the allocation of cellular resources. It can signal synthesis and degradation of proteins as well as cellular fate, not unlike the nutrient sensitive mammalian target of rapamycin (mTOR) pathway [276,277] and therefore these may be utilizing similar mechanisms to promote longevity.

One aspect of the mCAT proteome, however, is novel compared to other interventions thus far: antagonistic pleiotropy. While old mCAT mice are benefited with a more youthful pattern of proteome half-life and abundance, corresponding with longer life [18] and numerous healthspan benefits [56,61,72,73], the young mCAT proteome assumes an “older” phenotype in a young animal, in both protein abundance and half-life. Antagonistic pleiotropy is typically seen as an effect that is beneficial to an organism’s fitness early in life, but which causes functional decline and aging phenotypes later in life. In this case we observe the opposite in mCAT mice. Hence, we refer to this effect, illustrated in Figure 6-7, as reverse antagonistic pleiotropy.

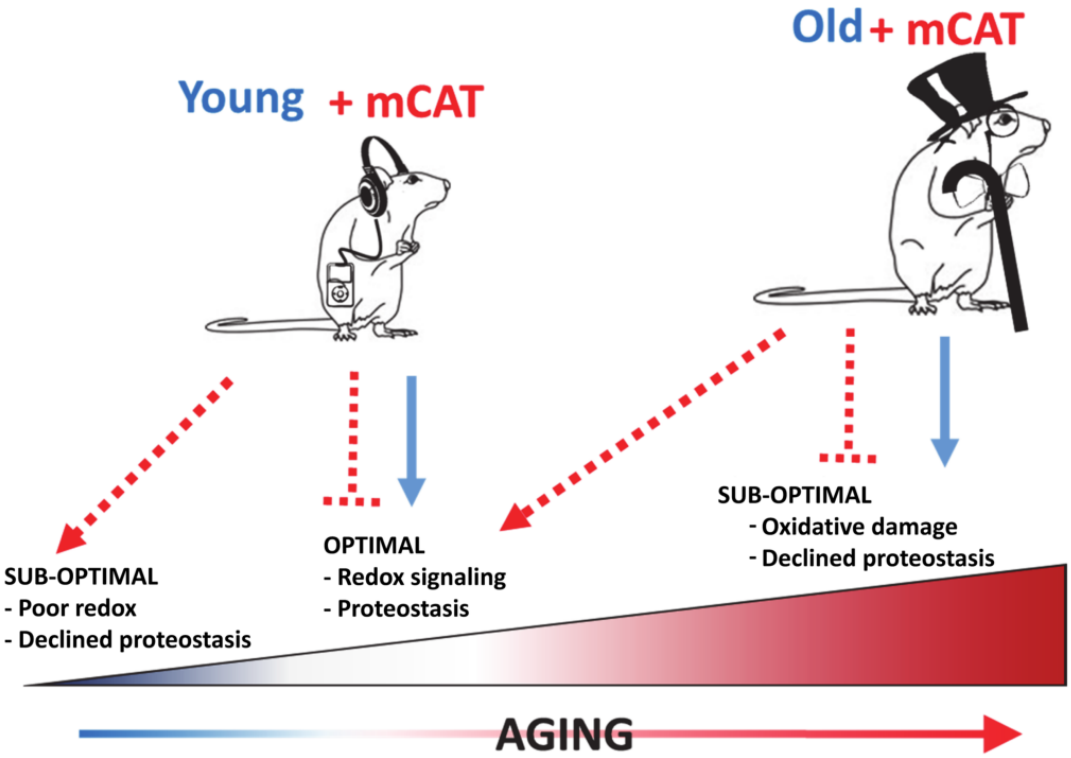

Figure 6 9 Model of mCAT "reverse" antagonistic pleiotropy

At moderate or low levels, ROS are increasingly being found to serve important physiological signaling roles that may be important for metabolism, protein turnover, cellular differentiation, stress response, and apoptosis [278,279], while damaging effects may not be apparent until ROS reaches high levels. For example, low level ROS is important for the renewal of stem cells and it has been shown that suppression of ROS significantly limits renewal of stem cells and suppresses neurogenesis in mice [280]. Thus, overexpression of mitochondria targeted catalase might lead to similar effects. In fact, a recent study has reported that while low levels of transgenic mCAT expression were beneficial in a cardiac Mfn2 knockout background, "super-suppression" of ROS by higher levels of mCAT exacerbated the cardiac phenotype and suppressed compensatory autophagy [281]. A separate study found that bactericidal activity is impaired in young mCAT mice [282]. At high levels, ROS cause oxidative damage, such as in cardiac hypertrophy and failure, and in this setting high and low levels of mCAT are both protective [76]. In the present study, the proteomic changes from mCAT overexpression in unstressed, young animals mimic a number of changes that occur with aging. Taken together, these studies suggest that mitochondrial antioxidant may not be universally beneficial, and the beneficial effects are observed in a setting when oxidative stress or

a high burst of ROS is anticipated. Thus, as with many drugs, mitochondrial antioxidants likely have a therapeutic windows and this may be age-dependent. It is also possible that such therapeutic windows vary by genetic background and organism.

These observations are also consistent with the notion of a ROS continuum, at the center of which is a physiologically necessary level of mitochondrial ROS [283] (SFig 7). At lower extremes of the continuum redox signaling pathways may be impaired while at higher extremes "pathological" ROS damages important components of the cell. In aging, increasing levels of ROS and oxidative damage are widely documented, and were part of the support for the "free radical theory of aging" [284]. However, the mCAT effect in young mice is consistent with an adverse impact on the more beneficial effects of ROS, while mCAT suppression of pathological levels of ROS in old animals is protective. This also suggests that ROS itself exhibits conventional antagonistic pleiotropy, and would explain why stronger antioxidant mechanisms, such as mCAT, have not evolved under natural selection of young animals in nature.

It would be of interest to pursue assays of reproductive fitness in mCAT versus WT mice as a further test of the hypothesis of reverse antagonistic pleiotropy. We have not detected such an effect in the laboratory, however, such tradeoffs in fitness may only be present in natural environments. Alternatively, one could pursue surrogate functional assays, such as tests of fighting behavior [285] or endurance on treadmills [286]. Another area for future research would be to examine additional ages of mCAT and WT mice to test the unproven assumption that there is an approximately linear decline in the youthful status of the proteomes over the life course.

In conclusion, we show evidence of "reverse" antagonistic pleiotropy in the cardiac and hepatic proteomes of mice overexpressing mitochondria-targeted catalase. In old mice, mCAT overexpression leads to a youthful proteome and better health, while in young mice it confers an "older" proteome. This data supports a view of ROS in aging that is inclusive of the beneficial functional roles ROS plays, such as redox signaling, in addition to pathological effects of ROS mediated oxidative damage. Importantly, this data underscores the importance of dosage and age with respect to therapeutic interventions. In

particular, in order for mitochondrial antioxidants to have a desired effect in humans, it may be important to consider not only the correct dose, but also to adjust the dose (or any delivery at all) with age.

6.5 MATERIALS AND METHODS

6.5.1 Animals

We used two independent founder lines as described before [18], B6.C3H-Tg(mCAT)4033Wcl and B6.C3H-Tg(mCAT)4403Wcl were generated and back-crossed as hemizygotes onto the C57BL/6J background (Jackson Laboratories, Bar Harbor, ME) for more than 10 generations. Control animals were wild type (WT) littermates of MCAT transgenic animals. Mice were fed irradiated Picolab Rodent Diet 20 #5053 (PMI Nutrition International, Brentwood, MO) and provided reverse osmosis water. One week after arrival, all mice were started on a synthetic diet (Harlan Teklad diet #TD.99366) that was nutritionally similar to the NIH-31 standard for rodents. The use of this diet facilitated the subsequent substitution of heavy-labeled [5,5,5 – $^{2}H_{3}$] leucine for light leucine, which enabled the protein turnover measurements.

6.5.2 Stable Isotope labeling

After 10 weeks of diet regimens, all mice received a synthetic diet (TD.09846, Harlan Teklad, Madison,WI) with the light leucine fully replaced by 11 g/kg of deuterated [5,5,5 – $^{2}H_{3}$] – L – leucine (Cambridge Isotope Laboratory, Tewksbury, MA), with CR and RP cohort conditions continued as above. Three mice were euthanized for tissue collections and proteomics analysis at four time points: days 3, 7, 12 and 17 after switching to $^{2}H_{3}$ – leucine diet.

6.5.3 Mass spectrometry

Tissues were homogenized in cold isolation buffer (250 mM sucrose, 1 mM EGTA, 10 mM HEPES, 10 mM Tris-HCl pH7.4). These lysates were centrifuged at 800 x g for 10 minutes to get rid of the debris. Whole liver and heart tissue were homogenized as previously described [193], trypsin digested, and LC-MS/MS analysis performed with a Waters nanoAcquity UPLC and a Thermo Scientific LTQ Orbitrap Velos, as previously described [88].

6.5.4 Data Repository

The raw data from MS/MS and extended supplementary files are available at https://chorusproject.org/pages/blog.html#/678. In order to view the data, a free account must be obtained by following the instructions on the Chorus Project website. For R-scripts, spreadsheets, and other data please contact the corresponding author.

6.5.5 **MS Data Analysis**

MS data were processed with the Hardklor (v1.33) and Bullseye (v1.25) algorithms to refine precursor mass measurements[287,288], followed by database search against all mouse entries of the UniProt database (**UniProt release 2013_02**) with the SEQUEST algorithm (vUW2012.01.7) – searching a total of 74,888 protein entries that were designated Mus musculus (Mouse). A dynamic modification of 3.0188325 for leucine was set to account for [5,5,5-$^{2}H_{3}$]-leucine and a static modification of 57.021461 for cysteine was set for carbamidomethyl modifications. The precursor monoisotopic mass tolerance was set to ± 10 ppm and the fragment mass tolerance window was set to 0.36 m/z. Enzyme specificity was set to semi-tryptic, allowing for up to 2 missed cleavage sites per peptide. The false discovery rate for spectrum matches was determined by the Percolator algorithm (v2.04) using a reversed copy of the UniProt database as a decoy [221]. Only results with a q-value less than 0.01 were kept for further analysis. This filter was used as it allows a small number (1%) of false positives to the next portion of analysis while providing enough data for categorization and statistical analysis of subsets of proteins. In addition, less than 5% of accepted false positives are expected to pass a subsequent turnover score filter, described below. Topograph (v1.1.0.297) software was developed for the deconvolution and measurement of peptide isotopologue abundances from LC-MS chromatograms and the calculation of peptide turnover rates, as previously described [88]. (http://proteome.gs.washington.edu/software/topograph/). Prior to analysis of abundance and turnover, peptides with a turnover score less than 0.98 were filtered out of the data. Turnover score is a metric internal to Topograph, ranging from 0 to 1, which describes the closeness of each observed isotopologue distribution with its closest matching theoretical distribution. A cutoff score of 0.98 was derived by plotting a receiver operator curve of true positive results versus true negative results (not shown), where true positive was defined as any peptide measurement that fell within 2 standard deviations of the mean label enrichment for all peptides, and true negatives were results that did not meet these criteria. Relative peptide abundances were determined by integrating MS1 peaks. For peptides that were identified in one sample, the regression of the identified peptide's MS/MS scan number is used to estimate a window for the same peptide in the other samples and a matching chromatographic peak was identified within that time range. This method allows peaks areas to be measured even in samples in which they are low and otherwise difficult to identify [289].For two given LC-MS/MS

chromatograms, the MS/MS scan number for peptides identified in both samples were plotted against each other in a scatter plot. A LOESS regression was used to find the best-fit line through the data points as previously described [88].

Only peptides that uniquely mapped to a single UniProt protein accession for Mus Musculus (**UniProt release 2013_02**), consisting of 74,888 entries from UniProtKB/*Swiss-Prot* and UniProtKB/*TrEMBL*, were used for quantification of abundance and turnover. First, sequences were searched against Swiss-Prot (reviewed) entries and accepted in a unique match is found. If no match was found, a second search was performed on TrEMBL (unreviewed) entries and the unique matches were retained. All remaining peptides, consisting of peptides with either no matching proteins or greater than 1 matching protein, were filtered out. For the cases where a protein consisted of more than one peptide, statistical models were modified to appropriately account for the multiple peptides by using a blocking factor. For each protein we applied non-linear regression fits of first order exponential curves to the percent newly synthesized protein using: $y = 100 + \beta 1^{e\alpha t}$. To determine whether the rates of turnover (slopes, α) were statistically different between experimental groups, ANCOVA was used. Half-lives were calculated according to first order kinetics: $t1/2 = \ln^{166}/$ slope. For details see the methods supplement of Hsieh et al. 2012 [88].

For heatmaps and pathway enrichment, only proteins that had significantly changed (p-value < 0.05) with age (significantly different between YWT and OWT) were considered. The p-values and correlations of the bivariate plots in panels B and C of Figs. 4-5 were derived from a partial correlation of the plotted groups while controlling for covariance with young wild type samples. Partial correlation allows direct comparison of peak areas (abundances) while controlling for changing baseline intensity caused by peptide variation in ionization efficiency. The YWT treatment group was used as the baseline for all other groups. Heatmaps were created using the heatmap.2 function in the gplots package in R. Rows and columns were ordered by linkage clustering using a Euclidean distance measure.

Line plots displayed in Figure 7 were calculated using proteomic abundance values (peak areas) of all proteins that significantly changed in abundance with age below a p-value threshold of 0.05. To compare

the trajectories of wild type aging and mCAT aging, we condensed the proteomic changes into an index of the aging change by taking the average absolute magnitude of the fold changes in protein abundance from YWT to OWT (WT aging). By this metric, WT aging is an average 5.66 fold change in heart proteome abundance. YWT was then set to zero and all values are expressed as a percentage of the WT aging effect; thus the 5.66 fold change in OWT equals 100% (black line, Figure 6-8A). Young and Old mCAT were adjusted accordingly such that all differences from YWT in the same direction as aging were positive values and changes in the opposite direction were negative values. The mCAT aging line was then plotted by connecting two points representing YmCAT and OmCAT.

6.5.6 **Pathway analysis**

Top pathways were determined using QIAGEN'S® Ingenuity Pathway Analysis (IPA®, QIAGEN Redwood City, www.qiagen.com/ingenuity) on all proteins which were significantly changed (p-value < 0.05) in abundance or half-life by aging (OWT vs YWT) or mCAT (YmCAT vs YWT and OmCAT vs OWT) expression. IPA determines the p-values of enrichment into canonical pathways by Fischer exact test.

All significantly changed proteins were then grouped by IPA canonical pathway and z-scores were visualized on a heatmap created in R using the gplots package. Values within each pathway category were clustered by Ward's method.

6.5.7 **Immunoblotting and ELISA**

A portion of each tissue was aliquotted into separate tubes containing cold isolation buffer (250 mM sucrose, 1 mM EGTA, 10 mM HEPES, 10 mM Tris-HCl pH7.4) as well as protease and phosphatase inhibitors(Pierce #87786 and #78420, Waltham, MA, USA) at the time of harvest, and stored at -80 degrees Celsius to be used for immunoblotting and other bench assays as necessary. Western blotting was done on the NuPAGE® Bis-Tris gel system (Life Technologies #WG1403BOX, Carlsbad, CA, USA) according to the manufacturer protocols with primary antibody concentrations of 1,000X and secondary antibody concentrations of 10,000X. The following primary antibodies were used: rabbit anti-human erythrocyte catalase(Athens Research & Technology #01-05-030000, Athens, GA, USA), UQCRC2(Abcam #ab103616, Cambridge, UK), VDAC(Thermo Scientific #PA1-954A, Waltham, MA, USA), Lamp2a(Invitrogen #51-2200, Waltham, MA, USA), mouse anti mouse multi-ubiquitin(MBL #D058-3, Wooburn, MA, USA), eEF2(Santa Cruz Biotechnology #sc-166415, Dallas, TX, USA), LC3II/I(Cell

Signaling #4108, Denver, MA, USA), Beclin1(Cell Signaling #3495, Denver, MA, USA), PGC1a(Abcam #ab54481, Cambridge, UK), COX-IV(Abcam #ab14744, Cambridge, UK). Secondary antibodies: Donkey anti Rabbit [290PI31458, Waltham, MA, USA], Goat anti Mouse [290PI31432, Waltham, MA, USA], and Rabbit anti Goat [290AP106P, Waltham, MA, USA]. Protein carbonylation was measured using an OxiSelect™ Protein Carbonyl ELISA Kit (Cell Biolabs, Inc. #STA-310, San Diego, CA, USA).

6.5.8 **Mitochondria Copy Number and mCAT gene expression**

In order to quantify mitochondria copy number per cell, we isolated DNA from hearts and livers using a PureLink® Genomic DNA Mini Kit, as per the manufacturer's instructions (Invitrogen K1820-02, Waltham, MA, USA). Mitochondrial DNA copy number was quantified using quantitative PCR of total DNA extracts from cardiac tissues. Mitochondrial DNA copies were estimated by the ratio of the amount of mitochondrial gene NADH dehydrogenase 1 (ND1) and a single-copy nuclear gene cytochrome P4501A1 (cyp1A1). Primers used were: ND1 (For: GAACGCAAAATCTTAGGGTACATACA, Rev: GCCGTATGGACCAACAATGTT, probe: 6FAM-CTACGAAAAGGCCC) and cyp1A1 (For:GACACAGTGATTGGCAGAGATC, Rev:AACGGATCTATGGTCTGACCTGT, probe: 6FAMCTCAGCTGCCCTATCTGGAGG CCTTC). Mitochondrial catalase qPCR was performed using forward and reverse primer sets for human catalase.

References

1 Pearson, J. L., North Dakota. State Department of Health. & North Dakota. State Department of Health and Consolidated Laboratories. *AIDS and North Dakota : a plan for action*. (North Dakota State Dept. of Health and Consolidated Laboratories, 1987).

2 Martin, G. M., LaMarco, K., Strauss, E. & K, L. K. Research on aging: the end of the beginning. *Science (New York, N.Y.)* **299**, 1339-1341, doi:10.1126/science.299.5611.1339 (2003).

3 Mah, D. C., Shihab-el-Deen, A., Price, G. B. & Zannis-Hadjopoulos, M. ORS12, a mammalian autonomously replicating DNA sequence, is present at the centromere of CV-1 cell chromosomes. *Experimental cell research* **203**, 435-442 (1992).

4 Trimpin, S. & Brizzard, B. Analysis of insoluble proteins. *BioTechniques* **46**, 321-326, doi:10.2144/000113135 (2009).

5 Medawar, P. An unsolved problem in biology. *HK Lewis, London* (1952).

6 de Magalhães, J. P. From cells to ageing: a review of models and mechanisms of cellular senescence and their impact on human ageing. *Exp Cell Res* **300**, 1-10, doi:10.1016/j.yexcr.2004.07.006 (2004).

7 Mattson, M. P., Duan, W. & Maswood, N. How does the brain control lifespan? *Ageing Res Rev* **1**, 155-165 (2002).

8 Kowald, A. & Kirkwood, T. B. Towards a network theory of ageing: a model combining the free radical theory and the protein error theory. *J Theor Biol* **168**, 75-94, doi:10.1006/jtbi.1994.1089 (1994).

9 *Centers for Disease Control and Prevention, National Center for Health Statistics. Compressed Mortality File 1999-2010 on CDC WONDER Online Database*.

10 Niccoli, T. & Partridge, L. Ageing as a risk factor for disease. *Curr Biol* **22**, R741-752, doi:10.1016/j.cub.2012.07.024 (2012).

11 Koga, H., Kaushik, S. & Cuervo, A. M. Protein homeostasis and aging: The importance of exquisite quality control. *Ageing Res Rev* **10**, 205-215, doi:10.1016/j.arr.2010.02.001 (2011).

12 Douglas, P. M. & Dillin, A. Protein homeostasis and aging in neurodegeneration. *J Cell Biol* **190**, 719-729, doi:10.1083/jcb.201005144 (2010).

13 Christians, E. S. & Benjamin, I. J. Proteostasis and REDOX state in the heart. *Am J Physiol Heart Circ Physiol* **302**, H24-37, doi:10.1152/ajpheart.00903.2011 (2012).

14 Hedhli, N., Pelat, M. & Depre, C. Protein turnover in cardiac cell growth and survival. *Cardiovasc Res* **68**, 186-196, doi:10.1016/j.cardiores.2005.06.025 (2005).

15 Surguchev, A. & Surguchov, A. Conformational diseases: looking into the eyes. *Brain Res Bull* **81**, 12-24, doi:10.1016/j.brainresbull.2009.09.015 (2010).

16 Vinciguerra, M., Musaro, A. & Rosenthal, N. Regulation of muscle atrophy in aging and disease. *Adv Exp Med Biol* **694**, 211-233 (2010).

17 Dai, D. F., Chen, T., Johnson, S. C., Szeto, H. & Rabinovitch, P. S. Cardiac aging: from molecular mechanisms to significance in human health and disease. *Antioxid Redox Signal* **16**, 1492-1526, doi:10.1089/ars.2011.4179 (2012).

18 Schriner, S. E. *et al.* Extension of murine life span by overexpression of catalase targeted to mitochondria. *Science* **308**, 1909-1911, doi:10.1126/science.1106653 (2005).

19 Perier, C. *et al.* Apoptosis-inducing factor deficiency sensitizes dopaminergic neurons to parkinsonian neurotoxins. *Ann Neurol* **68**, 184-192, doi:10.1002/ana.22034 (2010).

20 Marzetti, E., Calvani, R., Bernabei, R. & Leeuwenburgh, C. Apoptosis in skeletal myocytes: a potential target for interventions against sarcopenia and physical frailty - a mini-review. *Gerontology* **58**, 99-106, doi:10.1159/000330064 (2012).

21 Stanfel, M. N., Shamieh, L. S., Kaeberlein, M. & Kennedy, B. K. The TOR pathway comes of age. *Biochim Biophys Acta* **1790**, 1067-1074, doi:10.1016/j.bbagen.2009.06.007 (2009).

22 Puglielli, L. Aging of the brain, neurotrophin signaling, and Alzheimer's disease: is IGF1-R the common culprit? *Neurobiol Aging* **29**, 795-811, doi:10.1016/j.neurobiolaging.2007.01.010 (2008).

23 Abbas, A., Grant, P. J. & Kearney, M. T. Role of IGF-1 in glucose regulation and cardiovascular disease. *Expert Rev Cardiovasc Ther* **6**, 1135-1149, doi:10.1586/14779072.6.8.1135 (2008).

24 Kapahi, P. *et al.* With TOR, less is more: a key role for the conserved nutrient-sensing TOR pathway in aging. *Cell Metab* **11**, 453-465, doi:10.1016/j.cmet.2010.05.001 (2010).

25 Harrison, D. E. *et al.* Rapamycin fed late in life extends lifespan in genetically heterogeneous mice. *Nature* **460**, 392-395, doi:10.1038/nature08221 (2009).

26 Johnson, S. C., Rabinovitch, P. S. & Kaeberlein, M. mTOR is a key modulator of ageing and age-related disease. *Nature* **493**, 338-345, doi:10.1038/nature11861 (2013).

27 Morimoto, R. I. & Cuervo, A. M. Protein homeostasis and aging: taking care of proteins from the cradle to the grave. *J Gerontol A Biol Sci Med Sci* **64**, 167-170, doi:10.1093/gerona/gln071 (2009).

28 Wong, E. & Cuervo, A. M. Integration of clearance mechanisms: the proteasome and autophagy. *Cold Spring Harbor perspectives in biology* **2**, a006734, doi:10.1101/cshperspect.a006734 (2010).

29 Ravikumar, B., Duden, R. & Rubinsztein, D. C. Aggregate-prone proteins with polyglutamine and polyalanine expansions are degraded by autophagy. *Hum Mol Genet* **11**, 1107-1117 (2002).

30 Jung, C. H., Ro, S. H., Cao, J., Otto, N. M. & Kim, D. H. mTOR regulation of autophagy. *FEBS letters* **584**, 1287-1295, doi:10.1016/j.febslet.2010.01.017 (2010).

31 Robinson, P. A. Protein stability and aggregation in Parkinson's disease. *Biochem J* **413**, 1-13, doi:10.1042/bj20080295 (2008).

32 Madeo, F., Tavernarakis, N. & Kroemer, G. Can autophagy promote longevity? *Nat Cell Biol* **12**, 842-846, doi:10.1038/ncb0910-842 (2010).

33 Pyo, J. O. *et al.* Overexpression of Atg5 in mice activates autophagy and extends lifespan. *Nat Commun* **4**, 2300, doi:10.1038/ncomms3300 (2013).

34 Jana, N. R. Protein homeostasis and aging: role of ubiquitin protein ligases. *Neurochem Int* **60**, 443-447, doi:10.1016/j.neuint.2012.02.009 (2012).

35 Landles, C. & Bates, G. P. Huntingtin and the molecular pathogenesis of Huntington's disease. Fourth in molecular medicine review series. *EMBO Rep* **5**, 958-963, doi:10.1038/sj.embor.7400250 (2004).

36 Bedford, L. *et al.* Depletion of 26S proteasomes in mouse brain neurons causes neurodegeneration and Lewy-like inclusions resembling human pale bodies. *J Neurosci* **28**, 8189-8198, doi:10.1523/jneurosci.2218-08.2008 (2008).

37 Keck, S., Nitsch, R., Grune, T. & Ullrich, O. Proteasome inhibition by paired helical filament-tau in brains of patients with Alzheimer's disease. *J Neurochem* **85**, 115-122 (2003).

38 Li, W., Gao, B., Lee, S. M., Bennett, K. & Fang, D. RLE-1, an E3 ubiquitin ligase, regulates C. *elegans* aging by catalyzing DAF-16 polyubiquitination. *Dev Cell* **12**, 235-246, doi:10.1016/j.devcel.2006.12.002 (2007).

39 Rana, A., Rera, M. & Walker, D. W. Parkin overexpression during aging reduces proteotoxicity, alters mitochondrial dynamics, and extends lifespan. *Proc Natl Acad Sci U S A* **110**, 8638-8643, doi:10.1073/pnas.1216197110 (2013).

40 Tan, J. M. *et al.* Lysine 63-linked ubiquitination promotes the formation and autophagic clearance of protein inclusions associated with neurodegenerative diseases. *Hum Mol Genet* **17**, 431-439, doi:10.1093/hmg/ddm320 (2008).

41 Zinngrebe, J., Montinaro, A., Peltzer, N. & Walczak, H. Ubiquitin in the immune system. *EMBO reports* **15**, 28-45, doi:10.1002/embr.201338025 (2014).

42 Kraft, C., Peter, M. & Hofmann, K. Selective autophagy: ubiquitin-mediated recognition and beyond. *Nat Cell Biol* **12**, 836-841, doi:10.1038/ncb0910-836 (2010).

43 Haldar, A. K. *et al.* Ubiquitin systems mark pathogen-containing vacuoles as targets for host defense by guanylate binding proteins. *Proc Natl Acad Sci U S A*, doi:10.1073/pnas.1515966112 (2015).

44 McCay, C. M., Crowell, M. F. & Maynard, L. A. The effect of retarded growth upon the length of life span and upon the ultimate body size. 1935. *Nutrition* **5**, 155-171; discussion 172 (1989).

45 Kemnitz, J. W. *et al.* Dietary restriction increases insulin sensitivity and lowers blood glucose in rhesus monkeys. *The American journal of physiology* **266**, E540-547 (1994).

46 Weindruch, R., Walford, R. L., Fligiel, S. & Guthrie, D. The retardation of aging in mice by dietary restriction: longevity, cancer, immunity and lifetime energy intake. *The Journal of nutrition* **116**, 641-654 (1986).

47 Masoro, E. J. Overview of caloric restriction and ageing. *Mech Ageing Dev* **126**, 913-922, doi:10.1016/j.mad.2005.03.012 (2005).

48 Colman, R. J. *et al.* Caloric restriction delays disease onset and mortality in rhesus monkeys. *Science* **325**, 201-204, doi:10.1126/science.1173635 (2009).

49 Mattison, J. A. *et al.* Impact of caloric restriction on health and survival in rhesus monkeys from the NIA study. *Nature* **489**, 318-321, doi:10.1038/nature11432 (2012).

50 Osmulski, P. A. & Gaczynska, M. Rapamycin allosterically inhibits the proteasome. *Molecular pharmacology* **84**, 104-113, doi:10.1124/mol.112.083873 (2013).

51 Harman, D. Aging: A Theory Based on Free Radical and Radiation Chemistry. *Journal of Gerontology* **11**, 298-300, doi:10.1093/geronj/11.3.298 (1956).

52 Harman, D. The biologic clock: the mitochondria? *Journal of the American Geriatrics Society* **20**, 145-147 (1972).

53 Anderson, E. J. *et al.* Mitochondrial H2O2 emission and cellular redox state link excess fat intake to insulin resistance in both rodents and humans. *The Journal of clinical investigation* **119**, 573-581, doi:10.1172/jci37048 (2009).

54 Dodson, M., Darley-Usmar, V. & Zhang, J. Cellular metabolic and autophagic pathways: traffic control by redox signaling. *Free Radic Biol Med* **63**, 207-221, doi:10.1016/j.freeradbiomed.2013.05.014 (2013).

55 Fisher-Wellman, K. H. & Neufer, P. D. Linking mitochondrial bioenergetics to insulin resistance via redox biology. *Trends in endocrinology and metabolism: TEM* **23**, 142-153, doi:10.1016/j.tem.2011.12.008 (2012).

56 Dai, D. F. *et al.* Global proteomics and pathway analysis of pressure-overload-induced heart failure and its attenuation by mitochondrial-targeted peptides. *Circ Heart Fail* **6**, 1067-1076, doi:10.1161/circheartfailure.113.000406 (2013).

57 Tsutsui, H., Ide, T. & Kinugawa, S. Mitochondrial oxidative stress, DNA damage, and heart failure. *Antioxid Redox Signal* **8**, 1737-1744, doi:10.1089/ars.2006.8.1737 (2006).

58 Wang, X., Su, H. & Ranek, M. J. Protein quality control and degradation in cardiomyocytes. *Journal of molecular and cellular cardiology* **45**, 11-27, doi:10.1016/j.yjmcc.2008.03.025 (2008).

59 Brieger, K., Schiavone, S., Miller, F. J. & Krause, K. H. Reactive oxygen species: from health to disease. *Swiss Med Wkly* **142**, w13659, doi:10.4414/smw.2012.13659 (2012).

60 Arai, H. Oxidative modification of lipoproteins. *Subcell Biochem* **77**, 103-114, doi:10.1007/978-94-007-7920-4_9 (2014).

61 Lee, H. Y. *et al.* Targeted expression of catalase to mitochondria prevents age-associated reductions in mitochondrial function and insulin resistance. *Cell Metab* **12**, 668-674, doi:10.1016/j.cmet.2010.11.004 (2010).

62 Forman, H. J., Ursini, F. & Maiorino, M. An overview of mechanisms of redox signaling. *J Mol Cell Cardiol* **73**, 2-9, doi:10.1016/j.yjmcc.2014.01.018 (2014).

63 Goodman, M., Bostick, R. M., Kucuk, O. & Jones, D. P. Clinical trials of antioxidants as cancer prevention agents: past, present, and future. *Free Radic Biol Med* **51**, 1068-1084, doi:10.1016/j.freeradbiomed.2011.05.018 (2011).

64 Golbidi, S. & Laher, I. Antioxidant therapy in human endocrine disorders. *Med Sci Monit* **16**, RA9-24 (2010).

65 Kris-Etherton, P. M. *et al.* Antioxidant vitamin supplements and cardiovascular disease. *Circulation* **110**, 637-641, doi:10.1161/01.cir.0000137822.39831.f1 (2004).

66 Bjelakovic, G., Nikolova, D., Gluud, L. L., Simonetti, R. G. & Gluud, C. Antioxidant supplements for prevention of mortality in healthy participants and patients with various diseases. *Cochrane Database Syst Rev* **3**, CD007176, doi:10.1002/14651858.CD007176.pub2 (2012).

67 Albanes, D. *et al.* Alpha-Tocopherol and beta-carotene supplements and lung cancer incidence in the alpha-tocopherol, beta-carotene cancer prevention study: effects of base-line characteristics and study compliance. *Journal of the National Cancer Institute* **88**, 1560-1570 (1996).

68 Omenn, G. S. *et al.* Risk factors for lung cancer and for intervention effects in CARET, the Beta-Carotene and Retinol Efficacy Trial. *Journal of the National Cancer Institute* **88**, 1550-1559 (1996).

69 Lee, S. J., Hwang, A. B. & Kenyon, C. Inhibition of respiration extends C. *elegans* life span via reactive oxygen species that increase HIF-1 activity. *Curr Biol* **20**, 2131-2136, doi:10.1016/j.cub.2010.10.057 (2010).

70 Pérez, V. I. *et al.* Is the oxidative stress theory of aging dead? *Biochim Biophys Acta* **1790**, 1005-1014, doi:10.1016/j.bbagen.2009.06.003 (2009).

71 Treuting, P. M. *et al.* Reduction of age-associated pathology in old mice by overexpression of catalase in mitochondria. *J Gerontol A Biol Sci Med Sci* **63**, 813-822 (2008).

72 Mao, P. *et al.* Mitochondria-targeted catalase reduces abnormal APP processing, amyloid β production and BACE1 in a mouse model of Alzheimer's disease: implications for neuroprotection and lifespan extension. *Hum Mol Genet* **21**, 2973-2990, doi:10.1093/hmg/dds128 (2012).

73 Dai, D. F. *et al.* Overexpression of catalase targeted to mitochondria attenuates murine cardiac aging. *Circulation* **119**, 2789-2797, doi:10.1161/circulationaha.108.822403 (2009).

74 Parihar, V. K. *et al.* Targeted overexpression of mitochondrial catalase prevents radiation-induced cognitive dysfunction. *Antioxid Redox Signal* **22**, 78-91, doi:10.1089/ars.2014.5929 (2015).

75 Dai, D. F. *et al.* Mitochondrial proteome remodelling in pressure overload-induced heart failure: the role of mitochondrial oxidative stress. *Cardiovasc Res* **93**, 79-88, doi:10.1093/cvr/cvr274 (2012).

76 Dai, D. F. *et al.* Mitochondrial oxidative stress mediates angiotensin II-induced cardiac hypertrophy and Galphaq overexpression-induced heart failure. *Circ Res* **108**, 837-846, doi:10.1161/circresaha.110.232306 (2011).

77 Fletcher, M. J. & Sanadi, D. R. Turnover of rat-liver mitochondria. *Biochim Biophys Acta* **51**, 356-360 (1961).

78 Beattie, D. S., Basford, R. E. & Koritz, S. B. The turnover of the protein components of mitochondria from rat liver, kidney, and brain. *The Journal of biological chemistry* **242**, 4584-4586 (1967).

79 Schoenheimer, R., Rittenberg, D., Foster, G. L., Keston, A. S. & Ratner, S. The Application of the Nitrogen Isotope N15 for the Study of Protein Metabolism. *Science (New York, N.Y.)* **88**, 599-600, doi:10.1126/science.88.2295.599 (1938).

80 Christiano, R., Nagaraj, N., Frohlich, F. & Walther, T. C. Global proteome turnover analyses of the Yeasts S. cerevisiae and S. pombe. *Cell reports* **9**, 1959-1965, doi:10.1016/j.celrep.2014.10.065 (2014).

81 Jones, P. J. & Leatherdale, S. T. Stable isotopes in clinical research: safety reaffirmed. *Clinical science* **80**, 277-280 (1991).

82 Doherty, M. K. & Beynon, R. J. Protein turnover on the scale of the proteome. *Expert review of proteomics* **3**, 97-110, doi:10.1586/14789450.3.1.97 (2006).

83 Wu, C. C., MacCoss, M. J., Howell, K. E., Matthews, D. E. & Yates, J. R., 3rd. Metabolic labeling of mammalian organisms with stable isotopes for quantitative proteomic analysis. *Anal Chem* **76**, 4951-4959, doi:10.1021/ac049208j (2004).

84 Kim, T. Y. *et al.* Metabolic labeling reveals proteome dynamics of mouse mitochondria. *Mol Cell Proteomics* **11**, 1586-1594, doi:10.1074/mcp.M112.021162 (2012).

85 Miller, B. F., Robinson, M. M., Bruss, M. D., Hellerstein, M. & Hamilton, K. L. A comprehensive assessment of mitochondrial protein synthesis and cellular proliferation with age and caloric restriction. *Aging Cell* **11**, 150-161, doi:10.1111/j.1474-9726.2011.00769.x (2012).

86 Hellerstein, M. K. & Neese, R. A. Mass isotopomer distribution analysis: a technique for measuring biosynthesis and turnover of polymers. *The American journal of physiology* **263**, E988-1001 (1992).

87 Hellerstein, M. K. & Neese, R. A. Mass isotopomer distribution analysis at eight years: theoretical, analytic, and experimental considerations. *The American journal of physiology* **276**, E1146-1170 (1999).

88 Hsieh, E. J. *et al.* Topograph, a software platform for precursor enrichment corrected global protein turnover measurements. *Mol Cell Proteomics* **11**, 1468-1474, doi:10.1074/mcp.O112.017699 (2012).

89 Claydon, A. J., Thom, M. D., Hurst, J. L. & Beynon, R. J. Protein turnover: measurement of proteome dynamics by whole animal metabolic labelling with stable isotope labelled amino acids. *Proteomics* **12**, 1194-1206, doi:10.1002/pmic.201100556 (2012).

90 North, B. J. & Sinclair, D. A. The intersection between aging and cardiovascular disease. *Circ Res* **110**, 1097-1108, doi:10.1161/circresaha.111.246876 (2012).

91 Dai, D. F. *et al.* Altered proteome turnover and remodeling by short-term caloric restriction or rapamycin rejuvenate the aging heart. *Aging Cell* **13**, 529-539, doi:10.1111/acel.12203 (2014).

92 Kruse, S. E. *et al.* Age Modifies Respiratory Complex I and Protein Homeostasis in a Muscle Type-specific Manner. *Aging Cell* **IN PRESS** (2015).

93 Price, J. C., Guan, S., Burlingame, A., Prusiner, S. B. & Ghaemmaghami, S. Analysis of proteome dynamics in the mouse brain. *Proc Natl Acad Sci U S A* **107**, 14508-14513, doi:10.1073/pnas.1006551107 (2010).

94 Wohlgemuth, S. E., Calvani, R. & Marzetti, E. The interplay between autophagy and mitochondrial dysfunction in oxidative stress-induced cardiac aging and pathology. *J Mol Cell Cardiol* **71**, 62-70, doi:10.1016/j.yjmcc.2014.03.007 (2014).

95 Dutta, D., Xu, J., Kim, J. S., Dunn, W. A., Jr. & Leeuwenburgh, C. Upregulated autophagy protects cardiomyocytes from oxidative stress-induced toxicity. *Autophagy* **9**, 328-344, doi:10.4161/auto.22971 (2013).

96 Taneike, M. *et al.* Inhibition of autophagy in the heart induces age-related cardiomyopathy. *Autophagy* **6**, 600-606, doi:10.4161/auto.6.5.11947 (2010).

97 Pagan, J., Seto, T., Pagano, M. & Cittadini, A. Role of the ubiquitin proteasome system in the heart. *Circ Res* **112**, 1046-1058, doi:10.1161/circresaha.112.300521 (2013).

98 Mouli, P. K., Twig, G. & Shirihai, O. S. Frequency and selectivity of mitochondrial fusion are key to its quality maintenance function. *Biophysical journal* **96**, 3509-3518, doi:10.1016/j.bpj.2008.12.3959 (2009).

99 Ong, S. B., Hall, A. R. & Hausenloy, D. J. Mitochondrial dynamics in cardiovascular health and disease. *Antioxidants & redox signaling* **19**, 400-414, doi:10.1089/ars.2012.4777 (2013).

100 Schieke, S. M. *et al.* The mammalian target of rapamycin (mTOR) pathway regulates mitochondrial oxygen consumption and oxidative capacity. *J Biol Chem* **281**, 27643-27652, doi:10.1074/jbc.M603536200 (2006).

101 Palmer, C. S. *et al.* Adaptor proteins MiD49 and MiD51 can act independently of Mff and Fis1 in Drp1 recruitment and are specific for mitochondrial fission. *The Journal of biological chemistry* **288**, 27584-27593, doi:10.1074/jbc.M113.479873 (2013).

102 Liesa, M., Palacin, M. & Zorzano, A. Mitochondrial dynamics in mammalian health and disease. *Physiological reviews* **89**, 799-845, doi:10.1152/physrev.00030.2008 (2009).

103 Chen, H. *et al.* Mitofusins Mfn1 and Mfn2 coordinately regulate mitochondrial fusion and are essential for embryonic development. *The Journal of cell biology* **160**, 189-200, doi:10.1083/jcb.200211046 (2003).

104 Chen, H. *et al.* Mitochondrial fusion is required for mtDNA stability in skeletal muscle and tolerance of mtDNA mutations. *Cell* **141**, 280-289, doi:10.1016/j.cell.2010.02.026 (2010).

105 Narula, J. *et al.* Apoptosis in heart failure: release of cytochrome c from mitochondria and activation of caspase-3 in human cardiomyopathy. *Proc Natl Acad Sci U S A* **96**, 8144-8149 (1999).

106 Phaneuf, S. & Leeuwenburgh, C. Cytochrome c release from mitochondria in the aging heart: a possible mechanism for apoptosis with age. *American journal of physiology. Regulatory, integrative and comparative physiology* **282**, R423-430, doi:10.1152/ajpregu.00296.2001 (2002).

107 Beltrami, C. A. *et al.* Structural basis of end-stage failure in ischemic cardiomyopathy in humans. *Circulation* **89**, 151-163 (1994).

108 Suen, D. F., Norris, K. L. & Youle, R. J. Mitochondrial dynamics and apoptosis. *Genes Dev* **22**, 1577-1590, doi:10.1101/gad.1658508 (2008).

109 Youle, R. J. & Karbowski, M. Mitochondrial fission in apoptosis. *Nature reviews. Molecular cell biology* **6**, 657-663, doi:10.1038/nrm1697 (2005).

110 Samant, S. A. *et al.* SIRT3 deacetylates and activates OPA1 to regulate mitochondrial dynamics during stress. *Mol Cell Biol* **34**, 807-819, doi:10.1128/MCB.01483-13 (2014).

111 Ikeda, Y. *et al.* Molecular mechanisms mediating mitochondrial dynamics and mitophagy and their functional roles in the cardiovascular system. *J Mol Cell Cardiol* **78**, 116-122, doi:10.1016/j.yjmcc.2014.09.019

10.1016/j.yjmcc.2014.09.019. Epub 2014 Oct 7. (2015).

112 Knowlton, A. A., Chen, L. & Malik, Z. A. Heart failure and mitochondrial dysfunction: the role of mitochondrial fission/fusion abnormalities and new therapeutic strategies. *Journal of cardiovascular pharmacology* **63**, 196-206, doi:10.1097/01.fjc.0000432861.55968.a6 (2014).

113 Bhandari, P., Song, M. & Dorn, G. W., 2nd. Dissociation of mitochondrial from sarcoplasmic reticular stress in Drosophila cardiomyopathy induced by molecularly distinct mitochondrial fusion defects. *J Mol Cell Cardiol* **80**, 71-80, doi:10.1016/j.yjmcc.2014.12.018 10.1016/j.yjmcc.2014.12.018. Epub 2014 Dec 30. (2015).

114 Zepeda, R. *et al.* Drp1 loss-of-function reduces cardiomyocyte oxygen dependence protecting the heart from ischemia-reperfusion injury. *Journal of cardiovascular pharmacology* **63**, 477-487, doi:10.1097/FJC.0000000000000071 (2014).

115 Givvimani, S., Pushpakumar, S., Veeranki, S. & Tyagi, S. C. Dysregulation of Mfn2 and Drp-1 proteins in heart failure. *Canadian journal of physiology and pharmacology* **92**, 583-591, doi:10.1139/cjpp-2014-0060 (2014).

116 Ravikumar, B., Berger, Z., Vacher, C., O'Kane, C. J. & Rubinsztein, D. C. Rapamycin pre-treatment protects against apoptosis. *Hum Mol Genet* **15**, 1209-1216, doi:10.1093/hmg/ddl036 (2006).

117 Dias, V., Junn, E. & Mouradian, M. M. The role of oxidative stress in Parkinson's disease. *J Parkinsons Dis* **3**, 461-491, doi:10.3233/jpd-130230 (2013).

118 Ashrafi, G., Schlehe, J. S., LaVoie, M. J. & Schwarz, T. L. Mitophagy of damaged mitochondria occurs locally in distal neuronal axons and requires PINK1 and Parkin. *J Cell Biol* **206**, 655-670, doi:10.1083/jcb.201401070 (2014).

119 Matsuda, S., Kitagishi, Y. & Kobayashi, M. Function and characteristics of PINK1 in mitochondria. *Oxid Med Cell Longev* **2013**, 601587, doi:10.1155/2013/601587 (2013).

120 Rochet, J. C., Hay, B. A. & Guo, M. Molecular insights into Parkinson's disease. *Prog Mol Biol Transl Sci* **107**, 125-188, doi:10.1016/b978-0-12-385883-2.00011-4 (2012).

121 Sparling, P. B., Millard-Stafford, M. & Snow, T. K. Development of a cadence curl-up test for college students. *Research quarterly for exercise and sport* **68**, 309-316, doi:10.1080/02701367.1997.10608012 (1997).

122 Greene, A. W. *et al.* Mitochondrial processing peptidase regulates PINK1 processing, import and Parkin recruitment. *EMBO Rep* **13**, 378-385, doi:10.1038/embor.2012.14 (2012).

123 Hammerling, B. C. & Gustafsson, A. B. Mitochondrial quality control in the myocardium: cooperation between protein degradation and mitophagy. *J Mol Cell Cardiol* **75**, 122-130, doi:10.1016/j.yjmcc.2014.07.013

10.1016/j.yjmcc.2014.07.013. Epub 2014 Jul 30. (2014).

124 Thomas, R. L. & Gustafsson, A. B. Mitochondrial autophagy--an essential quality control mechanism for myocardial homeostasis. *Circ J* **77**, 2449-2454 (2013).

125 Huang, C. *et al.* Preconditioning involves selective mitophagy mediated by Parkin and p62/SQSTM1. *PLoS One* **6**, e20975, doi:10.1371/journal.pone.0020975 (2011).

126 Piquereau, J. *et al.* Protective role of PARK2/Parkin in sepsis-induced cardiac contractile and mitochondrial dysfunction. *Autophagy* **9**, 1837-1851, doi:10.4161/auto.26502 (2013).

127 Kubli, D. A. *et al.* Parkin protein deficiency exacerbates cardiac injury and reduces survival following myocardial infarction. *J Biol Chem* **288**, 915-926, doi:10.1074/jbc.M112.411363 (2013).

128 Kubli, D. A., Quinsay, M. N. & Gustafsson, A. B. Parkin deficiency results in accumulation of abnormal mitochondria in aging myocytes. *Commun Integr Biol* **6**, e24511, doi:10.4161/cib.24511 (2013).

129 Jimenez, R. E., Kubli, D. A. & Gustafsson, A. B. Autophagy and mitophagy in the myocardium: therapeutic potential and concerns. *Br J Pharmacol* **171**, 1907-1916, doi:10.1111/bph.12477 (2014).

130 Siddall, H. K. *et al.* Loss of PINK1 increases the heart's vulnerability to ischemia-reperfusion injury. *PLoS One* **8**, e62400, doi:10.1371/journal.pone.0062400 (2013).

131 Billia, F. *et al.* PTEN-inducible kinase 1 (PINK1)/Park6 is indispensable for normal heart function. *Proc Natl Acad Sci U S A* **108**, 9572-9577, doi:10.1073/pnas.1106291108 (2011).

132 Speakman, J. R. & Mitchell, S. E. Caloric restriction. *Molecular aspects of medicine* **32**, 159-221, doi:10.1016/j.mam.2011.07.001 (2011).

133 Taffet, G. E., Pham, T. T. & Hartley, C. J. The Age-Associated Alterations in Late Diastolic Function in Mice Are Improved by Caloric Restriction. *The Journals of Gerontology Series A: Biological Sciences and Medical Sciences* **52A**, B285-B290, doi:10.1093/gerona/52A.6.B285 (1997).

134 Niemann, B., Chen, Y., Issa, H., Silber, R. E. & Rohrbach, S. Caloric restriction delays cardiac ageing in rats: role of mitochondria. *Cardiovasc Res* **88**, 267-276, doi:10.1093/cvr/cvq273 (2010).

135 Shinmura, K. *et al.* Impact of long-term caloric restriction on cardiac senescence: caloric restriction ameliorates cardiac diastolic dysfunction associated with aging. *J Mol Cell Cardiol* **50**, 117-127, doi:10.1016/j.yjmcc.2010.10.018 (2011).

136 Maeda, H. *et al.* Nutritional influences on aging of Fischer 344 rats: II. Pathology. *J Gerontol* **40**, 671-688 (1985).

137 Kenyon, C. J. The genetics of ageing. *Nature* **464**, 504-512, doi:nature08980 [pii] 10.1038/nature08980 [doi] (2010).

138 Miller, R. A. *et al.* Rapamycin, but not resveratrol or simvastatin, extends life span of genetically heterogeneous mice. *J Gerontol A Biol Sci Med Sci* **66**, 191-201, doi:10.1093/gerona/glq178 (2011).

139 Steffen, K. K. *et al.* Yeast life span extension by depletion of 60s ribosomal subunits is mediated by Gcn4. *Cell* **133**, 292-302, doi:10.1016/j.cell.2008.02.037 (2008).

140 Guertin, D. A. & Sabatini, D. M. Defining the role of mTOR in cancer. *Cancer Cell* **12**, 9-22, doi:S1535-6108(07)00151-1 [pii] 10.1016/j.ccr.2007.05.008 [doi] (2007).

141 Sengupta, S., Peterson, T. R. & Sabatini, D. M. Regulation of the mTOR complex 1 pathway by nutrients, growth factors, and stress. *Molecular cell* **40**, 310-322, doi:10.1016/j.molcel.2010.09.026 (2010).

142 Selman, C. *et al.* Ribosomal protein S6 kinase 1 signaling regulates mammalian life span. *Science* **326**, 140-144, doi:10.1126/science.1177221 (2009).

143 Zid, B. M. *et al.* 4E-BP extends lifespan upon dietary restriction by enhancing mitochondrial activity in Drosophila. *Cell* **139**, 149-160, doi:10.1016/j.cell.2009.07.034 (2009).

144 Wessells, R. *et al.* d4eBP acts downstream of both dTOR and dFoxo to modulate cardiac functional aging in Drosophila. *Aging Cell* **8**, 542-552, doi:10.1111/j.1474-9726.2009.00504.x (2009).

145 McMullen, J. R. *et al.* Inhibition of mTOR signaling with rapamycin regresses established cardiac hypertrophy induced by pressure overload. *Circulation* **109**, 3050-3055, doi:10.1161/01.cir.0000130641.08705.45 (2004).

146 Laplante, M. & Sabatini, D. M. mTOR signaling in growth control and disease. *Cell* **149**, 274-293, doi:10.1016/j.cell.2012.03.017 (2012).

147 Al-Qassab, H. *et al.* Dominant role of the p110beta isoform of PI3K over p110alpha in energy homeostasis regulation by POMC and AgRP neurons. *Cell Metab* **10**, 343-354, doi:10.1016/j.cmet.2009.09.008 (2009).

148 Sipula, I. J., Brown, N. F. & Perdomo, G. Rapamycin-mediated inhibition of mammalian target of rapamycin in skeletal muscle cells reduces glucose utilization and increases fatty acid oxidation. *Metabolism* **55**, 1637-1644, doi:S0026-0495(06)00282-4 [pii]

10.1016/j.metabol.2006.08.002 [doi] (2006).

149 Kolwicz, S. C., Jr. & Tian, R. Metabolic therapy at the crossroad: how to optimize myocardial substrate utilization? *Trends in cardiovascular medicine* **19**, 201-207, doi:S1050-1738(09)00183-2 [pii]

10.1016/j.tcm.2009.12.005 [doi] (2009).

150 Zhang, Y. *et al.* Insulin-like growth factor 1 alleviates high-fat diet-induced myocardial contractile dysfunction: role of insulin signaling and mitochondrial function. *Hypertension* **59**, 680-693, doi:HYPERTENSIONAHA.111.181867 [pii]

10.1161/HYPERTENSIONAHA.111.181867 [doi] (2012).

151 Li, Q., Ceylan-Isik, A. F., Li, J. & Ren, J. Deficiency of insulin-like growth factor 1 reduces sensitivity to aging-associated cardiomyocyte dysfunction. *Rejuvenation research* **11**, 725-733, doi:10.1089/rej.2008.0717 (2008).

152 Lamming, D. W. *et al.* Rapamycin-induced insulin resistance is mediated by mTORC2 loss and uncoupled from longevity. *Science (New York, N.Y.)* **335**, 1638-1643, doi:10.1126/science.1215135 (2012).

153 Fang, Y. *et al.* Duration of rapamycin treatment has differential effects on metabolism in mice. *Cell metabolism* **17**, 456-462, doi:10.1016/j.cmet.2013.02.008 (2013).

154 Neff, F. *et al.* Rapamycin extends murine lifespan but has limited effects on aging. *The Journal of clinical investigation* **123**, 3272-3291, doi:67674 [pii]
10.1172/JCI67674 [doi] (2013).

155 Flynn, J. M. *et al.* Late-life rapamycin treatment reverses age-related heart dysfunction. *Aging Cell* **12**, 851-862, doi:10.1111/acel.12109 (2013).

156 Lakatta, E. G. & Levy, D. Arterial and cardiac aging: major shareholders in cardiovascular disease enterprises: Part I: aging arteries: a "set up" for vascular disease. *Circulation* **107**, 139-146 (2003).

157 Breusing, N. & Grune, T. Regulation of proteasome-mediated protein degradation during oxidative stress and aging. *Biol Chem* **389**, 203-209, doi:10.1515/BC.2008.029 [doi] (2008).

158 Miller, B. F. *et al.* Calorie restriction does not increase short-term or long-term protein synthesis. *The journals of gerontology. Series A, Biological sciences and medical sciences* **68**, 530-538, doi:10.1093/gerona/gls219 (2013).

159 Drake, J. C. *et al.* Assessment of mitochondrial biogenesis and mTORC1 signaling during chronic rapamycin feeding in male and female mice. *J Gerontol A Biol Sci Med Sci* **68**, 1493-1501, doi:10.1093/gerona/glt047 (2013).

160 Price, J. C. *et al.* The effect of long term calorie restriction on in vivo hepatic proteostatis: a novel combination of dynamic and quantitative proteomics. *Mol Cell Proteomics* **11**, 1801-1814, doi:10.1074/mcp.M112.021204 (2012).

161 Conn, C. S. & Qian, S. B. Nutrient signaling in protein homeostasis: an increase in quantity at the expense of quality. *Science signaling* **6**, ra24, doi:10.1126/scisignal.2003520 (2013).

162 Someya, S. *et al.* Sirt3 mediates reduction of oxidative damage and prevention of age-related hearing loss under caloric restriction. *Cell* **143**, 802-812, doi:S0092-8674(10)01138-4 [pii]
10.1016/j.cell.2010.10.002 [doi] (2010).

163 Seibenhener, M. L. *et al.* Sequestosome 1/p62 is a polyubiquitin chain binding protein involved in ubiquitin proteasome degradation. *Mol Cell Biol* **24**, 8055-8068, doi:10.1128/MCB.24.18.8055-8068.2004 [doi]
24/18/8055 [pii] (2004).

164 Yao, T. P. The role of ubiquitin in autophagy-dependent protein aggregate processing. *Genes Cancer* **1**, 779-786, doi:10.1177/1947601910383277 [doi] (2010).

165 Thoreen, C. C. *et al.* A unifying model for mTORC1-mediated regulation of mRNA translation. *Nature* **485**, 109-113, doi:nature11083 [pii]

10.1038/nature11083 [doi] (2012).

166 Wang, H. *et al.* Development and evaluation of a micro- and nanoscale proteomic sample preparation method. *J Proteome Res* **4**, 2397-2403, doi:10.1021/pr050160f (2005).

167 Schonhofen, P., de Medeiros, L. M., Chatain, C. P., Bristot, I. J. & Klamt, F. Cofilin/actin rod formation by dysregulation of cofilin-1 activity as a central initial step in neurodegeneration. *Mini reviews in medicinal chemistry* **14**, 393-400 (2014).

168 Finkel, T. & Holbrook, N. J. Oxidants, oxidative stress and the biology of ageing. *Nature* **408**, 239-247, doi:10.1038/35041687 (2000).

169 Hipkiss, A. R. Accumulation of altered proteins and ageing: causes and effects. *Exp Gerontol* **41**, 464-473, doi:10.1016/j.exger.2006.03.004 (2006).

170 Chondrogianni, N. & Gonos, E. S. Proteasome dysfunction in mammalian aging: steps and factors involved. *Exp Gerontol* **40**, 931-938, doi:10.1016/j.exger.2005.09.004 (2005).

171 Blackwell, B. N., Bucci, T. J., Hart, R. W. & Turturro, A. Longevity, body weight, and neoplasia in ad libitum-fed and diet-restricted C57BL6 mice fed NIH-31 open formula diet. *Toxicol Pathol* **23**, 570-582 (1995).

172 Sabatini, D. M., Erdjument-Bromage, H., Lui, M., Tempst, P. & Snyder, S. H. RAFT1: a mammalian protein that binds to FKBP12 in a rapamycin-dependent fashion and is homologous to yeast TORs. *Cell* **78**, 35-43 (1994).

173 Wilkinson, J. E. *et al.* Rapamycin slows aging in mice. *Aging Cell* **11**, 675-682, doi:10.1111/j.1474-9726.2012.00832.x (2012).

174 Choo, A. Y., Yoon, S. O., Kim, S. G., Roux, P. P. & Blenis, J. Rapamycin differentially inhibits S6Ks and 4E-BP1 to mediate cell-type-specific repression of mRNA translation. *Proc Natl Acad Sci U S A* **105**, 17414-17419, doi:10.1073/pnas.0809136105 (2008).

175 Gingras, A. C., Raught, B. & Sonenberg, N. Regulation of translation initiation by FRAP/mTOR. *Genes Dev* **15**, 807-826, doi:10.1101/gad.887201 (2001).

176 Beretta, L., Gingras, A. C., Svitkin, Y. V., Hall, M. N. & Sonenberg, N. Rapamycin blocks the phosphorylation of 4E-BP1 and inhibits cap-dependent initiation of translation. *The EMBO journal* **15**, 658-664 (1996).

177 Kaul, G., Pattan, G. & Rafeequi, T. Eukaryotic elongation factor-2 (eEF2): its regulation and peptide chain elongation. *Cell biochemistry and function* **29**, 227-234, doi:10.1002/cbf.1740 (2011).

178 Lewis, S. E., Goldspink, D. F., Phillips, J. G., Merry, B. J. & Holehan, A. M. The effects of aging and chronic dietary restriction on whole body growth and protein turnover in the rat. *Exp Gerontol* **20**, 253-263 (1985).

179 Goldspink, D. F., el Haj, A. J., Lewis, S. E., Merry, B. J. & Holehan, A. M. The influence of chronic dietary intervention on protein turnover and growth of the diaphragm and extensor digitorum longus muscles of the rat. *Exp Gerontol* **22**, 67-78 (1987).

180 Lambert, A. J. & Merry, B. J. Use of primary cultures of rat hepatocytes for the study of ageing and caloric restriction. *Exp Gerontol* **35**, 583-594 (2000).

181 Merry, B. J., Holehan, A. M., Lewis, S. E. & Goldspink, D. F. The effects of ageing and chronic dietary restriction on in vivo hepatic protein synthesis in the rat. *Mech Ageing Dev* **39**, 189-199 (1987).

182 el Haj, A. J., Lewis, S. E., Goldspink, D. F., Merry, B. J. & Holehan, A. M. The effect of chronic and acute dietary restriction on the growth and protein turnover of fast and slow types of rat skeletal muscle. *Comp Biochem Physiol A Comp Physiol* **85**, 281-287 (1986).

183 Hansen, M. *et al.* A role for autophagy in the extension of lifespan by dietary restriction in C. *elegans*. *PLoS Genet* **4**, e24, doi:10.1371/journal.pgen.0040024 (2008).

184 Alvers, A. L. *et al.* Autophagy is required for extension of yeast chronological life span by rapamycin. *Autophagy* **5**, 847-849 (2009).

185 Hipkiss, A. R. On why decreasing protein synthesis can increase lifespan. *Mech Ageing Dev* **128**, 412-414, doi:10.1016/j.mad.2007.03.002 (2007).

186 Cerqueira, F. M., Cunha, F. M., Laurindo, F. R. & Kowaltowski, A. J. Calorie restriction increases cerebral mitochondrial respiratory capacity in a NO•-mediated mechanism: impact on neuronal survival. *Free Radic Biol Med* **52**, 1236-1241, doi:10.1016/j.freeradbiomed.2012.01.011 (2012).

187 Dani, D. *et al.* Modulation of oxidative phosphorylation machinery signifies a prime mode of anti-ageing mechanism of calorie restriction in male rat liver mitochondria. *Biogerontology* **11**, 321-334, doi:10.1007/s10522-009-9254-y (2010).

188 Finley, L. W. *et al.* Skeletal muscle transcriptional coactivator PGC-1α mediates mitochondrial, but not metabolic, changes during calorie restriction. *Proc Natl Acad Sci U S A* **109**, 2931-2936, doi:10.1073/pnas.1115813109 (2012).

189 Cunningham, J. T. *et al.* mTOR controls mitochondrial oxidative function through a YY1-PGC-1alpha transcriptional complex. *Nature* **450**, 736-740, doi:10.1038/nature06322 (2007).

190 Ramanathan, A. & Schreiber, S. L. Direct control of mitochondrial function by mTOR. *Proc Natl Acad Sci U S A* **106**, 22229-22232, doi:10.1073/pnas.0912074106 (2009).

191 Fok, W. C. *et al.* Combined treatment of rapamycin and dietary restriction has a larger effect on the transcriptome and metabolome of liver. *Aging Cell* **13**, 311-319, doi:10.1111/acel.12175 (2014).

192 Yu, Z. *et al.* Rapamycin and Dietary Restriction Induce Metabolically Distinctive Changes in Mouse Liver. *J Gerontol A Biol Sci Med Sci*, doi:10.1093/gerona/glu053 (2014).

193 Zhang, J. *et al.* Systematic characterization of the murine mitochondrial proteome using functionally validated cardiac mitochondria. *Proteomics* **8**, 1564-1575, doi:10.1002/pmic.200700851 (2008).

194 Hipp, M. S., Park, S. H. & Hartl, F. U. Proteostasis impairment in protein-misfolding and -aggregation diseases. *Trends in cell biology*, doi:10.1016/j.tcb.2014.05.003 (2014).

195 Hetz, C., Chevet, E. & Oakes, S. A. Proteostasis control by the unfolded protein response. *Nature Cell Biology* **17**, 829-838, doi:10.1038/ncb3184 (2015).

196 Cannizzo, E. S. *et al.* Age-related oxidative stress compromises endosomal proteostasis. *Cell reports* **2**, 136-149, doi:10.1016/j.celrep.2012.06.005 (2012).

197 Jones, D. P. Redox theory of aging. *Redox biology* **5**, 71-79, doi:10.1016/j.redox.2015.03.004

10.1016/j.redox.2015.03.004. (2015).

198 Tsakiri, E. N. *et al.* Proteasome dysfunction in Drosophila signals to an Nrf2-dependent regulatory circuit aiming to restore proteostasis and prevent premature aging. *Aging Cell* **12**, 802-813, doi:10.1111/acel.12111 (2013).

199 Baskin, K. K. & Taegtmeyer, H. AMP-activated protein kinase regulates E3 ligases in rodent heart. *Circ Res* **109**, 1153-1161, doi:10.1161/CIRCRESAHA.111.252742

10.1161/CIRCRESAHA.111.252742. Epub 2011 Sep 15. (2011).

200 Brehm, A. & Kruger, E. Dysfunction in protein clearance by the proteasome: impact on autoinflammatory diseases. *Seminars in immunopathology* **37**, 323-333, doi:10.1007/s00281-015-0486-4

10.1007/s00281-015-0486-4. Epub 2015 May 12. (2015).

201 Karunadharma, P. P. *et al.* Subacute calorie restriction and rapamycin discordantly alter mouse liver proteome homeostasis and reverse aging effects. *Aging Cell*, doi:10.1111/acel.12317 (2015).

202 Jolly, R. D., Dalefield, R. R. & Palmer, D. N. Ceroid, lipofuscin and the ceroid-lipofuscinoses (Batten disease). *Journal of inherited metabolic disease* **16**, 280-283 (1993).

203 Corboy, M. J., Thomas, P. J. & Wigley, W. C. Aggresome formation. *Methods in molecular biology (Clifton, N.J.)* **301**, 305-327, doi:10.1385/1-59259-895-1:305 (2005).

204 Cuanalo-Contreras, K., Mukherjee, A. & Soto, C. Role of protein misfolding and proteostasis deficiency in protein misfolding diseases and aging. *International journal of cell biology* **2013**, 638083, doi:10.1155/2013/638083 (2013).

205 Rotteveel, J. J. & Mullaart, R. A. [Antioxidative therapy in ceroid lipofuscinosis]. *Tijdschrift voor kindergeneeskunde* **57**, 181-186 (1989).

206 Calise, J. & Powell, S. R. The ubiquitin proteasome system and myocardial ischemia. *Am J Physiol Heart Circ Physiol* **304**, H337-349, doi:10.1152/ajpheart.00604.2012 (2013).

207 Mi, L., Gan, N. & Chung, F. L. Aggresome-like structure induced by isothiocyanates is novel proteasome-dependent degradation machinery. *Biochem Biophys Res Commun* **388**, 456-462, doi:10.1016/j.bbrc.2009.08.047 (2009).

208 Semba, R. D., Nicklett, E. J. & Ferrucci, L. Does accumulation of advanced glycation end products contribute to the aging phenotype? *J Gerontol A Biol Sci Med Sci* **65**, 963-975, doi:10.1093/gerona/glq074 (2010).

209 Ferreira, M. E. *et al.* Oxidative Stress in Alzheimer's Disease: Should We Keep Trying Antioxidant Therapies? *Cellular and molecular neurobiology* **35**, 595-614, doi:10.1007/s10571-015-0157-y 10.1007/s10571-015-0157-y. Epub 2015 Jan 24. (2015).

210 Herter, S. *et al.* Dendritic cell aggresome-like-induced structure formation and delayed antigen presentation coincide in influenza virus-infected dendritic cells. *Journal of immunology* **175**, 891-898 (2005).

211 Solcia, E. *et al.* Particle-rich cytoplasmic structure (PaCS): identification, natural history, role in cell biology and pathology. *Biomolecules* **4**, 848-861, doi:10.3390/biom4030848 (2014).

212 Palmer, I. & Wingfield, P. T. Preparation and extraction of insoluble (inclusion-body) proteins from Escherichia coli. *Current protocols in protein science / editorial board, John E. Coligan ... [et al.]* **Chapter 6**, Unit6.3, doi:10.1002/0471140864.ps0603s70 (2012).

213 Harman, D. Alzheimer's disease: A hypothesis on pathogenesis. *Journal of the American Aging Association* **23**, 147-161, doi:10.1007/s11357-000-0017-6 10.1007/s11357-000-0017-6. (2000).

214 Buchan, J. R. & Parker, R. Eukaryotic stress granules: the ins and outs of translation. *Molecular cell* **36**, 932-941, doi:10.1016/j.molcel.2009.11.020 (2009).

215 Crawford, J. M. Histologic findings in alcoholic liver disease. *Clinics in liver disease* **16**, 699-716, doi:10.1016/j.cld.2012.08.004 (2012).

216 Bardag-Gorce, F. *et al.* The Role of the Ubiquitin–Proteasome Pathway in the Formation of Mallory Bodies. *Experimental and molecular pathology* **73**, 75-83, doi:10.1006/exmp.2002.2451 (2002).

217 Kato, M. Mallory Bodies in Hepatocytes of Alcoholic Liver Disease and Primary Biliary Cirrhosis Contain Nε-(Carboxymethyl)lysine-Modified Cytokeratin, but not those in Hepatic Carcinoma Cells. *Yonago Acta medica* **49**, 83-92 (2006).

218 Hanada, S. *et al.* Aging modulates susceptibility to mouse liver Mallory-Denk body formation. *The journal of histochemistry and cytochemistry : official journal of the Histochemistry Society* **60**, 475-483, doi:10.1369/0022155412441478 (2012).

219

220 Matsumoto, M. *et al.* Large-scale analysis of the human ubiquitin-related proteome. *Proteomics* **5**, 4145-4151, doi:10.1002/pmic.200401280 (2005).

221 Käll, L., Canterbury, J. D., Weston, J., Noble, W. S. & MacCoss, M. J. Semi-supervised learning for peptide identification from shotgun proteomics datasets. *Nature methods* **4**, 923-925, doi:10.1038/nmeth1113 (2007).

222 Finney, G. L. *et al.* Label-Free Comparative Analysis of Proteomics Mixtures Using Chromatographic Alignment of High-Resolution μLC−MS Data. *Analytical Chemistry* **80**, 961-971, doi:10.1021/ac701649e (2008).

223 Billingham, R. E., Krohn, P. L. & Medawar, P. B. Effect of locally applied cortisone acetate on survival of skin homografts in rabbits. *British medical journal* **2**, 1049-1053 (1951).

224 Brand, M. D. The sites and topology of mitochondrial superoxide production. *Exp Gerontol* **45**, 466-472, doi:10.1016/j.exger.2010.01.003 (2010).

225 Schonhofen, P., de Medeiros, L. M., Chatain, C. P., Bristot, I. J. & Klamt, F. Cofilin/actin rod formation by dysregulation of cofilin-1 activity as a central initial step in neurodegeneration. *Mini reviews in medicinal chemistry* **14**, 393-400 (2014).

226 Twig, G., Hyde, B. & Shirihai, O. S. Mitochondrial fusion, fission and autophagy as a quality control axis: the bioenergetic view. *Biochim Biophys Acta* **1777**, 1092-1097, doi:10.1016/j.bbabio.2008.05.001 (2008).

227 Tatsuta, T. & Langer, T. AAA proteases in mitochondria: diverse functions of membrane-bound proteolytic machines. *Research in microbiology* **160**, 711-717, doi:10.1016/j.resmic.2009.09.005 (2009).

228 Taylor, E. B. & Rutter, J. Mitochondrial quality control by the ubiquitin-proteasome system. *Biochemical Society transactions* **39**, 1509-1513, doi:10.1042/BST0391509 (2011).

229 Pellegrino, M. W., Nargund, A. M. & Haynes, C. M. Signaling the mitochondrial unfolded protein response. *Biochim Biophys Acta* **1833**, 410-416, doi:10.1016/j.bbamcr.2012.02.019 (2013).

230 Lionaki, E. & Tavernarakis, N. Oxidative stress and mitochondrial protein quality control in aging. *Journal of proteomics*, doi:10.1016/j.jprot.2013.03.022 (2013).

231 FLETCHER, M. J. & SANADI, D. R. Turnover of liver mitochondrial components in adult and senescent rats. *J Gerontol* **16**, 255-257 (1961).

232 Menzies, R. A. & Gold, P. H. The turnover of mitochondria in a variety of tissues of young adult and aged rats. *J Biol Chem* **246**, 2425-2429 (1971).

233 Cambridge, S. B. *et al.* Systems-wide proteomic analysis in mammalian cells reveals conserved, functional protein turnover. *J Proteome Res* **10**, 5275-5284, doi:10.1021/pr101183k (2011).

234 Schägger, H. & Pfeiffer, K. Supercomplexes in the respiratory chains of yeast and mammalian mitochondria. *EMBO J* **19**, 1777-1783, doi:10.1093/emboj/19.8.1777 (2000).

235 Genova, M. L., Bianchi, C. & Lenaz, G. Structural organization of the mitochondrial respiratory chain. *Ital J Biochem* **52**, 58-61 (2003).

236 Nelson, C. J., Li, L., Jacoby, R. P. & Millar, A. H. Degradation rate of mitochondrial proteins in Arabidopsis thaliana cells. *J Proteome Res* **12**, 3449-3459, doi:10.1021/pr400304r (2013).

237 Gao, X. *et al.* The crystal structure of mitochondrial cytochrome bc1 in complex with famoxadone: the role of aromatic-aromatic interaction in inhibition. *Biochemistry* **41**, 11692-11702 (2002).

238 Gledhill, J. R. & Walker, J. E. Inhibitors of the catalytic domain of mitochondrial ATP synthase. *Biochemical Society transactions* **34**, 989-992, doi:10.1042/BST0340989 (2006).

239 Iwata, S. *et al.* Complete structure of the 11-subunit bovine mitochondrial cytochrome bc1 complex. *Science* **281**, 64-71 (1998).

240 Solmaz, S. R. & Hunte, C. Structure of complex III with bound cytochrome c in reduced state and definition of a minimal core interface for electron transfer. *J Biol Chem* **283**, 17542-17549, doi:10.1074/jbc.M710126200 (2008).

241 Sun, F. *et al.* Crystal structure of mitochondrial respiratory membrane protein complex II. *Cell* **121**, 1043-1057, doi:10.1016/j.cell.2005.05.025 (2005).

242 Tsukihara, T. *et al.* The whole structure of the 13-subunit oxidized cytochrome c oxidase at 2.8 A. *Science* **272**, 1136-1144 (1996).

243 Angerer, H. *et al.* Tracing the tail of ubiquinone in mitochondrial complex I. *Biochim Biophys Acta* **1817**, 1776-1784, doi:10.1016/j.bbabio.2012.03.021 (2012).

244 Vogel, R. O., Smeitink, J. A. & Nijtmans, L. G. Human mitochondrial complex I assembly: a dynamic and versatile process. *Biochim Biophys Acta* **1767**, 1215-1227, doi:10.1016/j.bbabio.2007.07.008 (2007).

245 Vincow, E. S. *et al.* The PINK1-Parkin pathway promotes both mitophagy and selective respiratory chain turnover in vivo. *Proc Natl Acad Sci U S A* **110**, 6400-6405, doi:10.1073/pnas.1221132110 (2013).

246 Huynen, M. A., Duarte, I. & Szklarczyk, R. Loss, replacement and gain of proteins at the origin of the mitochondria. *Biochim Biophys Acta* **1827**, 224-231, doi:10.1016/j.bbabio.2012.08.001 (2013).

247 McKenzie, M. & Ryan, M. T. Assembly factors of human mitochondrial complex I and their defects in disease. *IUBMB Life* **62**, 497-502, doi:10.1002/iub.335 (2010).

248 Fox, T. D. Mitochondrial protein synthesis, import, and assembly. *Genetics* **192**, 1203-1234, doi:10.1534/genetics.112.141267 (2012).

249 Lau, E. *et al.* Substrate- and isoform-specific proteome stability in normal and stressed cardiac mitochondria. *Circ Res* **110**, 1174-1178, doi:10.1161/CIRCRESAHA.112.268359 (2012).

250 Gottlieb, R. A. & Carreira, R. S. Autophagy in health and disease. 5. Mitophagy as a way of life. *Am J Physiol Cell Physiol* **299**, C203-210, doi:10.1152/ajpcell.00097.2010 (2010).

251 Livnat-Levanon, N. & Glickman, M. H. Ubiquitin-proteasome system and mitochondria - reciprocity. *Biochim Biophys Acta* **1809**, 80-87, doi:10.1016/j.bbagrm.2010.07.005 (2011).

252 Heo, J. M. & Rutter, J. Ubiquitin-dependent mitochondrial protein degradation. *The international journal of biochemistry & cell biology* **43**, 1422-1426, doi:10.1016/j.biocel.2011.06.002 (2011).

253 Margineantu, D. H., Emerson, C. B., Diaz, D. & Hockenbery, D. M. Hsp90 inhibition decreases mitochondrial protein turnover. *PloS one* **2**, e1066, doi:10.1371/journal.pone.0001066 (2007).

254 Tatsuta, T. & Langer, T. Quality control of mitochondria: protection against neurodegeneration and ageing. *EMBO J* **27**, 306-314, doi:10.1038/sj.emboj.7601972 (2008).

255 Boisvert, F. M. *et al.* A quantitative spatial proteomics analysis of proteome turnover in human cells. *Mol Cell Proteomics* **11**, M111.011429, doi:10.1074/mcp.M111.011429 (2012).

256 Nelson, C. J., Alexova, R., Jacoby, R. P. & Millar, A. H. Proteins with high turnover rate in barley leaves estimated by proteome analysis combined with in planta isotope labeling. *Plant physiology* **166**, 91-108, doi:10.1104/pp.114.243014 (2014).

257 Doherty, M. K., Hammond, D. E., Clague, M. J., Gaskell, S. J. & Beynon, R. J. Turnover of the human proteome: determination of protein intracellular stability by dynamic SILAC. *J Proteome Res* **8**, 104-112, doi:10.1021/pr800641v (2009).

258 Musatov, A. & Robinson, N. C. Susceptibility of mitochondrial electron-transport complexes to oxidative damage. Focus on cytochrome c oxidase. *Free Radic Res* **46**, 1313-1326, doi:10.3109/10715762.2012.717273 (2012).

259 Goard, C. A. & Schimmer, A. D. Mitochondrial matrix proteases as novel therapeutic targets in malignancy. *Oncogene*, doi:10.1038/onc.2013.228 (2013).

260 Huth, W., Rolle, S. & Wunderlich, I. Turnover of matrix proteins in mammalian mitochondria. *Biochem J* **364**, 275-284 (2002).

261 Acín-Pérez, R., Fernández-Silva, P., Peleato, M. L., Pérez-Martos, A. & Enriquez, J. A. Respiratory active mitochondrial supercomplexes. *Mol Cell* **32**, 529-539, doi:10.1016/j.molcel.2008.10.021 (2008).

262 Lapuente-Brun, E. *et al.* Supercomplex assembly determines electron flux in the mitochondrial electron transport chain. *Science* **340**, 1567-1570, doi:10.1126/science.1230381 (2013).

263 Kubinyi, H. Vol. 247 107-119 (Analytica Chimica Acta, 1991).

264 Bokov, A., Chaudhuri, A. & Richardson, A. The role of oxidative damage and stress in aging. *Mech Ageing Dev* **125**, 811-826, doi:10.1016/j.mad.2004.07.009 (2004).

265 Bhardwaj, P. Oxidative stress and antioxidants in gastrointestinal diseases. *Trop Gastroenterol* **29**, 129-135 (2008).

266 Mecocci, P. & Polidori, M. C. Antioxidant clinical trials in mild cognitive impairment and Alzheimer's disease. *Biochim Biophys Acta* **1822**, 631-638, doi:10.1016/j.bbadis.2011.10.006 (2012).

267 Jalili, M., Kolahi, S., Aref-Hosseini, S. R., Mamegani, M. E. & Hekmatdoost, A. Beneficial role of antioxidants on clinical outcomes and erythrocyte antioxidant parameters in rheumatoid arthritis patients. *Int J Prev Med* **5**, 835-840 (2014).

268 Pérez, V. I. *et al.* The overexpression of major antioxidant enzymes does not extend the lifespan of mice. *Aging Cell* **8**, 73-75, doi:10.1111/j.1474-9726.2008.00449.x (2009).

269 Lewis, K. N., Andziak, B., Yang, T. & Buffenstein, R. The naked mole-rat response to oxidative stress: just deal with it. *Antioxid Redox Signal* **19**, 1388-1399, doi:10.1089/ars.2012.4911 (2013).

270 Itsara, L. S. *et al.* Oxidative stress is not a major contributor to somatic mitochondrial DNA mutations. *PLoS Genet* **10**, e1003974, doi:10.1371/journal.pgen.1003974 (2014).

271 Bartell, S. M. *et al.* FoxO proteins restrain osteoclastogenesis and bone resorption by attenuating H2O2 accumulation. *Nat Commun* **5**, 3773, doi:10.1038/ncomms4773 (2014).

272 Szeto, H. H. First-in-class cardiolipin-protective compound as a therapeutic agent to restore mitochondrial bioenergetics. *Br J Pharmacol* **171**, 2029-2050, doi:10.1111/bph.12461 (2014).

273 K, P. Vol. 60 (Proceedings of the Royal Society of London, 1987).

274 Michael Lynn, C. F. B. J. Vol. 22 (4) 327-341 (Journal of Applied Social Psychology, 1992).

275 Zolk, O., Schenke, C. & Sarikas, A. The ubiquitin–proteasome system: Focus on the heart. *Cardiovascular Research* **70**, 410-421, doi:10.1016/j.cardiores.2005.12.021 (2006).

276 Sarbassov, D. D. & Sabatini, D. M. Redox regulation of the nutrient-sensitive raptor-mTOR pathway and complex. *J Biol Chem* **280**, 39505-39509, doi:10.1074/jbc.M506096200 (2005).

277 Squier, T. C. Redox modulation of cellular metabolism through targeted degradation of signaling proteins by the proteasome. *Antioxid Redox Signal* **8**, 217-228, doi:10.1089/ars.2006.8.217 (2006).

278 Starkov, A. A. The role of mitochondria in reactive oxygen species metabolism and signaling. *Ann N Y Acad Sci* **1147**, 37-52, doi:10.1196/annals.1427.015 (2008).

279 Reczek, C. R. & Chandel, N. S. ROS-dependent signal transduction. *Curr Opin Cell Biol* **33**, 8-13, doi:10.1016/j.ceb.2014.09.010 (2015).

280 Le Belle, J. E. *et al.* Proliferative neural stem cells have high endogenous ROS levels that regulate self-renewal and neurogenesis in a PI3K/Akt-dependant manner. *Cell Stem Cell* **8**, 59-71, doi:10.1016/j.stem.2010.11.028 (2011).

281 Song, M. *et al.* Super-suppression of mitochondrial reactive oxygen species signaling impairs compensatory autophagy in primary mitophagic cardiomyopathy. *Circ Res* **115**, 348-353, doi:10.1161/circresaha.115.304384 (2014).

282 West, A. P. *et al.* TLR signalling augments macrophage bactericidal activity through mitochondrial ROS. *Nature* **472**, 476-480, doi:10.1038/nature09973 (2011).

283 Marcinek, D. J. & Siegel, M. P. Targeting redox biology to reverse mitochondrial dysfunction. *Aging (Albany NY)* **5**, 588-589 (2013).

284 Shi, Y., Buffenstein, R., Pulliam, D. A. & Van Remmen, H. Comparative studies of oxidative stress and mitochondrial function in aging. *Integr Comp Biol* **50**, 869-879, doi:10.1093/icb/icq079 (2010).

285 GM, M., D, M. & EP, B. in *FASEB* Vol. 19:20 (Federation Proceedings, Atlantic City, 1960).

286 Torma, F. *et al.* Exercise Increases Markers of Spermatogenesis in Rats Selectively Bred for Low Running Capacity. *PLoS One* **9**, e114075, doi:10.1371/journal.pone.0114075 (2014).

287 Hoopmann, M. R., Finney, G. L. & MacCoss, M. J. High-speed data reduction, feature detection, and MS/MS spectrum quality assessment of shotgun proteomics data sets using high-resolution mass spectrometry. *Anal Chem* **79**, 5620-5632, doi:10.1021/ac0700833 (2007).

288 Hsieh, E. J., Hoopmann, M. R., MacLean, B. & MacCoss, M. J. Comparison of database search strategies for high precursor mass accuracy MS/MS data. *J Proteome Res* **9**, 1138-1143, doi:10.1021/pr900816a (2010).

289 Kubinyi, H. Vol. 247 107-119 (Analytica Chimica Acta, 1991).

290 Rodriguez, K. A. *et al.* A cytosolic protein factor from the naked mole-rat activates proteasomes of other species and protects these from inhibition. *Biochim Biophys Acta*, doi:10.1016/j.bbadis.2014.07.005 (2014).